PHOSPHOLIPID REQUIREMENT FOR MITOCHONDRIAL CALCIUM CHANNEL AND ITS IMPLICATIONS IN BARTH SYNDROME

A Dissertation

by

SAGNIKA GHOSH

Submitted to the Graduate and Professional School of
Texas A&M University
in partial fulfillment of the requirements for the degree of

DOCTOR OF PHILOSOPHY

Chair of Committee,	Thomas D. Meek
Committee Members,	Vishal M. Gohil
	Michael Polymenis
	Steve W. Lockless
Head of Department,	Joshua A. Wand

December 2021

Major Subject: Biochemistry

ABSTRACT

Biochemical interactions between macromolecules form the basis of life. Among different macromolecular interactions present in living systems, we still lag in our understanding of how lipids influence the structure and function of proteins in biological membranes. To this end, I developed yeast *Saccharomyces cerevisiae* phospholipid mutants as a surrogate system to dissect the *in vivo* phospholipid requirements of the mitochondrial calcium import machinery – the uniporter complex.

I first focused on mitochondrial calcium uniporter (MCU), the pore-forming subunit of the uniporter complex, for the following reasons. First, it is an integral inner mitochondrial membrane protein that is a key regulator of mitochondrial bioenergetics. Second, MCU is not present in *S. cerevisiae*, providing a "clean" system to interrogate its phospholipid requirements in a physiologically relevant mitochondrial membrane. Third, mitochondrial calcium signaling has been implicated in a number of human diseases, however, the phospholipid requirements of MCU have remained unknown. I used heterologous expression to functionally reconstitute protozoan and human MCU in wild type yeast as well as in mutants defective in the biosynthesis of the most abundant mitochondrial phospholipids, phosphatidylcholine, phosphatidylethanolamine, or cardiolipin (CL), to uncover a CL-specific requirement for the stability and activity of MCU. My findings from the yeast model system are applicable to higher organisms as shown by the reduced abundance and activity of endogenous MCU in cells and cardiac tissue of Barth syndrome patients that have inherited deficiency in CL levels.

In a follow-up study, I showed that the partial loss of CL in Barth syndrome disease models also results in rapid turnover of mitochondrial calcium uptake 1 (MICU1), the principal regulator of the uniporter complex. The CL-deficiency induced decrease in MCU and MICU1 disrupts mitochondrial calcium signaling such that calcium-stimulated mitochondrial bioenergetic pathways are blunted in cellular models of Barth syndrome. These findings could explain common clinical features observed in Barth syndrome patients such as cardiac arrhythmia and proximal muscle myopathy.

In summary, my work shows that yeast phospholipid mutants can be leveraged to uncover specific phospholipid requirements of mitochondrial membrane proteins and suggests a role of mitochondrial calcium signaling in the pathogenesis of Barth syndrome.

DEDICATION

To my parents

ACKNOWLEDGEMENTS

I would like to thank my advisor Dr. Gohil for his unwavering guidance, dedication, and support throughout the course of this research and beyond. I would like to thank my committee members, Dr. Meek, Dr. Polymenis, and Dr. Lockless for their advice and suggestions regarding my research work. I thank Dr. Laganowsky for his input and availability for my dissertation defense. I would also like to thank Dr. Writoban Basu Ball for his constant encouragement and support, especially during the early days of my graduate course, and for all the exciting discussions about science and life. I would like to take this opportunity to thank all the former and current members of the Gohil lab for their constant help and assistance throughout my PhD journey, with a special mention to Dr. Charli Baker, Dr. Donna Iadarola, and Natalie Garza for being a constant support for me in and out of the lab. A special thanks to all the amazing friends I have made through this journey, without whom the ride would not have been as enjoyable and memorable. A special mention to Nairita Maitra, Sayan Banerjee, and Isita Jhulki for their constant care and support throughout the years and making it feel like home here in College Station. Finally, and most importantly, I would like to take this opportunity to thank my parents Dipak Ghosh and Jubilee Ghosh and my brother Sounak Ghosh for their unwavering love, encouragement, understanding, and support, which made this journey possible.

CONTRIBUTORS AND FUNDING SOURCES

This work was supported by a dissertation committee consisting of my advisor Dr. Vishal M. Gohil of the Department of Biochemistry and Biophysics and the Interdisciplinary Program in Genetics, Dr. Thomas D. Meek of the Department of Biochemistry and Biophysics, Dr. Michael Polymenis of the Department of Biochemistry and Biophysics and the Interdisciplinary Program in Genetics, and Dr. Steve W. Lockless of the Department of Biology. The head of the Biochemistry and Biophysics department, Dr. Joshua A. Wand, also supported this work.

Chapter I is partly a reprint of two review publications for which I am the first author and a middle author, respectively. I performed all the literature reviews and wrote all the sections in this chapter except for the sections “Cardiolipin biosynthesis” and “Barth syndrome disease models” written, respectively, by Drs. Donna M. Iadarola and Writoban Basu Ball of the Department of Biochemistry and Biophysics at the Texas A&M University. The review publications used in this chapter were supported by the Welch Foundation grant [A-1810] and the National Institutes of Health award [R01GM111672] to Vishal M. Gohil. The content is solely the responsibility of the authors and does not necessarily represent the official views of the National Institute of Health.

Chapter II is a reprint of a research article for which I am the first author. I performed all the experimental work described in this chapter except for the phospholipid measurement (Table 2.2) performed by Dr. Writoban Basu Ball of the Department of Biochemistry and Biophysics at Texas A&M University, and the

mitochondrial calcium uptake assays (Figure 2.11D and E) performed by Travis R. Madaris and Subramanya Srikantan in the lab of Dr. Muniswamy Madesh (Department of Medicine, Division of Nephrology, Center for Precision Medicine at the University of Texas Health Science Center at San Antonio). I thank Dr. Vamsi K. Mootha (Massachusetts General Hospital and Broad Institute) for generously providing the yeast plasmids used in this study. I also thank Dr. Miriam L. Greenberg (Wayne State University) for generously sharing yeast strains and mammalian cell lines and Drs. Sharon Ackerman, Chris Meisinger, Dennis R. Winge, Vincenzo Zara, and Jan Brix for their generous gift of antibodies. This work was supported by the Welch Foundation Grant [A-1810] and the National Institutes of Health awards [R01GM111672] to Vishal M. Gohil, [R01AR071942] to Vamsi K. Mootha and [R01GM109882] to Muniswamy Madesh. The content is solely the responsibility of the authors and does not necessarily represent the official views of the National Institutes of Health.

The work in Chapter III has not been previously published. I performed all the experimental work described in this chapter except for the mitochondrial calcium uptake assay (Figure 3.4) and NADH measurement (Figure 3.5D-F), which was performed by Travis R. Madaris and Subramanya Srikantan in the lab of Dr. Muniswamy Madesh (Department of Medicine, Division of Nephrology, Center for Precision Medicine at the University of Texas Health Science Center at San Antonio) and MCUR1 levels in CL-deficient yeast mutant (Figure 3.2C and D), which was performed by Dr. Mohammad Zulkifli of the Department of Biochemistry and Biophysics at Texas A&M University. I thank Dr. Muniswamy Madesh for generously providing the plasmid used in this study. I

thank Alaumy Joshi of the Department of Biochemistry and Biophysics at Texas A&M University for assisting me in the construction of the yeast expression plasmid used in this study. This work was supported by the Barth syndrome Foundation 'Idea Grant', the Welch Foundation Grant [A-1810], and the National Institutes of Health Award [R01GM111672] to Vishal M. Gohil. The content is solely the responsibility of the authors and does not necessarily represent the official views of the National Institutes of Health.

The work in Appendix A has not been previously published. I performed all the experimental work described in this appendix. I thank Dr. Miriam L. Greenberg (Wayne State University) for generously providing the mammalian cell line, Dr. Scot C. Leary (University of Saskatchewan) for providing the antibody used in this study and Dr. Prachi P. Trivedi for help with ELISA assays. This work was supported by the Welch Foundation Grant [A-1810] and the National Institutes of Health award [R01GM111672] to Vishal M. Gohil. The content is solely the responsibility of the authors and does not necessarily represent the official views of the National Institutes of Health.

NOMENCLATURE

MRC	Mitochondrial respiratory chain
IMM	Inner mitochondrial membrane
OMM	Outer mitochondrial membrane
PE	Phosphatidylethanolamine
PC	Phosphatidylcholine
CL	Cardiolipin
MCU	Mitochondrial calcium uniporter
MICU1	Mitochondrial calcium uptake 1
EMRE	Essential MCU regulator
MCUR1	Mitochondrial calcium uniporter regulator 1
BTHS	Barth syndrome
$[Ca^{2+}]_i$	Intracellular calcium concentration
AFP	α-fetoprotein

TABLE OF CONTENTS

Page

LIST OF FIGURES

Page

LIST OF TABLES

Page

CHAPTER I

INTRODUCTION

Membrane biogenesis requires synthesis and integration of both membrane proteins and phospholipids (Gohil and Greenberg, 2009). Phospholipids influence the structure and function of membrane proteins; however, the roles of individual phospholipids are not well understood. Mitochondrial membranes represent an excellent model system to systematically dissect the *in vivo* roles of individual phospholipids without impacting other subcellular compartments because mitochondria are not part of the endomembrane system (Horvath and Daum, 2013).

---

* Part of this chapter is reprinted with permission from "Mitochondrial dysfunctions in Barth syndrome" by Ghosh S, Iadarola DM, Basu Ball W, Gohil VM, 2019. *IUBMB Life*, 71(7): 791-801. Copyright (2019) by John Wiley and Sciences.

** Part of this chapter is reprinted with permission from "Molecular nature and physiological role of the mitochondrial calcium uniporter channel" by Alevriadou BR, Patel A, Noble M, Ghosh S, Gohil VM, Stathopulos PB, Madesh M, 2021. *Am J Physiol Cell Physiol.* 320(4): C465-C482. Copyright (2021) by The American Physiological Society.

Moreover, the phospholipid composition of the inner mitochondrial membrane (IMM) is highly conserved from yeast to humans, with phosphatidylcholine (PC), phosphatidylethanolamine (PE), and cardiolipin (CL) being the three most abundant phospholipids (Figure 1.1) (Basu Ball et al., 2018).

Prior literature has extensively reported specific roles of the mitochondrial phospholipids in driving mitochondrial respiratory chain (MRC) biogenesis and bioenergetics in yeast and mammalian cells (Baker et al., 2016, Bottinger et al., 2012, Pfeiffer et al., 2003, Tasseva et al., 2013). Specifically, it was shown that non-bilayer forming phospholipids, such as PE and CL, are essential for the activity and assembly of MRC complexes, respectively (Baker et al., 2016, Bottinger et al., 2012). Interestingly, the bilayer forming PC was found to be largely dispensable for MRC function or formation (Baker et al., 2016 and Schuler et al., 2016). These studies exploited the ability to genetically manipulate mitochondrial phospholipid composition in yeast to interrogate specific role(s) of individual phospholipids in the integration, assembly, stability, and activity of MRC proteins. However, the role of phospholipids on non-MRC proteins has not been widely studied.

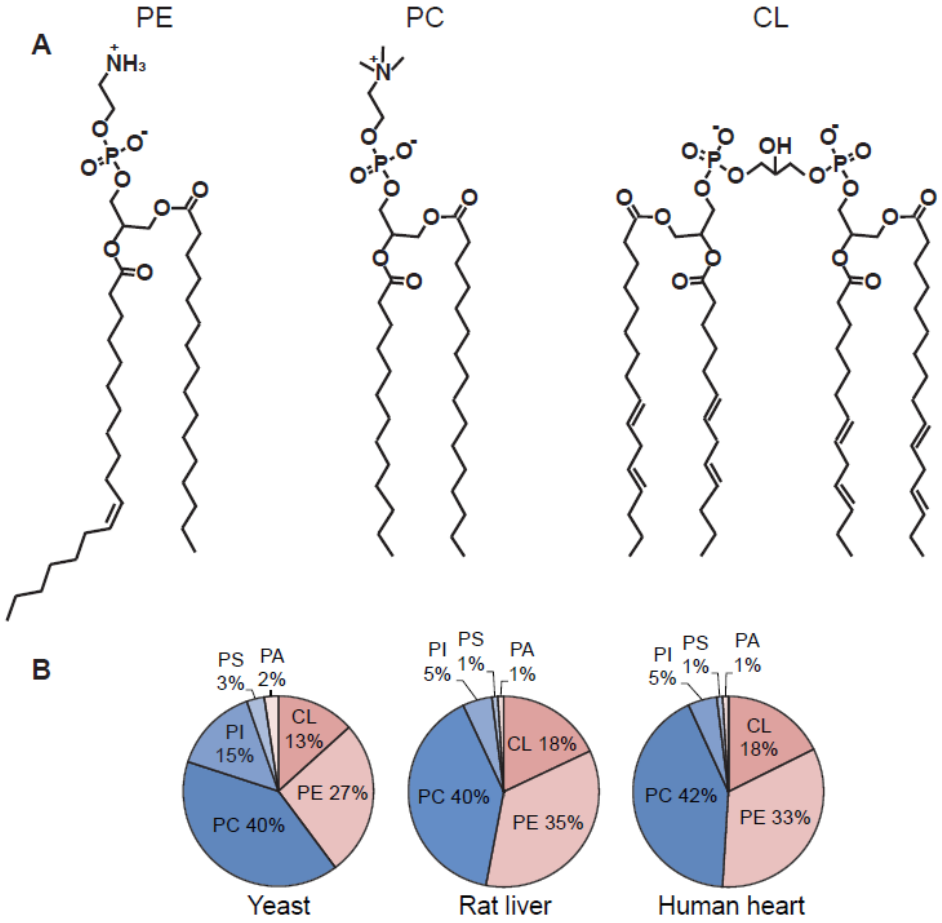

Figure 1.1 Structure and composition of mitochondrial membrane phospholipids
(A) Line diagrams of the most abundant mitochondrial phospholipids including phosphatidylethanolamine (PE), phosphatidylcholine (PC), and cardiolipin (CL). (B) The mitochondrial membrane phospholipid composition of yeast, rat liver, and human heart depicted as the percentage of total phospholipid phosphorus. PA, Phosphatidic acid; PI, Phosphatidylinositol; PS, Phosphatidylserine; PE, Phsophatidylethanolamine; PC, phosphatidylcholine; CL, cardiolipin. (Figure 1.1B is adapted from Basu Ball et al., 2018)

Mitochondrial calcium uniporter complex

One of the critical non-MRC regulators of mitochondrial bioenergetics is the recently discovered mitochondrial calcium uniporter complex, which is the major focus of this thesis (Perocchi et al., 2010, Baughman et al., 2011, De Stefani et al., 2011, Sancak et al., 2013). The IMM localized mitochondrial calcium uniporter (MCU)

constitutes the pore-forming subunit of the multimeric (~ 450-800 kDa) mitochondrial calcium uniporter complex. The uniporter complex enables mitochondria to take up large amounts of cytosolic calcium (Ca^{2+}) in response to physiological cues (Figure 1.2) (Kamer and Mootha, 2015).

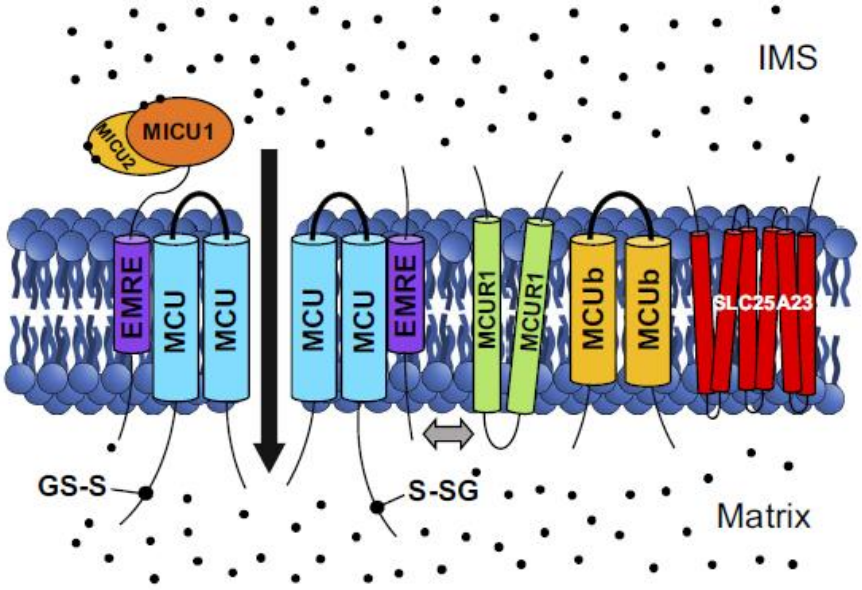

Figure 1.2 The mitochondrial calcium uniporter complex
The mitochondrial calcium uniporter complex is localized in the inner mitochondrial membrane, and each channel is composed of a tetramer of pore-forming mitochondrial calcium uniporter (MCU) subunits. Additional proteins making up the complex include essential MCU regulator (EMRE), mitochondrial calcium uptake 1/2 (MICU1/2), MCU regulator 1 (MCUR1), MCU dominant-negative β-subunit (MCUb), and solute carrier 25A23 (SLC25A23). Here, two out of the four MCU subunits, EMRE, and MICU1/2 are shown. MCUR1, MCUb, and SLC25A23 proteins are depicted integrating in and out of the MCU-EMRE-MICU core complex (integration is shown by a double-headed gray arrow). Transmembrane domains are represented as cylinders, and Ca^{2+} ions are represented as black dots. IMS, intermembrane space. (Figure modified and reprinted from Alevriadou et al., 2021).

In the uniporter complex, MCU associates with its regulatory proteins, including the MCU dominant negative β-subunit (MCUb), mitochondrial calcium uptake 1, 2, and 3 (MICU1, MICU2, MICU3), and the essential MCU regulator (EMRE) (Figure 1.2). MCU, MICU1, MICU2, and EMRE form the core components of the complex and

together they regulate the threshold and flux of Ca^{2+} import into the mitochondrial matrix (Kamer and Mootha, 2015). MCUR1 has been shown to act as a scaffold factor for building the uniporter complex (Tomar et al., 2016). Mitochondrial Ca^{2+} influx is an electrogenic process dependent on the large negative membrane potential across the IMM. Multiple recent cryo-electron microscopy (cryo-EM) studies of fungal and human MCU homologs have revealed that MCU exists as a tetramer in a 1:1 stoichiometry with EMRE. The MCU:EMRE heterooctamer then interacts with MICU1:MICU2 heterodimers forming the functional and regulated uniporter complex (Figure 1.3A and B) (Fan et al., 2020, Wang et al., 2020, Zhuo et al., 2021). According to the most recent structural studies, MICU1 is situated in the inter membrane space and blocks the MCU pore entrance to inhibit Ca^{2+} entry under low intracellular Ca^{2+} concentrations ($[Ca^{2+}]_i$) (Figure 1.3A) (Fan et al., 2020, Wang et al., 2020). A high $[Ca^{2+}]_i$ results in Ca^{2+} binding by the EF hand motifs of MICU1 and MICU2 and induces them to adopt a more open perpendicular conformation (Figure 1.3B) (Wang et al., 2020). This conformational change leads to weakened pore-blocking interactions between MICU1 and MCU and allows Ca^{2+} entry into the mitochondrial matrix (Fan et al., 2020, Wang et al., 2020).

Interestingly, another cryo-EM structure of a fungal MCU revealed the presence of lipid moieties on the membrane-exposed surfaces of MCU, however their molecular identities and roles were not determined (Baradaran et al., 2018).

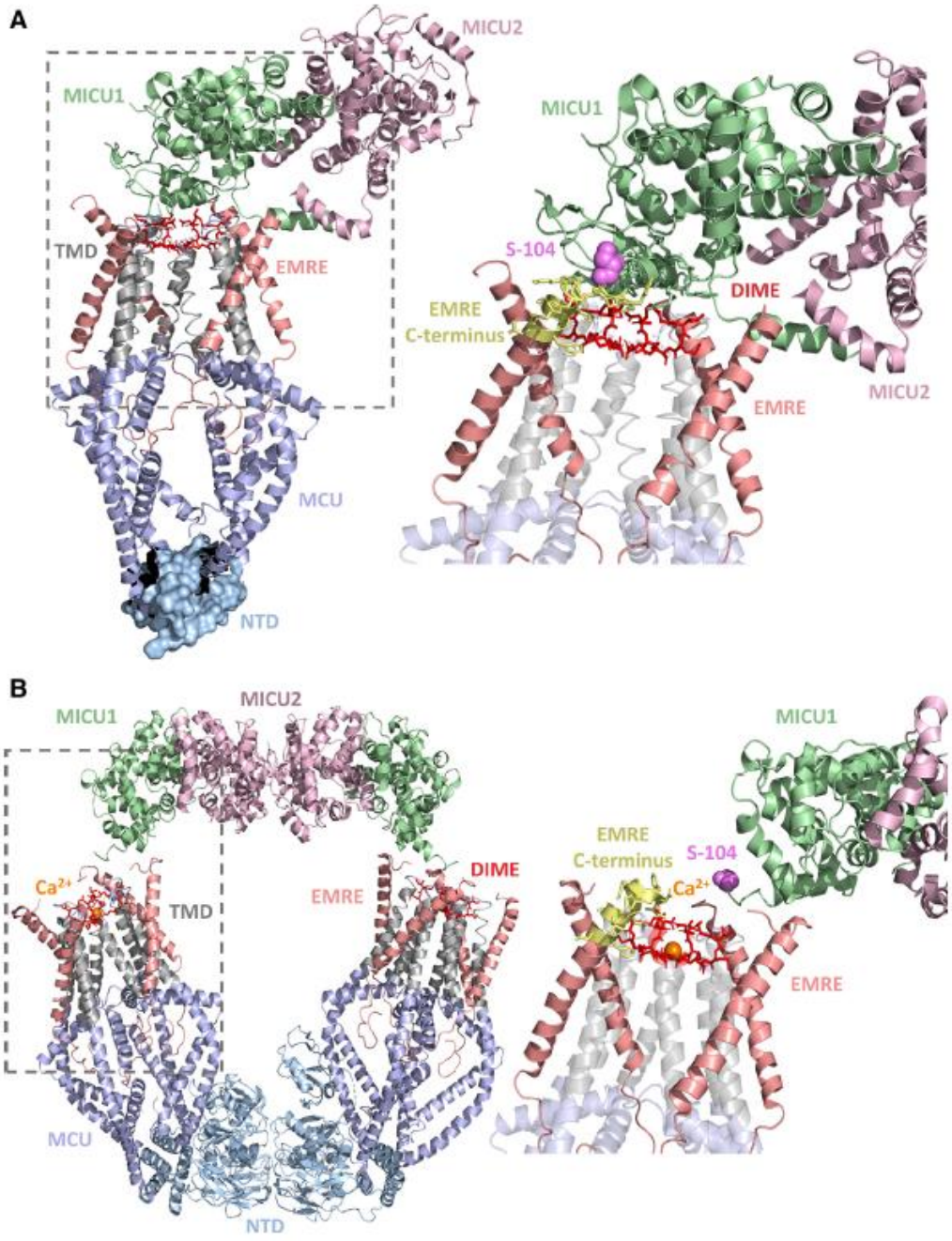

Figure 1.3 Structure of the human uniporter complex

(A) Structure of the pore-occluded MCU-EMRE-MICU1-MICU2 uniporter complex in low [Ca^{2+}]. Four human MCU subunits (blue and gray) are in complex with four EMRE peptides (salmon). The zoomed view of the MCU-EMRE-MICU1 interface (dashed box) is shown at right. The poly-basic region of the unresolved MICU1 NH_2 terminal region extends from S104 (magenta sphere) and likely contacts the unresolved poly-acidic COOH-terminal tail of EMRE, extending from the yellow cartoon. (B) Dimer of two pore-relieved human MCU-EMRE-

MICU1-MICU2 complexes in high [Ca^{2+}]. Four human MCU subunits (blue and gray) are in complex with four EMRE peptides (salmon). The zoomed view of the MCU-EMRE-MICU1 interface (dashed box) is shown at right. In (A) and (B), MICU1 and MICU2 are green and light pink, respectively, the DIME residues are red, the MCU NTDs are light blue, the MCU TMDs are gray, the NH_2-terminal Ser104 MICU1 residue is magenta, the COOH-terminal region of EMRE is yellow, and Ca^{2+} is orange. The structure figures were rendered in PyMOL using the 6WDO and 6WDN pdb coordinate files from Fan et al., 2020. MCU, mitochondrial calcium uniporter; EMRE, essential MCU regulator; MICU, mitochondrial Ca^{2+} uptake 1. (Figure reprinted from Alevriadou et al., 2021).

The physiological importance of mitochondrial calcium signaling

Ca^{2+} is a ubiquitous intracellular signaling messenger that is implicated in vital cellular processes including growth, secretion, metabolism, and neurotransmission as well as apoptotic and necrotic cell death pathways. The free $[Ca^{2+}]_i$ is tightly regulated by different intracellular Ca^{2+} stores as well as by the Ca^{2+} buffering proteins and Ca^{2+} transporting channels and pumps (Alevriadou et al., 2021). Mitochondria, owing to the capacity to buffer large amounts of Ca^{2+}, play a central role in maintaining the spatiotemporal patterning of intracellular Ca^{2+} signals. Specific mitochondrial Ca^{2+} influx and efflux proteins are responsible for maintaining the Ca^{2+} concentration inside the matrix (Kamer and Mootha, 2015). Elevation in mitochondrial matrix [Ca^{2+}] enhances mitochondrial respiration and ATP production by allosterically stimulating the activities of tricarboxylic acid cycle dehydrogenases (Kamer and Mootha, 2015). On the other hand, excessive Ca^{2+} accumulation in the mitochondria triggers mitochondrial pathways of apoptosis and necrosis (Kamer and Mootha, 2015, Hajnóczky et al., 2006). As such, mitochondrial Ca^{2+} homeostasis has been linked to several pathologies including ischemia-reperfusion injuries, cardiomyopathies, skeletal muscle myopathies, and neurodegeneration (Alevriadou et al., 2021).

Mitochondrial calcium uniporter complex in human diseases

Monogenic Mitochondrial Disorders: Whole exome sequencing of patients with neuromuscular disorders identified loss-of-function mutations in MICU1 as the pathogenic variants (Logan et al., 2014). Ca^{2+} sensing by MICU1 was impaired, and Ca^{2+} entry into mitochondria persisted even at low $[Ca^{2+}]_i$. These patients clinically presented with early onset proximal myopathy, learning difficulties, and a progressive and debilitating movement disorder (Logan et al., 2014). More recently, a homozygous MICU1 deletion of exon 1 was reported in two cousins diagnosed with severe exercise intolerance, fatigue, and lethargy in early childhood (Lewis Smith et al., 2016). As a result of this deletion, MICU1 protein was not detected in fibroblasts from these patients, leading to impaired mitochondrial Ca^{2+} uptake. Loss-of-function of MICU1 also induced a sarcolemma repair defect leading to skeletal muscle weakness and wasting (Debattisti et al., 2019).

Barth syndrome (BTHS) is another example of a monogenic disorder, where pathogenic mutations in the CL remodeling enzyme TAFAZZIN indirectly impact the MCU complex as described in chapters II and III of this thesis (Bione et al., 1996; Ghosh et al., 2020). Considering that BTHS patients share overlapping clinical features with MICU1 patients, including proximal muscle myopathy, exercise intolerance, and fatigue (Clarke et al., 2013), it is likely that a perturbation in MCU function contributes to some aspects of BTHS pathology.

Cardiovascular Disorders: Cardiac muscle relies heavily on mitochondria to meet energy demands, and mitochondrial buffering of $[Ca^{2+}]_i$ transients generated during

systole plays a critical role in this process (Griffiths et al., 2009). This process, referred to as excitation-contraction-bioenergetic coupling, has been implicated in various cardiac pathological conditions. For example, impaired mitochondrial Ca^{2+} signaling has been linked to cardiac hypertrophy and hereditary cardiomyopathy, leading to cardiomyocyte death and heart failure (Lu et al., 2013, Kuo et al., 2002). Mitochondrial Ca^{2+} uptake has also been shown to be reduced in diabetic cardiomyopathy (Flarsheim et al., 1996). Yet, rigorous testing of this theory has only become possible after the discovery of the MCU channel components. Genetic gain-of-function and loss-of-function experiments performed in murine neonatal cardiomyocytes showed that MCU is indeed responsible for the relay of $[Ca^{2+}]_i$ transients during cardiac contractions (Drago et al., 2012). It was recently shown that the stoichiometry of MICU1/MCU varies among different organs, with the heart containing a low MICU1/MCU ratio, which allows for a low $[Ca^{2+}]_i$ threshold for mitochondrial Ca^{2+} uptake and activation of oxidative metabolism (Paillard et al., 2017). These studies show that the uniporter serves as a crucial molecular assembly that decodes $[Ca^{2+}]_i$ transients and matches mitochondrial oxidative metabolism in cardiomyocytes. However, phenotypes observed in several whole body and cardiac-specific *Mcu-KO* mice have been rather mild (Mammucari et al., 2018). The first cardiac-specific model of MCU deficiency was constructed by expressing a dominant negative form of MCU with pore domain mutations that prevented Ca^{2+} entry (DN-MCU) in mouse hearts. DN-MCU mice exhibited normal resting heart rates but demonstrated impaired heart rate acceleration in cardiac pacemaker cells during agonist-induced fight-or-flight responses, resulting in an

inability to match mitochondrial OXPHOS and ATP production to increased energy demands (Wu et al., 2015). The stress induced cardiac defect phenotype was recapitulated in cardiac-specific *Mcu-KO* adult mice cardiomyocytes (Kwong et al., 2015, Luongo et al., 2015). MCU ablation offered cardioprotection after ischemia-reperfusion injury by preventing Ca^{2+} overload-induced opening of the mitochondrial permeability transition pore (Kwong et al., 2015, Luongo et al., 2015), but contrasting reports also exist (Pan et al., 2013). A study showed that MCU levels are increased in patient hearts exhibiting cardiac hypertrophy due to aortic stenosis (Zaglia et al., 2017). Studies of MCU deficiency in mice highlighted the importance of the uniporter in heart physiology, but the observed phenotypes were not striking, considering that the heart is one of the most metabolically active organs in the body. This could be partly because cardiac cells are rich in mitochondria (~33% by cell volume), and each mitochondrion contains ~200 molecules of MCU. Therefore, the Ca^{2+} current density through MCU in that tissue is maintained at a low level to prevent Ca^{2+} overload-mediated injury (Fieni et al., 2012). Furthermore, contrasting data obtained from models could be due to differences in experimental conditions, method of construction of the model, age, and genetic background of the organism. Based on the above, it appears that the contributions of MCU-mediated Ca^{2+} signaling in cardiac physiology might be subtler than previously predicted.

Skeletal Muscle Disorders: Mitochondrial Ca^{2+} signaling is crucial for skeletal muscle contraction and relaxation, as it must strategically coordinate ATP production with the metabolic demands required for generation of an action potential (Eisner et al.,

2013). Not surprisingly, mitochondrial Ca^{2+} signaling defects have been implicated in various types of muscle myopathies, including central core disease, an autosomal dominant myopathy characterized by hypotonia, proximal muscle weakness, delayed motor development, and reduced muscle bulk (Brini et al., 2005). Dysregulated mitochondrial Ca^{2+} uptake has also been implicated in a mouse model of Duchenne muscular dystrophy (Robert et al., 2001). Owing to its involvement in all voluntary movements, skeletal muscle exhibits one of the highest Ca^{2+} current densities and conductance through MCU compared with other tissues, like liver and kidney (Fieni et al., 2012). Global *Mcu-KO* mice were incapable of acute mitochondrial Ca^{2+} uptake, leading to impaired exercise capacity, muscle strength, and maximal muscle power output during strenuous work (Pan et al., 2013). Basal mitochondrial metabolism remained unaffected in these mice, suggesting that MCU is required to signal for increased mitochondrial ATP production when the muscle goes from a resting to an energized state. MCU activity was recently implicated in skeletal muscle trophism in mice; it was shown to be necessary and sufficient for the control of muscle fiber size both in postnatal and adult lives through a non-bioenergetic function (Mammucari et al., 2015). MCU overexpression in both young and adult mice resulted in a significant increase in myofiber size (hypertrophy), whereas its silencing decreased average fiber size in both age groups (atrophy) (Mammucari et al., 2015). The positive correlation between muscle size and MCU content was recapitulated in aged humans (>70 yr old), where extensive physical exercise increased MCU protein levels in their skeletal muscles (Zampieri et al., 2016). These studies point to a direct role of MCU-mediated

mitochondrial Ca^{2+} signaling in regulating skeletal muscle mass. Furthermore, MCU has been implicated in the repair mechanism of injured skeletal muscle fibers, owing to continuous strain, physical trauma, and aging (Horn et al., 2017). A non-bioenergetic role of mitochondria was reported for the repair of muscle fibers that involves mitochondrial Ca^{2+}-dependent generation of reactive oxygen species, which triggers F-actin accumulation for membrane repair (Horn et al., 2017).

Neurodegenerative Disorders: Ca^{2+} signaling regulates neuronal functions through fine-tuned spatiotemporal patterns of intraneuronal Ca^{2+} transients. Deregulated shaping of neuronal Ca^{2+} signals could lead to severe neurodegenerative disorders (Brini et al., 2014). The precise role of mitochondrial Ca^{2+} signaling in this process is only starting to be realized. Ever since the molecular discovery of MCU, the uniporter has been linked to several neurodegenerative conditions, emphasizing the important role of MCU in neuronal metabolism. Ca^{2+} transients signal a wide variety of cellular responses depending on factors, including type of neuron, size of neuron, transmitter system, location in the neural circuits, and source and sink of Ca^{2+} signal (Mammucari et al., 2018). Even at rest, the brain utilizes 20% of the total O_2 consumed by the body; this gets rapidly upregulated to raise ATP production during increased activity. The rise in ATP production is mediated by a Ca^{2+}-dependent increase in mitochondrial OXPHOS (Mink et al., 1981, Rangaraju et al., 2014). A siRNA library screen identified MCU and MICU1 as critical factors responsible for memory formation during development in *Drosophila* (Walkinshaw et al., 2015). Decreased mitochondrial Ca^{2+} signaling mediated by a dominant negative form of MCU led to dysfunction in size and synaptic content in

mushroom body neurons, whereas silencing of a MICU1 homolog impaired climbing activity in *Drosophila* (Drago et al., 2016, M'Angale et al., 2017).

In contrast, mitochondrial Ca^{2+} overload has been associated with amyloid-β Aβ plaque deposition and neuronal death in a mouse model of Alzheimer's disease. Secreted soluble Aβ applied onto healthy mouse brain resulted in increased mitochondrial [Ca^{2+}], which was rescued by inhibiting MCU activity (Calvo-Rodriguez et al., 2020). Neurons from Alzheimer's patient brains showed downregulation of mitochondrial Ca^{2+} uptake pathway genes and upregulation of Ca^{2+} efflux pathway genes, suggesting a possible compensatory mechanism to prevent mitochondrial Ca^{2+} overload (Calvo-Rodriguez et al., 2020). Impaired mitochondrial Ca^{2+} homeostasis has also been linked to Parkinson's disease, another major neurodegenerative disorder (Pchitskaya et al., 2018). In dopaminergic neurons isolated from genetic models of Parkinson's disease and other neurodegenerative disorders, mitochondrial Ca^{2+} was elevated, leading to mitochondrial enlargement and neuronal death (Lee et al., 2018). Furthermore, inhibition of MCU-mediated mitochondrial Ca^{2+} uptake restored mitochondrial integrity and function in zebrafish models of Parkinson's disease (Soman et al., 2019).

Cardiolipin

The major phospholipid that is the focus of this thesis is cardiolipin (CL), which is a unique dimeric phospholipid that is present almost exclusively in the mitochondrial membranes of a eukaryotic cell. CL biosynthesis is highly conserved from yeast to humans and occurs exclusively in the mitochondrial membranes (Gaspard and McMaster, 2015) (Figure 1.4 and Table 1.1).

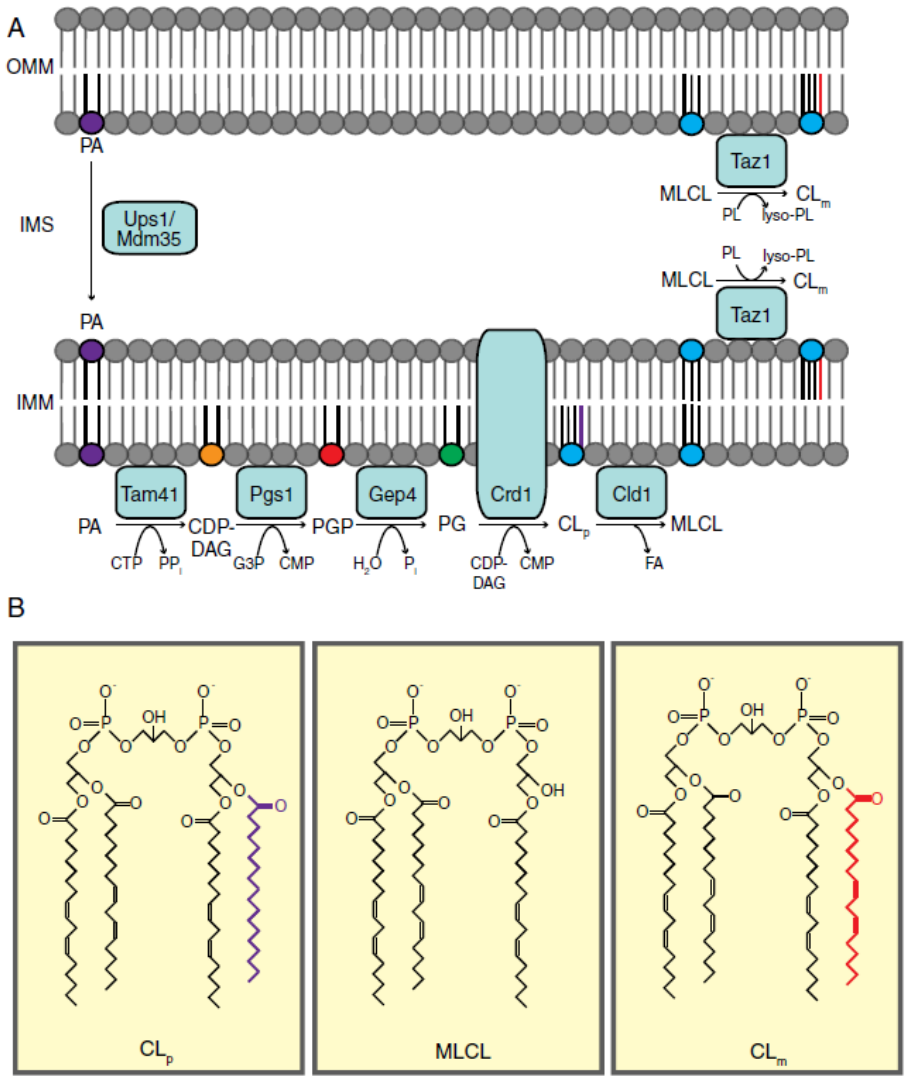

Figure 1.4 Cardiolipin biosynthetic pathway in yeast

(A) CL biosynthesis occurs exclusively in the mitochondria. CL precursor, PA, is transported from the OMM to the IMM via Ups1/Mdm35 to initiate the CL biosynthetic pathway. PA is converted to PG through three subsequent enzyme-catalyzed reactions by Tam41, Pgs1, and Gep4. Crd1 biosynthesizes nascent CL (CL_p) from PG. CL_p must then be remodeled to form mature CL (CL_m) through sequential deacylation and reacylation reactions catalyzed by Cld1 and Taz1, respectively. Taz1 is localized to the OMM and the IMM facing the IMS. (B) Structures of CL_p, MLCL, and CL_m. ATP, adenosine triphosphate; ADP, adenosine diphosphate; CTP, cytidine triphosphate; PPi, pyrophosphate; CDP-DAG, cytidine diphosphate-diacylglycerol; CMP, cytidine monophosphate; PA, phosphatidic acid; CL_p, premature cardiolipin; CL_m, mature cardiolipin; MLCL, monolysocardiolipin; PG, phosphatidylglycerol; PGP, phosphatidylglycerol phosphate; G3P, glycerol-3-phosphate; PL, phospholipid; FA, fatty acid; OMM, outer mitochondrial membrane; IMM, inner mitochondrial membrane; IMS, intermembrane space. (Figure reprinted from Ghosh et al., 2019).

CL biosynthesis requires phosphatidic acid (PA), which is transported from the outer mitochondrial membrane (OMM) to the IMM via the Ups1/Mdm35 lipid transport protein complex in yeast and PRELID1/TRIAP1 in humans (Figure 1.4 and Table 1.1). PA in the IMM is then converted to CDP-diacylglycerol (CDP-DAG) by the cytidylyltransferase Tam41/TAMM41 in yeast and humans, respectively (Blumson et al., 2018). In the committed step, the yeast mitochondrial enzyme Pgs1 and its mammalian counterpart PGS1 convert CDP-DAG into phosphatidylglycerolphosphate (PGP) through transfer of the phosphatidyl group from CDP-DAG onto the glycerol-3-phosphate (Figure 1.4 and Table 1.1). PGP is subsequently dephosphorylated to phosphatidylglycerol (PG) via a reaction catalyzed by the yeast enzyme Gep4 and its human homolog, PTPMT1 (Figure 1.4 and Table 1.1). Nascent CL (CL_p) is then biosynthesized via the condensation of PG and a phosphatidyl group from another CDP-DAG molecule by Crd1 in yeast and CLS1 in humans (Figure 1.4 and Table 1.1).

The acyl chains of newly synthesized CL (CL_p) are remodeled to yield mature CL (CL_m), by a process involving sequential deacylation and reacylation reactions in which the saturated acyl chains are replaced with unsaturated fatty acyl chains (Schlame et al., 2002, Beranek et al., 2009). In yeast, CL_p deacylation and reacylation reactions are catalyzed by the mitochondrial enzymes Cld1 and Taz1, respectively (Figure 1.4). Cld1 initiates the first step in CL remodeling by deacylating nascent CL to form monolysocardiolipin (MLCL) (Beranek et al., 2009). In *Drosophila*, the phospholipase $iPLA_2$ performs the function of Cld1 (Malhotra et al., 2009).

Yeast	Human	Function
Tam41	TAMM41	phosphatidate cytidylyltransferase
Pgs1	PGS1	phosphatidylglycerol synthase
Gep4	PTPMT1	phosphatidylglycerophosphatase
Crd1	CLS1	cardiolipin synthase
Cld1	?	cardiolipin-specific deacylase
Taz1	TAZ	transacylase

Table 1.1 CL biosynthesis and remodeling enzymes in yeast and humans
(Table reprinted from Ghosh et al., 2019)

The human homolog of Cld1 has not yet been identified (Table 1.1). MLCL generated from the deacylation of CL_p is then reacylated by Taz1 (TAFAZZIN or TAZ in human) to form mature CL_m (Figure 1.4 and Table 1.1) (Xu et al., 2006).

Barth syndrome

About four decades ago, physician Peter Barth reported a Dutch family with a history of inherited infantile cardiomyopathy involving abnormal mitochondria (Barth et al., 1983). This rare X-linked genetic disorder later came to be known as Barth syndrome (BTHS) (OMIM 302060). BTHS occurs at a frequency of 1 in 300,000 to 400,000 live births, but evidence is accumulating that this number is highly under-estimated (Clarke et al., 2013). BTHS is primarily characterized by cardiomyopathy, skeletal muscle myopathy, neutropenia, and growth delay in the affected individuals (Clarke et al., 2013). Initial observations indicating that BTHS is a mitochondrial disorder came from the electron microscopic examinations of patient tissues, which showed the presence of

abnormal mitochondria with aberrant cristae morphology and reduced respiratory chain function (Barth et al., 1983). The disease-causing mutation was subsequently mapped to the *TAZ* gene on chromosome X (Bione et al., 1996). Later, biochemical studies led to the identification of TAZ as an evolutionarily conserved phospholipid-lysophospholipid transacylase that remodels the acyl chains of CL (Xu et al., 2006), a signature phospholipid of the mitochondria. CL has a unique dimeric structure consisting of two phosphatidyl-moieties linked by a glycerol backbone (Figure 1.1 and 1.4). In the heart, CL is predominantly present as tetralinoleoyl-CL, however a remodeling defect due to *TAZ* mutations leads to deficiency of tetralinoleoyl-CL in BTHS patients (Schlame et al., 2002). *TAZ*-deficient mitochondria from all investigated BTHS disease models are characterized by an increased level of MLCL along with a decrease in total and remodeled CL levels (Malhotra et al., 2009, Gu et al., 2004, Acehan et al., 2011).

Although a number of causative mutations in *TAZ* have been identified, the large variability in clinical presentations is not fully understood, pointing to a gap in our knowledge about various contributing factors underlying the pathophysiology of BTHS (Clarke et al., 2013). The primary biochemical defect in BTHS is perturbation in the CL biosynthetic process; therefore, determining all CL-dependent mitochondrial functions can provide clues to the underlying causes of the variability in pathophysiology of this disorder.

Molecular Basis of Barth syndrome

The primary defect in BTHS is the accumulation of MLCL and a decrease in remodeled as well as total CL (Xu et al., 2006). Thus, the ensuing mitochondrial

dysfunction could be attributed to any combination of one or more of the above perturbations in CL species. An increased MLCL/CL ratio or a perturbation in content and composition of CL are proposed to be the molecular basis of BTHS. The strongest evidence for the detrimental role of an abnormal MLCL/CL ratio comes from studies on the yeast remodeling mutants *cld1*Δ and *taz1*Δ, where mitochondrial dysfunction associated with the yeast model of BTHS, *taz1*Δ, could be corrected by restoring the MLCL/CL ratio through deletion of *CLD1* (Ye et al., 2014, Baile et al., 2014). In addition, yeast *cld1*Δ cells, which have an MLCL/CL ratio similar to wild type cells but contain an aberrant CL composition, do not have any mitochondrial phenotypes associated with BTHS (Beranek et al., 2009, Ye et al., 2014, Baile et al., 2014). Further evidence in support of the role of the elevated MLCL/CL ratio in BTHS pathology comes from *Drosophila* studies, where deletion of the *Drosophila* equivalent of *CLD1* gene in a fly model of BTHS rescues the male sterility phenotype while partially restoring the MLCL/CL ratio (Malhotra et al., 2009). A human genetic study on BTHS patients with ameliorated clinical phenotypes showed that the severity of clinical presentations correlates with the MLCL/CL ratio (Bowron et al., 2015). In fact, the MLCL/CL ratio has proven to be a robust diagnostic marker for BTHS (Bowron et al., 2015).

Over 100 different pathogenic mutations in *TAZ* have been identified to date (www.barthsyndrome.org). These pathogenic mutations include a wide range of missense, nonsense, and splicing mutations, full or partial deletions, and frame-shifts throughout the entire open reading frame (Johnston et al., 1997, Whited et al., 2013).

The development of a genetically tractable yeast model of BTHS, *taz1*Δ, has greatly facilitated the study of these loss-of-function mutations because human TAZ can complement yeast *taz1*Δ cells (Ma et al., 2004). Claypool and colleagues classified a number of BTHS patient mutations by expressing them in *taz1*Δ cells (Whited et al., 2013). The majority of BTHS-associated mutations give rise to non-functional TAZ proteins. However, it has been difficult to establish a correlation between the type of mutation and the clinical presentations. In fact, Ronvelia et al. showed that a single mutation (genotype) gives rise to different clinical symptoms (phenotypes) (Ronvelia et al., 2012). Similarly, 9 out of 14 BTHS pedigrees showed no correlation between the type of mutation and clinical presentations (Johnston et al., 1997). These observations indicate that there are additional modifying factors that act as key determinants of BTHS pathogenesis. It will be crucial to identify these additional factors or processes that lead to the disease state in order to develop therapeutic strategies.

Mitochondrial dysfunctions in Barth syndrome

BTHS-associated disease phenotypes originate from a disruption in membrane-related functions including mitochondrial bioenergetics and dynamics, owing to defects in the biosynthesis of CL. To gain a better understanding of BTHS pathophysiology and to answer questions regarding the source of variability in the clinical symptoms presented in different patients, it is imperative to catalog the wide range of mitochondrial dysfunctions caused by CL deficiency.

Cardiolipin and mitochondrial ultrastructure: The most direct evidence for the role of mitochondria in BTHS pathology comes from the electron microscopic studies on BTHS patient tissues and various BTHS models. Electron micrographs of heart, liver, and skeletal muscle mitochondria from BTHS patients have shown enlarged mitochondria with stacked and disarrayed cristae (Bissler et al., 2005). Ultrastructural deformities have also been observed in the flight muscle mitochondria of a *Drosophila* model of BTHS, which is characterized by hyperdense cristae (Xu et al., 2006). Similarly, a murine model of BTHS exhibited enlarged mitochondria harboring circularly stacked cristae in cardiac and skeletal muscles (Acehan et al., 2011).

A decrease in CL, as observed in BTHS mitochondria, is expected to perturb mitochondrial cristae structure owing to its non-bilayer promoting propensities (Basu Ball et al., 2018). Although in theory the non-bilayer promoting properties of CL could explain the observed ultrastructure defects in BTHS mitochondria, yeast mitochondria completely devoid of CL have only minor defects in cristae length (Baile et al., 2014). However, it is difficult to directly correlate mitochondrial ultrastructure abnormalities to CL levels because CL deficiency in yeast cells triggers accumulation of PE, another non-bilayer forming phospholipid that may mitigate the ultrastructure phenotype (Basu Ball et al., 2018). Notably, synthetic lethal interaction between CL and mitochondrial PE biosynthetic pathways has been reported, which indicates overlapping roles of these two phospholipids in maintaining mitochondrial integrity (Gohil et al., 2005).

Another possible explanation for the abnormal cristae morphology of BTHS mitochondria is the interaction of CL with the Mitochondrial Contact Site and Cristae

Organizing System (MICOS) complex, which has been implicated in the maintenance of cristae shape and organization (Rampelt et al., 2018, Friedman et al., 2015). A molecular basis for this observation is provided by an *in vitro* study by Rampelt et al., which showed that Mic10, a MICOS subunit, requires CL for its oligomerization, a process essential for mature MICOS complex formation (Rampelt et al., 2018). Thus, deficiency of CL could alter mitochondrial morphology by impairing MICOS function. Together, these observations point to the crucial role of CL in maintaining mitochondrial ultrastructure, which in turn is required for efficient respiratory chain functions (Friedman et al., 2015).

Cardiolipin and mitochondrial dynamics: Mitochondria exist as a network, which is maintained by two opposing processes: fusion and fission. Fusion involves the merging of two mitochondria, whereas fission involves division of mitochondria. Both of these processes are mediated by evolutionarily conserved dynamin-related GTPases, including OPA1 for fusion (Ban et al., 2017) and DRP1 for fission (Francy et al., 2017). OPA1 is critical for fusion of the IMM, which is enriched in CL. A recent *in vitro* study showed that membrane fusion of OPA1-containing liposomes is dependent on the presence and abundance of CL (Ban et al., 2017). Interestingly, it was found that the presence of OPA1 in one liposome and a critical amount of CL in the other was sufficient to induce membrane fusion, indicating the novel finding that CL alone is capable of priming membranes for fusion (Ban et al., 2017). Importantly, the authors went on to show that the longer length and higher degree of unsaturation of CL acyl chains facilitated the fusion process, thus implicating a crucial role for CL remodeling

by TAZ in the mitochondrial fusion process. Mgm1, a yeast homolog of OPA1, has also been shown to require CL for its dimerization and activation of GTPase activity for membrane fusion (DeVay et al., 2009). Thus, CL has an evolutionarily conserved role in mitochondrial fusion.

In yeast, mitochondrial fission is mediated by Drp1, which requires CL for its recruitment onto the mitochondrial membranes and activation of its GTPase activity through lipid-protein interactions (Stepanyants et al., 2015). Drp1 is recruited to a CL dense region of the OMM where CL molecules organize around the protein. This organization induces phase transition of the membrane from a bilayer arrangement to an inverted hexagonal non-bilayer configuration, resulting in localized OMM constrictions that lead to fission (Stepanyants et al., 2015). A balance between fusion and fission is required to maintain mitochondrial homeostasis. Thus, an important role of CL in both of these processes suggests defects in mitochondrial dynamics are potential contributors to BTHS pathology.

Cardiolipin and mitochondrial respiratory chain biogenesis: The mitochondrial respiratory chain (MRC) consists of four multimeric protein complexes (complex I-IV) that are integral to the IMM. The MRC couples respiration to the generation of a proton gradient, which is harnessed by ATP synthase to produce mitochondrial ATP. The MRC complexes assemble into supramolecular structures, known as supercomplexes, which increase their stability as well as efficiency. In yeast, MRC complexes III and IV associate in different stoichiometries, forming large (III_2/IV_2) and small (III_2/IV) supercomplexes (Schagger et al., 2000). In mammals,

different combinations of individual MRC complexes can produce different supercomplexes, of which the cryo-EM structures of $I/III_2/IV$ and I/III_2 have been determined (Wu et al., 2016). Blue native gel electrophoresis on mitochondria isolated from CL-deficient yeast cells demonstrated a critical requirement of CL for the stability of supercomplexes (Pfeiffer et al., 2003). Consistent with this role, supercomplex levels are decreased in the yeast model of BTHS and patient lymphoblasts (Brandner et al., 2005, McKenzie et al., 2006).

Recent cryo-EM based structural studies have provided clues to the potential role of CL in supercomplex formation. CL, along with two abundant mitochondrial phospholipids PE and PC, have been found in purified yeast and mammalian supercomplexes (Wu et al., 2016, Mileykovskaya et al., 2012). It has been proposed that these phospholipid molecules might occupy the space between the individual complexes to stabilize the supercomplex (Wu et al., 2016). Phospholipid quantification of the purified yeast III_2/IV_2 supercomplex revealed the presence of ~50 molecules of CL (Mileykovskaya et al., 2012). Direct evidence for the role of CL in maintaining the stability of yeast supercomplexes came from a study by Wenz et al., which showed that mutation of a specific CL binding site in a yeast complex III subunit results in a loss of III_2/IV_2 supercomplex formation (Wenz et al., 2009). The elimination of CL binding to complex III results in a weakened interaction with complex IV and the subsequent destabilization of the supercomplex. The authors suggest that this phenomenon arises primarily due to the charge sensitivity of supercomplex formation, because simultaneously mutating the adjacent positively charged CL-binding residues restores

supercomplex assembly by neutralizing the loss of two negative charges contributed by CL (Wenz et al., 2009). The *in vitro* reconstitution of yeast complexes III and IV into proteoliposomes exhibited an absolute requirement of CL for the formation of stable III_2/IV and III_2/IV_2 supercomplexes (Bazan et al., 2013). The presence of PE and PC alone in the proteoliposome was not sufficient for supercomplex formation, while the addition of CL alone restored the same (Bazan et al., 2013). Recent *in vivo* studies in yeast have suggested that supercomplex formation is a function of the overall abundance of complex III and IV subunits (Cui et al., 2014). Thus, it is possible that the decreased abundance of supercomplexes in CL-deficient cells is due to a reduced expression or enhanced turnover of individual MRC subunits. Notably, decreased translation of MRC complex IV subunit in CL-deficient yeast cells has been reported (Su et al., 2006) and forced overexpression of the same subunit restored supercomplex formation (Cui et al., 2014, Basu Ball et al., 2018). Moreover, pharmacological stimulation of mitochondrial biogenesis also led to enhanced supercomplex formation in BTHS lymphoblasts (Xu et al., 2016).

A number of studies performed on mammalian systems have demonstrated a CL requirement for maintaining the steady-state levels of individual MRC complexes. For example, complex I and IV levels were found to be lowered in BTHS patient lymphoblasts (McKenzie et al., 2006) and the abundance and activity of complex II is reduced in BTHS murine cardiomyocytes (Dudek et al., 2016). Finally, a reduction in complex III activity was also reported in the mouse model of BTHS (Dudek et al., 2016,

Kiebish et al., 2013). Thus, CL deficiency results in a general disintegration of MRC structure and function.

Cardiolipin and mitochondrial bioenergetics: CL has been shown to be essential for the efficient coupling of respiration to ATP synthesis, classically defined as the P/O ratio (amount of ATP formed per molecule of oxygen consumed). A complete loss of CL in yeast *crd1*Δ mitochondria led to reduced energetic coupling during fast respiration driven by NADH as the substrate (Koshkin et al., 2002). The same group later went on to show that a similar respiratory coupling defect was also present in CL-deficient *taz1*Δ cells (Ma et al., 2004). While oxidative phosphorylation was not severely impacted under optimal conditions, CL was required for efficient energy transformation under osmotic and temperature stress (Koshkin et al., 2002). In addition to the coupling defect, a reduction in the activity of complex V (ATP synthase) was observed in a BTHS mouse model (Kiebish et al., 2013). In yeast, the assembly and activity of the mitochondrial ATP/ADP carrier, AAC2, which mediates transport of ATP from the matrix to the intermembrane space in exchange for ADP, was shown to be highly dependent on CL (Jiang et al., 2000). A subsequent study showed that yeast AAC2 also interacts with supercomplexes and that this interaction is impaired in yeast mitochondria lacking CL (Claypool et al., 2008). Thus, impaired function of AAC2 might act synergistically with the disruption of MRC activity to compromise mitochondrial energy generation.

Mitochondria undergo swelling and shrinking during respiration. Yeast mitochondria lacking CL exhibits increased swelling as compared to wild type

mitochondria when placed in a hypotonic solution, suggesting a possible role of CL in maintaining mitochondrial osmotic stability (Ma et al., 2004, Koshkin et al., 2002). Interestingly, CL-deficient mitochondria also lose their ability to shrink back to their original size when returned to an isotonic medium, suggesting that CL deficient mitochondrial membranes lose their elasticity. Deterioration of CL-dependent biophysical properties of the IMM also likely contributes to membrane "leakiness", leading to decreased membrane potential and overall efficiency of mitochondrial energy generation. Thus, CL deficiency impairs mitochondrial bioenergetics, which perturbs the function of high energy demanding tissues specifically affected in BTHS, such as the heart and skeletal muscles. Recent advances in tools and technologies to simultaneously assess different mitochondrial bioenergetic functions, such as the extracellular flux analyzer (Agilent Technologies) and high-resolution respirometry (Oroboros Instruments), may facilitate higher resolution mapping of CL-dependent mitochondrial bioenergetic functions.

Barth syndrome disease models

Pioneering studies in a simple eukaryotic yeast model of BTHS have uncovered many key mitochondrial defects, as described in previous sections. However, yeast cells do not exhibit the complexity of mammalian cells and cannot be used to study tissue and organ specific defects observed in BTHS patients. Over the last decade, multiple invertebrate and vertebrate models of BTHS, including the fly, fish, and mouse, have been developed (Table 1.2). All these model systems display the characteristic biochemical defects underlying BTHS, including reduced levels of mitochondrial CL,

increased MLCL, and altered acyl chain composition of CL. The availability of these model organisms, which faithfully recapitulate many of the biochemical defects observed in BTHS patients (Table 1.2), have proved critical in developing our understanding of BTHS pathology and they could also serve as useful tools in developing therapeutics for BTHS.

Cellular and organoid models of BTHS: Many mammalian cellular models are available for BTHS including patient-derived lymphoblasts (McKenzie et al., 2006), fibroblasts (Barth et al., 1996), and induced-Pluripotent Stem Cells (iPSCs) (Dudek et al., 2013, Wang et al. 2014). Recently, a CRISPR-mediated stable *Taz-KO* mouse C2C12 myoblast cell line has also been generated (Lou et al., 2018). Abnormal mitochondrial morphology is observed in patient-derived fibroblasts (Barth et al., 1996) and BTHS iPSC cardiomyocytes (Wang et al., 2014).

Model Organism	Mitochondrial Defects
Yeast *(Saccharomyces cerevisiae)*	• Reduced stability of MRC supercomplexes • Increased oxidative stress • Reduced mitophagy • Partial uncoupling • Reduced osmotic stability
Fly (*Drosophila melanogaster*)	• Abnormal mitochondrial morphology in flight muscles • Swelling and disruption of cristae membrane • Reduced ATP synthase dimer rows in cristae membrane
Mouse (*Mus musculus*)	• Abnormal mitochondrial morphology • Reduced cristae density • Disruption of the parallel alignment between mitochondria and sarcomeres • Reduced MRC supercomplex levels in cardiac mitochondria • Reduced MRC complex II levels and activity in cardiac mitochondria

Table 1.2 BTHS associated mitochondrial dysfunctions in BTHS disease models
(Table reprinted from Ghosh et al., 2019)

A hallmark of mitochondrial CL deficiency is the loss of MRC supercomplexes. Consistent with this role of CL, studies with patient-derived BTHS lymphoblasts and BTHS iPSCs from dermal fibroblasts showed reduced stability of MRC supercomplexes containing complex I, III, and IV (McKenzie et al., 2006, Dudek et al., 2013). Another common feature observed in multiple cellular models of BTHS is increased oxidative stress (Dudek et al., 2013). *Taz-KO* in mouse C2C12 myoblasts displayed mitochondrial defects consistent with other models of BTHS and was associated with impairment of myocyte differentiation to myotubes, which may explain the skeletal myopathy observed in BTHS patients (Lou et al., 2018).

Advances in the study of cardiac disorders are restricted by the lack of available organoid models. The invasive nature of the methods used to obtain cardiac tissue is a major obstacle for research in this area. However, Wang et al. developed a heart-on-chip model of BTHS (Wang et al., 2014). In this model, the BTHS iPSC tissues developed a significantly lower twitch and peak systolic stress, suggesting reduced contractile functions compared to the control tissue, indicating that engineered myocardial tissue recapitulates the BTHS myopathic phenotype. Analysis of mitochondrial function in this model is required to assess the role of mitochondrial bioenergetics on various physiological phenotypes reported.

***Drosophila* model of BTHS**: *Drosophila* is a useful model system for BTHS because it has specialized flight muscles with abundant mitochondria and, like humans, it expresses several *TAZ* transcripts (Xu et al., 2006). The *Drosophila* model of BTHS was constructed by the imprecise excision of a P element inserted upstream of the coding region of the *TAZ* gene, which caused similar changes in CL species profile as seen in Barth syndrome patients (Xu et al., 2006). BTHS flies showed reduced locomotor activity, and their flight muscles displayed frequent mitochondrial abnormalities, mostly in the cristae membranes (Xu et al., 2006). In a subsequent study, the same group found that TAZ deficiency in *Drosophila* disrupts the final stage of spermatogenesis-spermatid individualization, causing male sterility (Malhotra et al., 2009). Interestingly, it was found that male sterility in TAZ-deficient flies can be genetically suppressed by the inactivation of a calcium-independent phospholipase,

iPLA$_2$-VIA, which prevents MLCL accumulation, restoring the MLCL/CL ratio (Malhotra et al., 2009).

Zebrafish model of BTHS: Zebrafish embryos offer a powerful model for studying pediatric disorders and are particularly suitable for studying infantile hypertrophic cardiomyopathy because: 1) they are transparent and develop outside of the mother, enabling observation of organ development; 2) they do not require a functional cardiovascular system for the first 4-5 days post-fertilization, as their small size allows sufficient passive oxygen diffusion; and 3) compared to mouse models, zebrafish are inexpensive and knockdowns and knockouts can be easily generated and titrated. The zebrafish BTHS model was generated by antisense morpholino-based knockdown of Taz protein (Khuchua et al., 2006). *taz-KD* zebrafish embryos exhibit severe bradycardia, pericardial effusions, and generalized edema that resembles cardiac failure in BTHS patients. In this study, mitochondrial bioenergetic functions were not measured; therefore, it is difficult to assign cardiac defects to mitochondrial dysfunction. However, mitochondrial dysfunction in zebrafish does give rise to a similar cardiac phenotype as described in BTHS zebrafish (Khuchua et al., 2006); therefore, it is likely that the cardiac defects are caused by a disruption in CL-dependent mitochondrial functions. In the future, a stable CRISPR based *taz-KO* model of zebrafish could prove valuable in understanding the developmental defects observed in BTHS.

Mouse model of BTHS: A doxycycline-induced shRNA-mediated *Taz-KD* mouse recapitulates many of the disease phenotypes of BTHS, including cardiomyopathy and skeletal muscle myopathy (Acehan et al., 2011, Dudek et al., 2016,

Soustek et al., 2011, Phoon et al., 2012). These studies were performed on the same mouse model, but they differed in the dosage, timing, and mode of doxycycline administration. Two independent studies by Acehan et al. (Acehan et al., 2011) and Soustek et al. (Soustek et al., 2011) reported initial characterization of inducible shRNA *Taz-KD* mice. Mice were administered doxycycline in their diets pre- and post-natally. Remarkably, these mice did not exhibit an overt phenotype until much later in life. Soustek et al. reported skeletal muscle defects in 2-month old *Taz-KD* mice, but cardiac defects were apparent only after 7-10 months of age. Similarly, Acehan et al. also observed mitochondrial defects in skeletal muscle at 2 months of age, and cardiac mitochondrial defects became evident at 8 months. Both of these studies reported defects in cardiac function, including left ventricular dilation, left ventricular mass reduction, and ejection fraction in *Taz-KD* mice. In a study by Phoon et al., (Phoon et al., 2012) pregnant dams were treated with doxycycline early in gestation leading to the knockdown of *Taz* in the embryonic stage. These mice exhibited increased pre- and post-natal death, suggesting that the mode of delivery of doxycycline has a major impact on the severity of phenotype, because unlike previous studies, where doxycycline was administered in chow, in this study doxycycline was administered in water (Phoon et al., 2012). Electron microscopy of cardiac tissue from these mice demonstrated ultrastructural abnormalities in mitochondria at both embryonic and newborn stages. Early diastolic dysfunction was evident from echocardiography studies. Histological examination of embryonic day 13.5 and newborn *Taz-KD* mice showed myocardial thinning, hypertrabeculation and noncompaction, and defective ventricular septation

(Phoon et al., 2012). A more recent report by Dudek et al. identified reduced MRC supercomplexes at a pre-onset stage of the disease in the *Taz-KD* mice. Moreover, their analyses demonstrated a cardiac-specific loss of succinate dehydrogenase (MRC complex II) in mouse and patient cell-derived cardiomyocytes (Dudek et al., 2016). Notably, these MRC defects were not observed in mitochondria isolated from kidneys and livers of age-matched *Taz-KD* mice, suggesting that MRC complex II dysfunction is an important contributor to BTHS-associated cardiomyopathy (Dudek et al., 2016).

Recently, *Taz-KO* mice have also been generated, which display reproductive defects in males; the testes from the *Taz-KO* mice were smaller than their control counterparts, and this was associated with a disruption of spermatogenesis by meiosis (Cadalbert et al., 2015). Spermatocytes in the mutant animals failed to progress past the pachytene stage of meiosis, had higher levels of DNA double strand damage, and mutant males were infertile, a phenotype similar to the *Drosophila* model of BTHS (Xu et al., 2006). Together, these data reveal an evolutionarily conserved role of *Taz* in male fertility. The results from various BTHS models indicate that CL-dependent mitochondrial functions are critical for heart and muscle development and function. The usefulness of the mouse models of BTHS lies in the fact that in *Taz*-depleted mice, the cardiac defects observed reproduce many of the relevant cardiac parameters noted in BTHS patients, providing an excellent opportunity to test potential therapeutic targets in a mammalian model system.

Yeast as a model system to study the phospholipid requirements of MCU

Since phospholipid biosynthetic pathways are essential in mammals, it has been difficult to definitively dissect their precise role in MRC function. The yeast, *Saccharomyces cerevisiae*, serves as a powerful surrogate system to identify the phospholipid requirements of integral IMM proteins such as MCU in a physiologically relevant mitochondrial membrane milieu because: 1) the mitochondrial phospholipid composition is highly conserved from yeast to humans (Basu Ball et al., 2018), 2) the mitochondrial phospholipid composition can be genetically and nutritionally manipulated in yeast without loss of viability and gross ultrastructural changes to the mitochondria (Baker et al., 2016), and 3) *S. cerevisiae* does not contain the uniporter machinery (Bick et al., 2012), providing a "clean" system to study the effect of phospholipids on heterologously expressed MCU. These attributes of the yeast surrogate system can be exploited to dissect specific lipid requirements of other IMM ion channels, though in this thesis the focus has been uniporter components, MCU and MICU1, as described in chapters II and III of this thesis.

CHAPTER II

AN ESSENTIAL ROLE FOR CARDIOLIPIN IN THE STABILITY AND FUNCTION OF THE MITOCHONDRIAL CALCIUM UNIPORTER*

Summary

Calcium uptake by the mitochondrial calcium uniporter coordinates cytosolic signaling events with mitochondrial bioenergetics. During the past decade all protein components of the mitochondrial calcium uniporter have been identified, including MCU, the pore-forming subunit. However, the specific lipid requirements, if any, for the function and formation of this channel complex are currently not known. Here we utilize yeast, which lacks the mitochondrial calcium uniporter, as a model system to address this problem.

* Reprinted with permission from "An essential role for cardiolipin in the stability and function of the mitochondrial calcium uniporter" by Ghosh S, Basu Ball W, Madaris TR, Srikantan S, Madesh M, Mootha VK, Gohil VM. 2020. *Proc Natl Acad Sci U S A*. 117 (28) 16383-16390. Copyright (2020) by National Academy of Sciences.

We use heterologous expression to functionally reconstitute human uniporter machinery both in wild type yeast as well as in mutants defective in the biosynthesis of phosphatidylethanolamine, phosphatidylcholine, or cardiolipin (CL). We uncover a specific requirement of CL for *in vivo* reconstituted MCU stability and activity. The CL requirement of MCU is evolutionarily conserved with loss of CL triggering rapid turnover of MCU homologs and impaired calcium transport. Furthermore, we observe reduced abundance and activity of endogenous MCU in mammalian cellular models of Barth syndrome, which is characterized by a partial loss of CL. MCU abundance is also decreased in the cardiac tissue of Barth syndrome patients. Our work raises the hypothesis that impaired mitochondrial calcium transport contributes to the pathogenesis of Barth syndrome, and more generally, showcases the utility of yeast phospholipid mutants in dissecting the phospholipid requirements of ion channel complexes.

Significance

The assembly and function of membrane proteins depend on the lipid milieu. In recent years, the protein components of the mitochondrial calcium uniporter have been identified, but its specific phospholipid requirements are not known. Utilizing yeast mutants defective in their ability to synthesize different phospholipids, we identify a specific requirement of cardiolipin (CL) in the stability and function of the mitochondrial uniporter. Our findings are translatable to higher organisms because endogenous uniporter abundance is decreased in patient-derived cells and cardiac tissue from Barth syndrome, an inherited deficiency in CL levels. This work shows that yeast phospholipid mutants can be leveraged to uncover specific lipid requirements of membrane proteins and suggests impaired mitochondrial calcium signaling in the pathogenesis of Barth syndrome.

Introduction

The mitochondrial calcium uniporter is a highly selective calcium (Ca^{2+}) channel complex present in the inner mitochondrial membrane (IMM) and is distributed widely across eukaryotic life with lineage specific losses (Baughman et al., 2011, De Stefani et al., 2011, Bick et al., 2012). In response to physiological cues, the uniporter enables mitochondria to take up large amounts of Ca^{2+} from the cytoplasm, which contributes to the clearance of cytosolic Ca^{2+} transients and activates mitochondrial matrix dehydrogenases (Clapham 2007, Kamer and Mootha 2015). Although the physiological processes associated with mitochondrial Ca^{2+} uptake has been known for over six decades, the molecular identity of the uniporter has only been revealed in the past decade. The uniporter holocomplex is composed of the pore-forming subunit, MCU and small transmembrane subunit, EMRE, which are necessary and sufficient for Ca^{2+} transport, as well as the regulatory subunits MICU1, MICU2, and MCUb (Sancak et al., 2013, Perocchi et al., 2010, Plovanich et al., 2013, Raffaello et al., 2013).

Localization of the uniporter holocomplex in the IMM predicts that its function is likely influenced by the phospholipid milieu. Previous studies have shown that the function and assembly of a number of IMM protein complexes, including the mitochondrial respiratory chain supercomplexes and the ADP/ATP translocase requires cardiolipin (CL), the signature phospholipid of mitochondria (Zhang et al., 2002, Pfeiffer et al., 2003, Claypool et al., 2008). More recent studies have identified the critical requirements of phosphatidylethanolamine (PE) for the catalytic activities of the respiratory complexes and phosphatidylcholine (PC) for the stabilization of the IMM

protein translocase Tim23 (Baker et al., 2016, Tasseva et al., 2013, Schuler et al., 2016). The structural evidence for the role of phospholipids in MCU function comes from a recent cryo-electron microscopy (EM) study that identified four lipid molecules on the membrane exposed surfaces of MCU, the pore-forming subunit (Baradaran et al., 2018). However, the molecular identities and the roles of these lipids in MCU function were not determined.

Deciphering the phospholipid requirements of the uniporter is challenging in part because we currently lack a robust *in vitro* biochemical reconstitution system in which to investigate the channel complex. Here, we have utilized yeast, *Saccharomyces cerevisiae*, as a facile, *in vivo* genetic system to address this problem. Our choice of yeast was guided by the following three considerations. First, the phospholipid composition of the IMM is highly conserved from yeast to mammals, with PC, PE, and CL being the three most abundant phospholipids (Basu Ball et al., 2018). Second, the phospholipid composition of the IMM can be genetically and nutritionally manipulated in yeast without disrupting the gross structure of mitochondria (Baker et al. 2016). Third, *S. cerevisiae* do not contain any homologs of uniporter machinery (Bick et al., 2012), and previous studies have shown that it is possible to functionally reconstitute uniporter activity in yeast through heterologous expression of the uniporter machinery (Kovács-Bogdán et al., 2014). Thus, yeast represents a suitable *in vivo* reconstitution system for dissecting the phospholipid requirements of the non-native uniporter in a physiologically relevant mitochondrial membrane milieu (Kovács-Bogdán et al., 2014, Yamamoto et al., 2016). In this study, we engineered isogenic yeast mutants with defined perturbations in

the levels of PC, PE, and CL to uncover a CL-specific requirement for MCU stability and function. We validated the evolutionarily conserved requirement of CL for MCU in a mouse muscle cell line and in CL-depleted cardiac tissue of Barth syndrome (BTHS) patients.

Results

A yeast system to determine specific phospholipid requirements of MCU

To test the specific phospholipid requirement of MCU, we utilized isogenic yeast mutants of CL, PE, and PC biosynthetic pathways with deletions in *CRD1*, *PSD1*, and *PEM2*, respectively (Figure 2.1A).

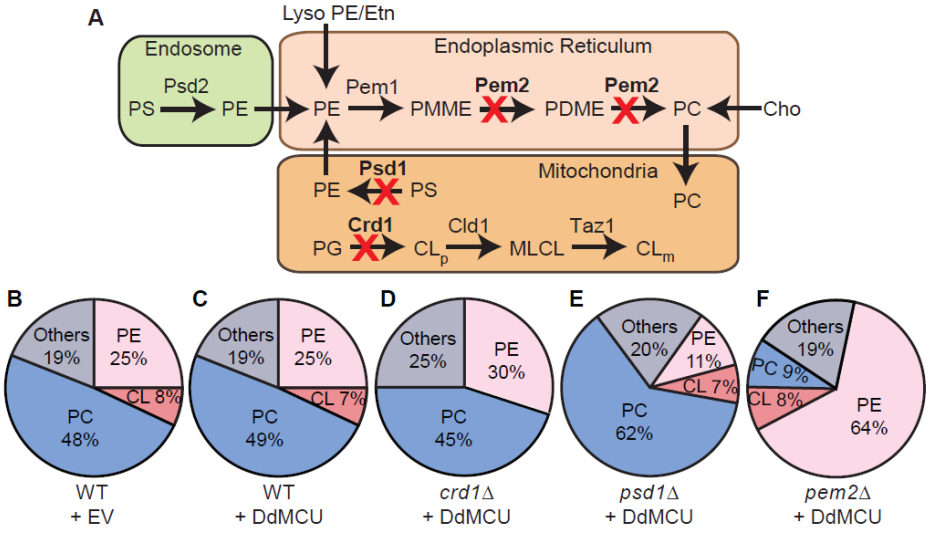

Figure 2.1 Yeast mutants with defined perturbations in mitochondrial phospholipid composition

(A) A schematic of yeast biosynthetic pathways of the most abundant mitochondrial phospholipids CL, PE, and PC. The enzymes for CL, PE, and PC biosynthesis that are deleted for phospholipid perturbation are highlighted in bold. PS, phosphatidylserine; PE, phosphatidylethanolamine; lysoPE, lysophosphatidylethanolamine; Etn, ethanolamine; Cho, choline; PMME, phosphatidylmonomethylethanolamine; PDME, phosphatidyldimethylethanolamine; PC, phosphatidylcholine; CL, cardiolipin; PG, phosphatidylglycerol; MLCL; monolysocardiolipin; CL_p, premature CL; CL_m, mature CL. (B-F) Pie-charts depicting levels of major mitochondrial phospholipids, including CL, PE, and PC are

expressed as % of total phospholipid phosphorus in mitochondria isolated from WT cells expressing EV (empty vector) (B), and WT cells (C), *crd1Δ* cells (D), *psd1Δ* cells (E), and *pem2Δ* cells (F) expressing DdMCU, respectively. Data shown as mean from three independent experiments. WT, wild type. (Figure reprinted from Ghosh et al., 2020).

We focused on these three abundant mitochondrial phospholipids because together they form ~80–90% of the total mitochondrial phospholipidome (Figure 2.1B) (Basu Ball et al., 2018) and are thus expected to influence membrane protein function. Previous work has shown that heterologous expression of membrane proteins in yeast can itself perturb the phospholipid composition (Chen et al., 2018), which can confound our study. Therefore, we first tested the effect of expressing MCU on the phospholipid composition of wild type (WT) yeast cells. Heterologous expression of *Dictyostelium discoideum* MCU (DdMCU), an MCU homolog that can conduct Ca^{2+} independent of any other protein, did not alter the mitochondrial phospholipid composition (Figure 2.1B and C and Table 2.1).

Phospholipids	WT + EV	WT + DdMCU	*crd1Δ* + DdMCU	*psd1Δ* + DdMCU	*pem2Δ* + DdMCU
Cardiolipin (CL)	7.9 ± 2.2	6.5 ± 1.6	N.D.	6.4 ± 0.9	8.4 ± 2.1
Phosphatidylethanolamine (PE)	24.8 ± 1.4	24.4 ± 0.9	29.1 ± 1.9	11.3 ± 1.4	63.8 ± 4.3#
Phosphatidylcholine (PC)	47.8 ± 4.1	49.1 ± 2.1	45.4 ± 0.9	62.2 ± 1.4	8.9 ± 1.7
Phosphatidylinositol (PI)	10.3 ± 0.7	12.1 ± 2.3	13.5 ± 1.2	11.4 ± 0.5	13.1 ± 2.2
Phosphatidylserine (PS)	5.1 ± 0.7	3.8 ± 0.5	4.2 ± 1.1	5.8 ± 2.2	3.3 ± 0.3
Phosphatidic acid (PA)	2.4 ± 0.9	2.5 ± 1.1	2.4 ± 0.4	2.9 ± 1.9	2.4 ± 2.1
Phosphatidylglycerol (PG)	N.D.	N.D.	5.3 ± 2	N.D.	N.D.

Table 2.1 Yeast mutants with defined perturbations in mitochondrial phospholipids.
Levels of all major mitochondrial phospholipids are expressed as % of total phospholipid phosphorus in the indicated yeast mutants expressing either empty vector (EV) or DdMCU. Data shown as mean ± SD, n=3. #represents sum of PE and PMME that are not resolved by the 2D-TLC method used in this study. The three major phospholipids targeted in this study are

highlighted in different colored boxes. WT, wild type; N.D., Not detected; PMME, phosphatidyl-monomethylethanolamine. (Table reprinted from Ghosh et al., 2020).

We then expressed DdMCU in *crd1*Δ, *psd1*Δ, and *pem2*Δ cells that are characterized by a complete absence of CL, ~2.5-fold decrease in PE, and a ~5-fold decrease in PC, respectively (Figure 2.1D–F and Table 2.1). These mutants are viable and exhibit normal growth in galactose-containing media, which allowed us to dissect the specific requirement of phospholipids for MCU function.

MCU stability and abundance are reduced in CL-deficient mitochondria

We next sought to determine how perturbations in these phospholipids impact the steady-state levels of DdMCU. Consistent with a previous report (Kovács-Bogdán et al., 2014), we found that DdMCU is expressed as a mature ~32 kDa protein in yeast mitochondria (Figure 2.2A).

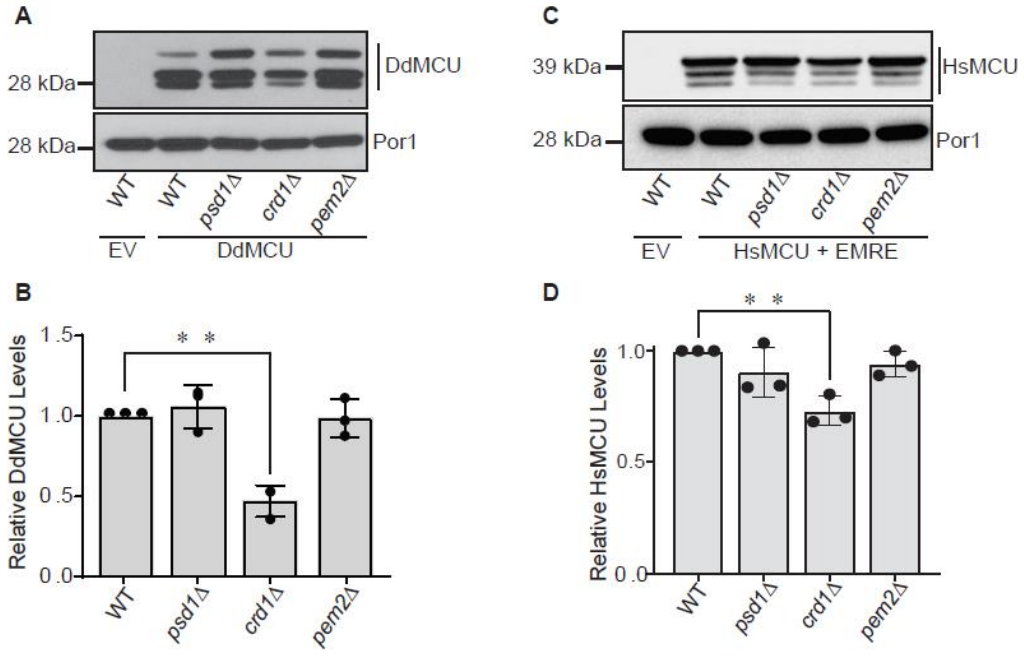

Figure 2.2 MCU abundance is reduced in CL-deficient yeast

A) SDS-PAGE immunoblot analysis of FLAG-tagged DdMCU in mitochondria isolated from the indicated yeast phospholipid mutants. Por1 was used as a loading control. (B) Quantification of DdMCU protein levels from (A) by densitometry using ImageJ software. (C) SDS-PAGE immunoblot analysis of FLAG-tagged HsMCU co-expressed with EMRE in mitochondria isolated from the indicated yeast phospholipid mutants. Por1 was used as a loading control. (D) Quantification of HsMCU protein levels from (C) by densitometry using ImageJ software. WT, wild type. Data shown as mean ± SD, n=3. $^{**}p < 0.005$. (Figure reprinted from Ghosh et al., 2020).

Notably, DdMCU levels in CL-deficient *crd1*Δ mitochondria were reduced by ~50% (Figure 2.2A and B), an effect not seen in PE- and PC-depleted *psd1*Δ and *pem2*Δ mitochondria, respectively (Figure 2.2A and B). DdMCU monomers form higher-order oligomers when reconstituted in yeast (Kovács-Bogdán et al., 2014). Consistent with the decrease in DdMCU monomers, Blue Native-polyacrylamide gel electrophoresis (BN-PAGE) immunoblot experiments showed a pronounced decrease in the abundance of DdMCU oligomeric complexes in *crd1*Δ mitochondria (Figure 2.3A). In contrast, depletion of PE and PC did not impact the oligomeric assembly of DdMCU in *psd1*Δ and *pem2*Δ cells, respectively (Figure 2.3A).

Next, we asked if CL requirement of MCU was evolutionarily conserved. To address this question, we reconstituted the human MCU (HsMCU) in our yeast phospholipid mutants. A previous study aimed at reconstitution of HsMCU in yeast showed that HsMCU alone is not sufficient for Ca^{2+} uptake and requires co-expression with EMRE- both of which are necessary and sufficient to reconstitute the uniporter activity (Kovács-Bogdán et al., 2014). Therefore, we co-expressed HsMCU and EMRE in the yeast phospholipid mutants and found a specific reduction in monomeric (Figure 2.2C and D) and oligomeric HsMCU (Figure 2.3B) in CL-deficient mitochondria. Notably, the decrease in the oligomeric assemblies of MCU (both DdMCU and HsMCU)

is more pronounced compared to its overall abundance, which suggests a critical role of CL for the assembly of higher-order MCU complexes in the IMM.

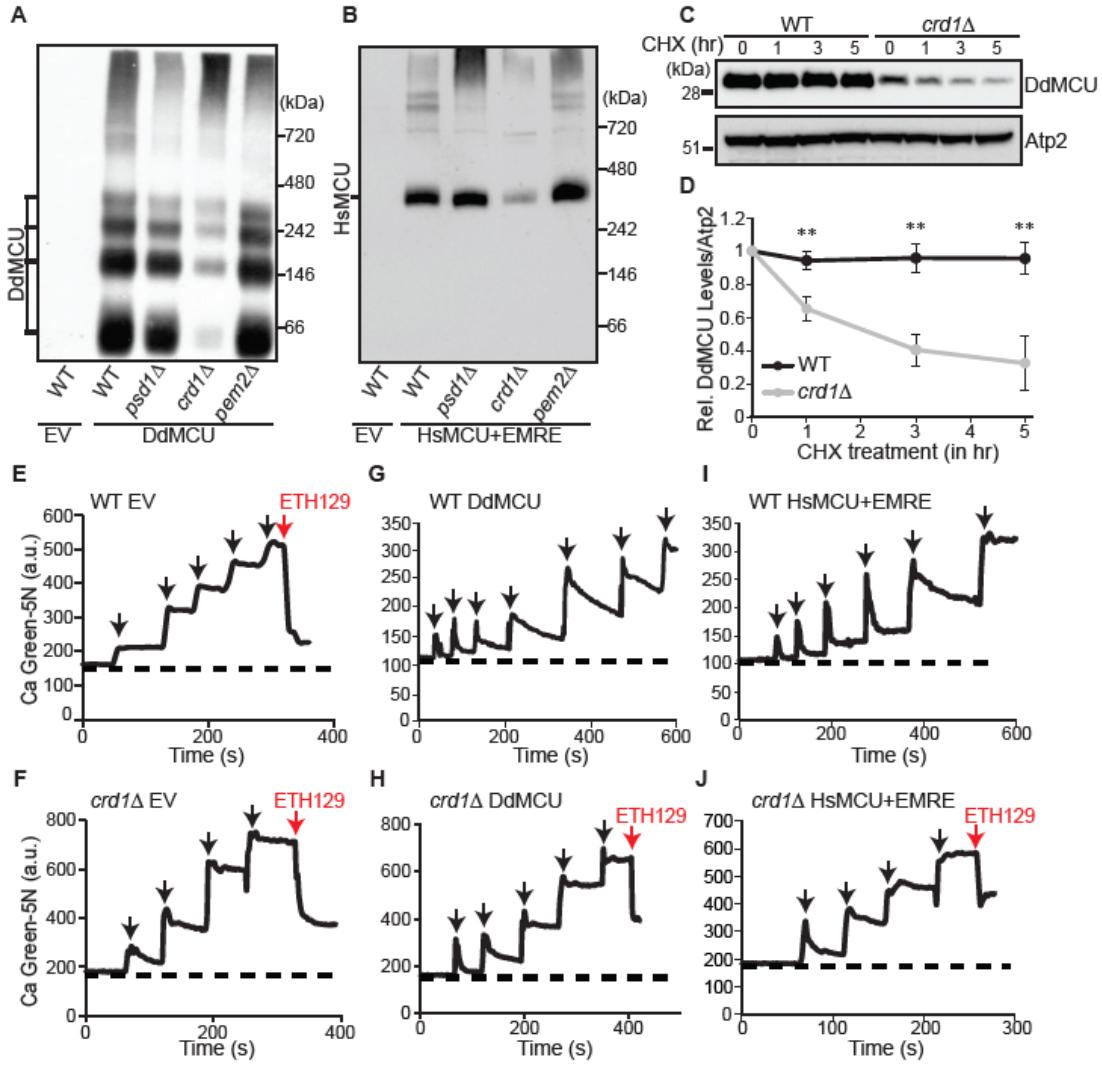

Figure 2.3 MCU stability and activity are reduced in CL-deficient yeast

(A) BN-PAGE immunoblot analysis of FLAG-tagged DdMCU in digitonin-solubilized mitochondria from the indicated yeast phospholipid mutants expressing empty vector (EV) or DdMCU. Blot is representative of three independent experiments. (B) BN-PAGE immunoblot analysis of FLAG-tagged HsMCU in digitonin-solubilized mitochondria from the indicated yeast phospholipid mutants expressing EV or co-expressing HsMCU and EMRE. Blot is representative of three independent experiments. (C) SDS-PAGE immunoblot analysis of FLAG-tagged DdMCU in cell lysates from WT and *crd1Δ* yeast treated with protein translation inhibitor cycloheximide (CHX) for the indicated time-points. Atp2 is used as loading control. (D) Quantification of relative DdMCU levels from (C), normalized to 0 hr of CHX treatment, by

densitometry using ImageJ software. Data shown as mean ± SD, n=3. $^{**}p < 0.005$. (E and F) Representative traces monitoring extra-mitochondrial Ca^{2+} levels by Calcium Green-5N following repeated 10 μM $CaCl_2$ additions (black arrows) to mitochondria isolated from WT (E) and *crd1Δ* cells (F) transformed with empty vector (EV). ETH129 is used as a Ca^{2+} ionophore (red arrow). (G and H) Representative traces monitoring extra-mitochondrial Ca^{2+} levels by Calcium Green-5N following repeated 10 μM $CaCl_2$ additions (black arrows) to mitochondria isolated from DdMCU expressing WT (G) and *crd1Δ* cells (H). ETH129 is used as a Ca^{2+} ionophore (red arrow) in (H). (I and J) Representative traces monitoring extra-mitochondrial Ca^{2+} levels by Calcium Green-5N following repeated 10 μM $CaCl_2$ additions (black arrows) to mitochondria isolated from HsMCU and EMRE expressing WT (I) and *crd1Δ* cells (J). ETH129 is used in (J) (red arrow). All traces are representative of three independent experiments. WT, wild type. (Figure reprinted from Ghosh et al., 2020).

Given that loss of CL decreased the abundance of HsMCU, we asked if increasing CL would lead to an elevation in HsMCU. We manipulated CL levels by growing WT yeast in different carbon sources. Levels of CL tend to be much higher when yeast is grown in galactose or in lactate compared with glucose as the main carbon source. Under these conditions of increased CL levels, we also observed a concomitant increase in the abundance of HsMCU oligomers as assessed by BN-PAGE/immunoblotting (Figure 2.4). Collectively, our genetic "loss-of-function" and carbon source-based "gain-of-function" experiments perturbing CL levels show a consistent and concordant impact on MCU levels.

Reduced biosynthesis or an increased turnover of MCU could explain a decrease in the steady-state levels of MCU in CL-deficient cells. Because we observed decreased MCU protein levels in yeast where DdMCU was expressed under strong non-native promoter, we argued that CL deficiency is unlikely to impact the expression of MCU but may affect its stability in the mitochondrial membrane. Therefore, we used a cycloheximide chase assay to test if MCU protein turnover *in vivo* is dependent on CL levels. DdMCU expressing WT and *crd1*Δ yeast cells were treated with cycloheximide

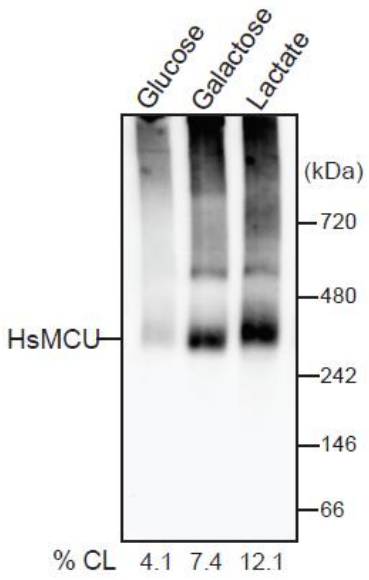

Figure 2.4 MCU abundance increases with increasing levels of cardiolipin
BN-PAGE immunoblot analysis of FLAG-tagged HsMCU in mitochondria isolated from wild type yeast cells grown in synthetic media containing either glucose, galactose, or lactate as the sole carbon source. Levels of cardiolipin are represented as % of total phospholipid phosphorus in mitochondrial lysates obtained from indicated growth media. % CL is average of three independent experiments and blot is representative of three independent experiments. CL, cardiolipin. (Figure reprinted from Ghosh et al., 2020).

to inhibit nascent protein translation from cytosolic ribosomes, and samples were collected over time to measure the turnover rate of DdMCU. We observed rapid turnover of DdMCU in CL-deficient *crd1*Δ cells compared to WT cells, where DdMCU was stable even after 5 h of cycloheximide treatment (Figure 2.3C and D). Thus, the decreased abundance of MCU in CL-deficient cells could be attributed to its reduced stability in the IMM.

Uniporter activity is diminished in yeast cardiolipin mutants

A decrease in uniporter abundance is expected to cause a reduction in mitochondrial Ca^{2+} uptake in CL-deficient mitochondria. To test this, we used

membrane impermeable Ca^{2+} indicator Calcium Green-5N (Ca Green-5N), which fluoresces upon binding with free Ca^{2+}, to measure Ca^{2+} uptake in isolated mitochondria. When pulses of Ca^{2+} were added to WT yeast mitochondria, which lack endogenous Ca^{2+} uptake machinery, the Ca Green-5N fluorescence increased with every pulse because exogenously added Ca^{2+} remained outside of mitochondria and accessible to Ca Green-5N (Figure 2.3E). Since mitochondrial integrity and membrane potential ($\Delta\Psi_m$) are crucial for Ca^{2+} uptake, we tested the intactness of these parameters by using the Ca^{2+} ionophore ETH129, which transports Ca^{2+} across the intact mitochondrial membrane in a $\Delta\Psi_m$-dependent manner (Kovács-Bogdán et al., 2014). Experiments with ETH129 confirmed that these parameters were intact in our experimental system (Figure 2.3E and F), although, we did notice that the ETH129-mediated Ca^{2+} buffering capacity of *crd1*Δ mitochondria is slightly lower than WT mitochondria (Figure 2.3E and F). We further confirmed the requirement of $\Delta\Psi_m$ for mitochondrial Ca^{2+} uptake by using an uncoupler (CCCP) or a respiratory chain inhibitor (antimycin), both of which abolished Ca^{2+} uptake (Figure 2.5A and B).

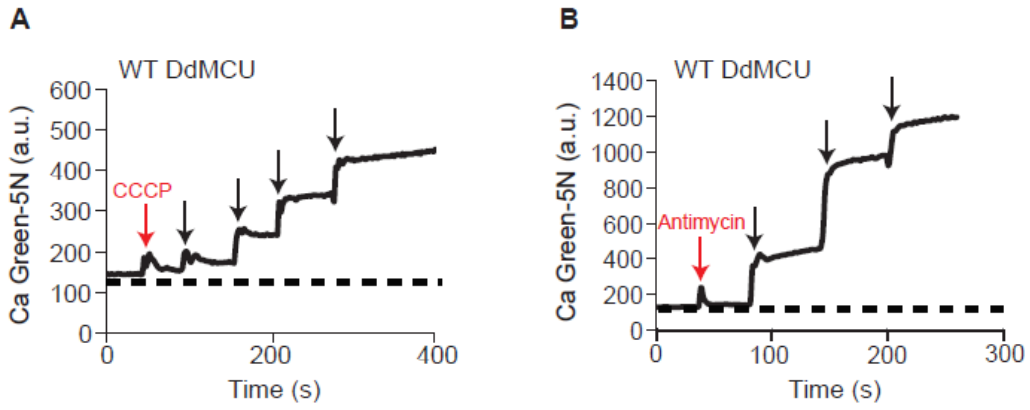

Figure 2.5 DdMCU mediated mitochondrial Ca^{2+} uptake is dependent on mitochondrial membrane potential and functional respiratory chain

(A) Representative traces monitoring extra-mitochondrial Ca^{2+} levels by Ca Green-5N following 10 μM $CaCl_2$ addition (black arrows) to DdMCU expressing WT yeast mitochondria pre-incubated with 1 μM CCCP (red arrow). Traces are representative of two independent experiments. (B) Representative traces monitoring extra-mitochondrial Ca^{2+} levels by Ca Green-5N following 10 μM $CaCl_2$ addition (black arrows) to DdMCU expressing WT yeast mitochondria pre-incubated with 1 μM antimycin (red arrow). Traces are representative of two independent experiments. (Figure reprinted from Ghosh et al., 2020).

After validating our assay, we measured mitochondrial Ca^{2+} uptake in DdMCU expressing WT and *crd1*Δ mitochondria. WT yeast mitochondria expressing DdMCU were able to take up multiple pulses of 10 μM Ca^{2+}, thereby rendering the added Ca^{2+} inaccessible to the membrane impermeable Ca Green-5N and lowering its fluorescence signal (Figure 2.3G). In contrast, *crd1*Δ mitochondria expressing DdMCU could uptake only two pulses of 10 μM Ca^{2+}, although it maintained sufficient $\Delta\Psi_m$ to allow ETH129-mediated Ca^{2+} uptake (Figure 2.3H). Consistent with these results, we observed a marked decrease in mitochondrial Ca^{2+} uptake in *crd1*Δ mitochondria when we co-expressed HsMCU and EMRE, despite the fact that ETH129-mediated Ca^{2+} uptake remained partially preserved (Figure 2.3I and J). Quantitative analysis showed reduced specific activity of HsMCU Ca^{2+} uptake kinetics in CL-deficient mitochondria (Figure 2.6), suggesting that lack of CL impairs mitochondrial Ca^{2+} uptake by decreasing both MCU abundance and activity. Taken together, these results demonstrate an evolutionarily conserved role of CL in MCU function.

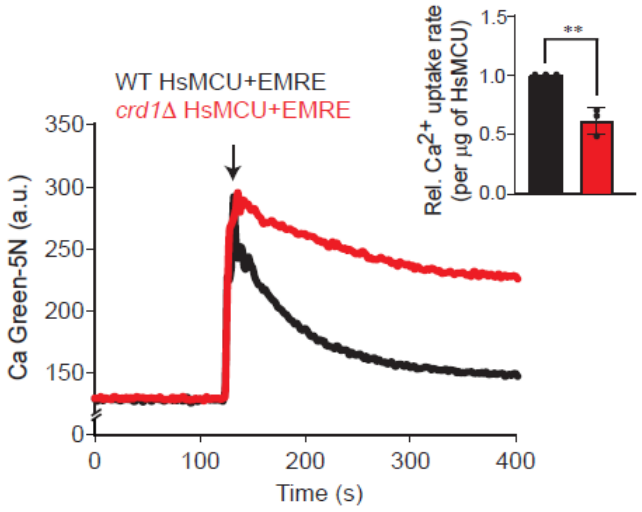

Figure 2.6 Specific Ca^{2+} uptake rate of HsMCU is reduced in *crd1*Δ yeast cells
Representative traces monitoring extra-mitochondrial Ca^{2+} levels using Ca Green-5N, following 25 µM $CaCl_2$ addition (black arrow) to mitochondria isolated from WT and *crd1*Δ yeast expressing HsMCU and EMRE. Inset shows quantification of uptake rate of Ca^{2+}, defined as the slope of linear fits between 150-200s, normalized to per µg of HsMCU protein in WT and *crd1*Δ mitochondria. Data shown as mean ± SD, n=3. $^{**}p < 0.005$. WT, wild type. (Figure reprinted from Ghosh et al., 2020).

MCU function is impaired in a CL-depleted yeast model of BTHS

We next asked whether a partial loss of mitochondrial CL, as observed in BTHS patients and disease models, may perturb MCU abundance and activity. BTHS is a rare genetic disorder characterized by loss-of-function mutations in a conserved CL remodeling enzyme Taz1, referred to as TAZ or TAFAZZIN in mammals. Loss of Taz1 leads to a reduction in the levels of CL and an accumulation of its precursor, monolysocardiolipin (MLCL) (Figure 2.7A). We used yeast model of BTHS, *taz1*Δ cells, to determine if MCU function was compromised in yeast cells that are partially depleted in CL. We validated *taz1*Δ cells by measuring its mitochondrial phospholipid composition, which showed an expected ~50% reduction in CL with a concomitant increase in MLCL (Figure 2.7B). Consistent with our results in CL-deficient *crd1*Δ cells,

we observed a modest decrease in the steady-state levels of DdMCU (Figure 2.8A and B) and HsMCU, which was expressed along with EMRE, (Figure 2.8C and D) in *taz1*Δ mitochondria.

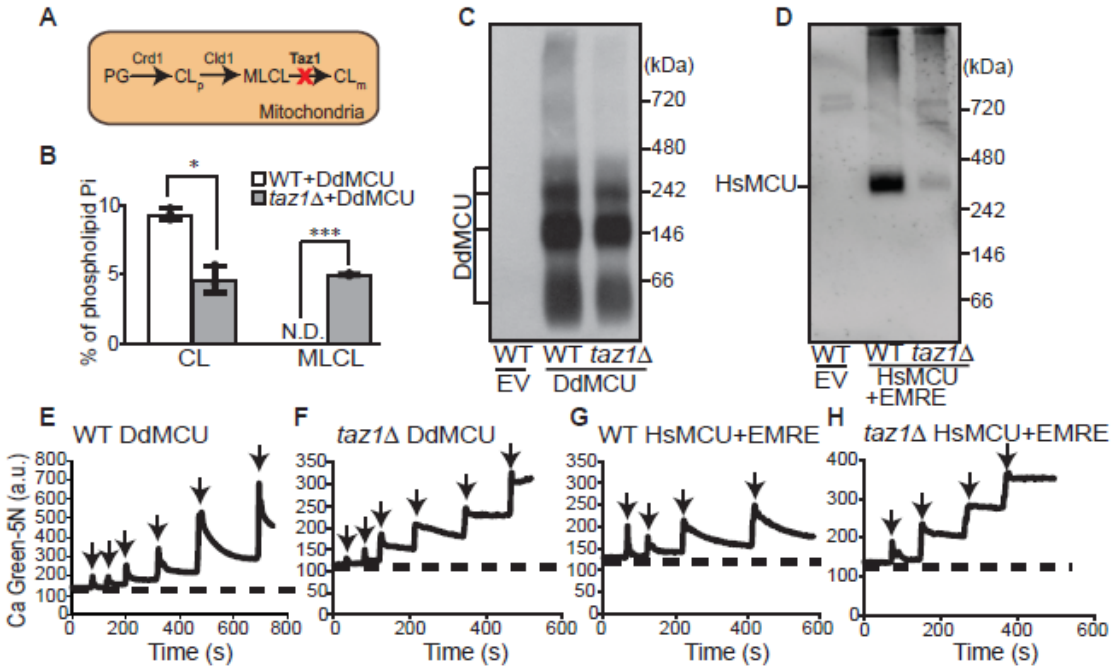

Figure 2.7 MCU abundance and activity are reduced in *taz1*Δ cells, a yeast model of BTHS

(A) A schematic of CL biosynthetic and remodeling pathway in yeast. (B) CL and MLCL levels in mitochondria isolated from WT and *taz1*Δ cells expressing DdMCU. Data are shown as mean ± SD, n=3. **p* < 0.05; ****p* < 0.0005. N.D., not detected. (C) BN-PAGE immunoblot analysis of FLAG-tagged DdMCU in digitonin-solubilized mitochondria from WT and *taz1*Δ cells expressing empty vector (EV) or DdMCU. Blot is representative of three independent experiments. (D) BN-PAGE immunoblot analysis of FLAG-tagged HsMCU in digitonin-solubilized mitochondria from WT and *taz1*Δ cells expressing EV or co-expressing HsMCU and EMRE. Blot is representative of three independent experiments. (E-H) Representative traces monitoring extra-mitochondrial Ca^{2+} levels with Calcium Green-5N following repeated 10 µM $CaCl_2$ additions (black arrows) to mitochondria isolated from WT and *taz1*Δ cells expressing either DdMCU (E and F) or HsMCU and EMRE (G and H). All traces are representative of three independent experiments. WT, wild type; PG, phosphatidylglycerol; CL, cardiolipin; CL_p, premature CL; CL_m, mature CL; MLCL, monolysocardiolipin. (Figure reprinted from Ghosh et al., 2020).

The oligomeric assemblies of both DdMCU and HsMCU/EMRE were also reduced in *taz1*Δ mitochondria, with the reduction being more pronounced for HsMCU (Figure 2.7C and D). As shown previously (Basu Ball et al., 2018, Baile et al., 2014), we find that a complete or partial loss of CL in *crd1*Δ and *taz1*Δ cells, respectively, does not lead to a universal decrease in the levels of IMM proteins or their supramolecular assemblies (Figure 2.9A and B).

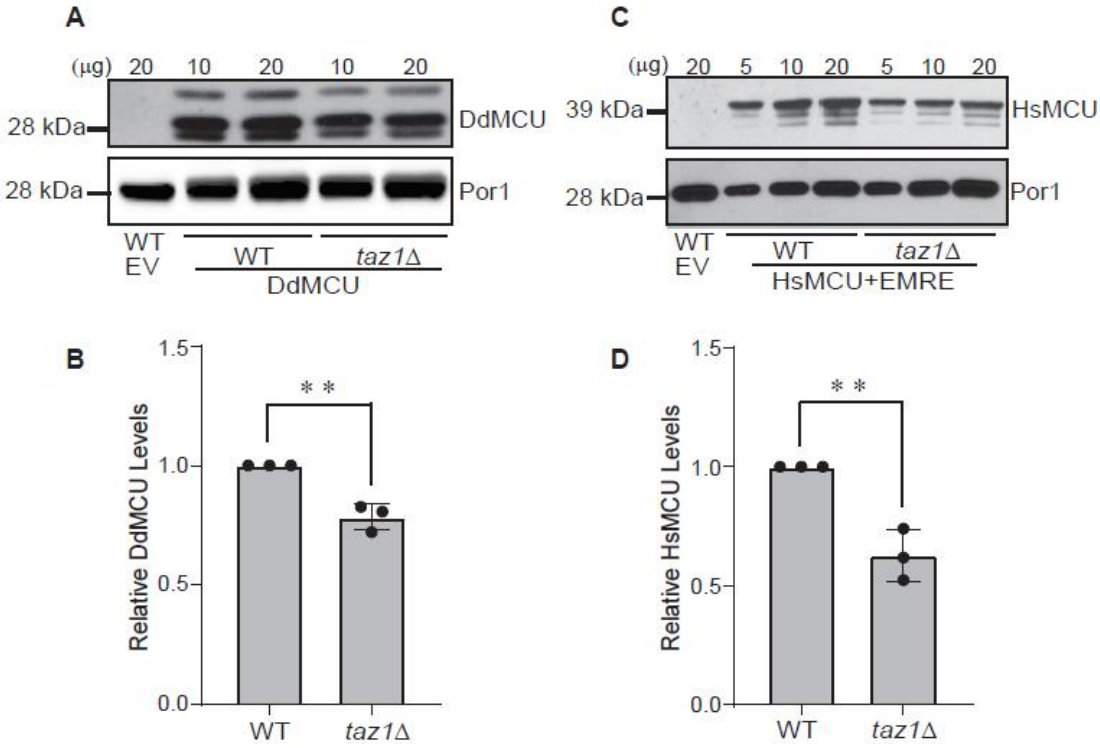

Figure 2.8 Steady-state levels of DdMCU and HsMCU are reduced in *taz1*Δ cells
(A) SDS-PAGE immunoblot analysis of FLAG-tagged DdMCU expressed in WT and *taz1*Δ yeast mitochondria. Por1 was used as a loading control. (B) Quantification of DdMCU protein levels from (A) using ImageJ software. (C) SDS-PAGE immunoblot analysis of FLAG-tagged HsMCU expressed in WT and *taz1*Δ yeast mitochondria. Por1 was used as a loading control. (D) Quantification of HsMCU protein levels from (C) using ImageJ software. Data shown as mean ± SD, n=3. ** $p < 0.005$. WT, wild type. (Figure reprinted from Ghosh et al., 2020).

In fact, none of the IMM protein levels were decreased in *taz1*Δ cells and levels of the respiratory chain subunits (Sdh1 and Atp2) and the protein import machinery (Tim44

and Tom70) were not reduced in *crd1*Δ cells either when these cells were cultured in galactose containing media (Figure 2.9A). Thus, a decrease in the levels of DdMCU and HsMCU in *crd1*Δ and *taz1*Δ cells highlights their specific requirement of CL. In accordance with the reduced abundance of DdMCU and HsMCU in *taz1*Δ mitochondria, the mitochondrial Ca^{2+} uptake was also diminished in DdMCU (Figure 2.7E and F) and HsMCU/EMRE (Figure 2.7G and H) expressing *taz1*Δ mitochondria.

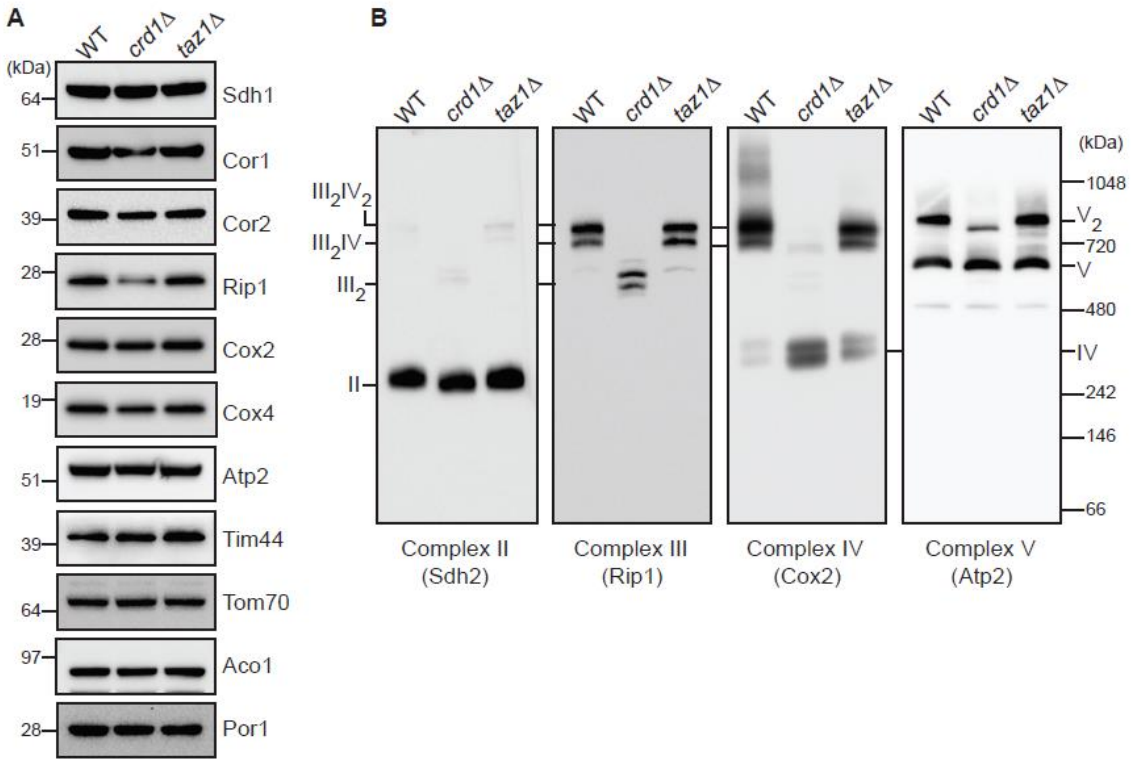

Figure 2.9 Specific effects of CL deficiency on the abundance and assembly of mitochondrial membrane proteins

(A) SDS-PAGE immunoblot analysis of mitochondrial proteins in mitochondria isolated from the indicated yeast CL-deficient mutants. Por1 is used as a loading control. (B) BN-PAGE immunoblot analysis of mitochondrial respiratory chain complexes in mitochondria isolated from the indicated yeast CL-deficient mutants. (Figure reprinted from Ghosh et al., 2020).

Again, quantitative analysis of mitochondrial Ca^{2+} uptake kinetics showed reduced Ca^{2+} uptake rate by HsMCU in CL-depleted *taz1*Δ mitochondria (Figure 2.10). These results suggest that a partial loss of CL in *taz1*Δ mutant impairs MCU abundance, assembly, and activity.

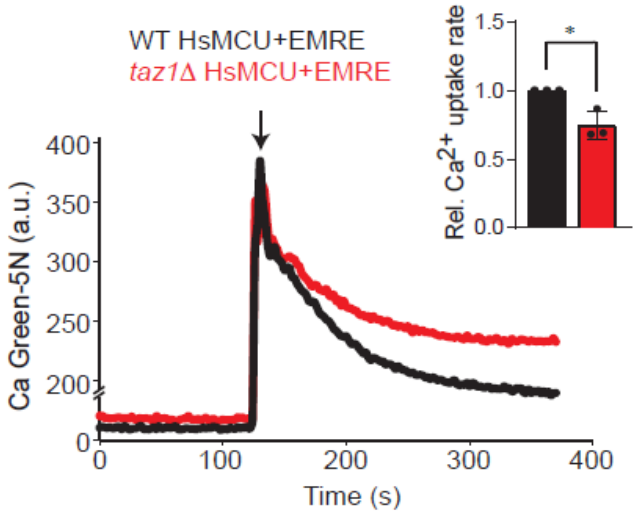

Figure 2.10 Ca^{2+} uptake rate of HsMCU is reduced in *taz1*Δ yeast cells
Representative traces monitoring extra-mitochondrial Ca^{2+} levels using Ca Green-5N, following 25 μM $CaCl_2$ addition (black arrow) to mitochondria isolated from WT and *taz1*Δ yeast expressing HsMCU and EMRE. Inset shows quantification of uptake rate of Ca^{2+}, defined as the slope of linear fits between 150-200s. Data shown as mean ± SD, n=3. *$p < 0.05$. WT, wild type. (Figure reprinted from Ghosh et al., 2020).

MCU function is disrupted in C2C12 murine myoblast model of BTHS

We wondered whether our findings with non-native MCU expressed in yeast CL-deficient and CL-depleted mutants are applicable to endogenous MCU in mammalian cells. To this end, we utilized a *Taz-KO* C2C12 murine myoblast cell line, which has recently been developed as a murine skeletal muscle model of BTHS, a disease characterized by skeletal and cardiomyopathy (Lou et al., 2018). An expected decline in the levels of CL with a concomitant elevation in MLCL validated the *Taz-KO* C2C12

cells as a disease model of BTHS (Table 2.2). Using this model of BTHS, we found that the steady-state levels of monomeric MCU and MCU-containing uniporter complexes were significantly reduced in *Taz-KO* cells when compared to WT (Figure 2.11A-C). A cycloheximide chase assay in *Taz-KO* C2C12 cells showed an increase in the turnover of

Phospholipids	WT	*Taz-KO*
Cardiolipin	12.1	5.5
Monolysocardiolipin	N.D.	7.1
Phosphatidylethanolamine	35.2	35.4
Phosphatidylcholine	49.2	45.1
Phopshatidylinositol	2.1	2.3
Phosphatidylserine	0.6	0.7
Phosphatidic acid	0.8	1.7
Phosphatidylglycerol	N.D.	2.2

Table 2.2 Mitochondrial phospholipid composition of C2C12 myoblasts
Levels of major mitochondrial phospholipids are expressed as % of total phospholipid phosphorus in WT and *Taz-KO* C2C12 cells. Data shown as mean values. n=2. WT, wild type; N.D., Not detected. (Table reprinted from Ghosh et al., 2020).

endogenous MCU in *Taz-KO* cells compared to WT (Figure 2.12), suggesting that depletion of unsaturated CL or accumulation of MLCL reduces the stability of endogenous MCU.

Next, we utilized permeabilized WT and *Taz-KO* C2C12 cells to test the role of CL on MCU-mediated mitochondrial Ca^{2+} uptake. After the permeabilized cells had reached a steady-state $\Delta\Psi_m$, we applied a 10 μM Ca^{2+} pulse and monitored the reduction in extramitochondrial Ca^{2+} ($[Ca^{2+}]_{out}$). Compared to WT, *Taz-KO* cells exhibited a delayed clearance of $[Ca^{2+}]_{out}$, indicating compromised mitochondrial Ca^{2+} uptake

(Figure 2.11D and E). Collectively, these results reveal that optimal levels of CL are essential for maintaining endogenous MCU abundance and activity in the mouse muscle cell line model of BTHS.

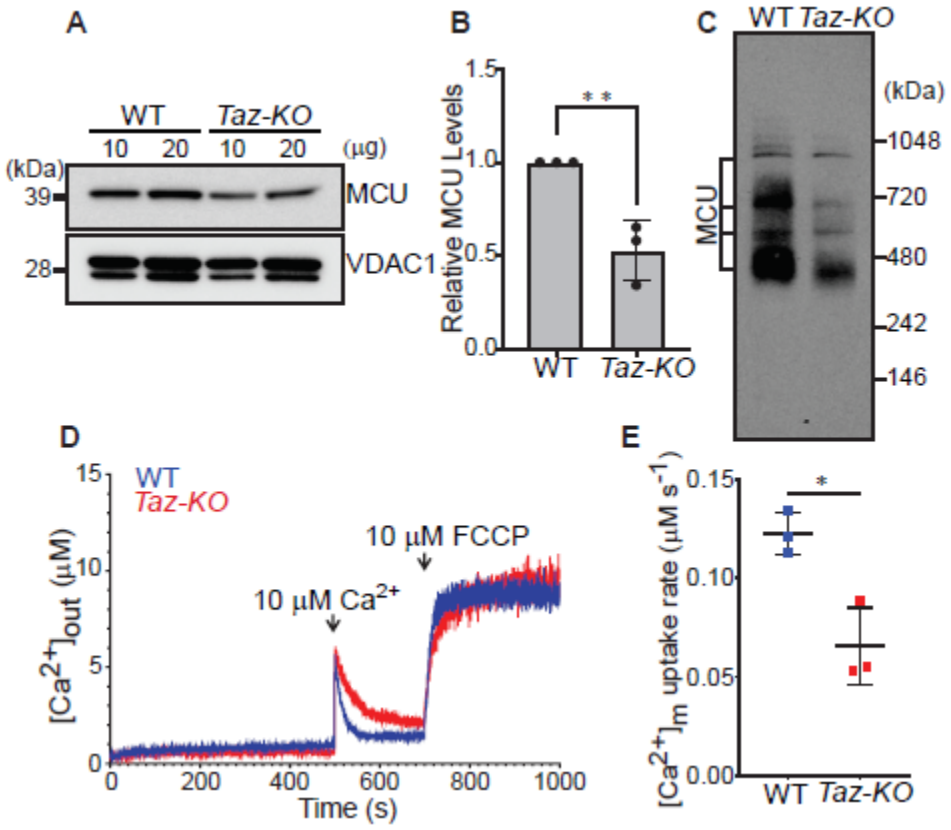

Figure 2.11 Endogenous MCU abundance and activity are reduced in *Taz-KO* C2C12 myoblasts

(A) SDS-PAGE immunoblot analysis of MCU in mitochondria isolated from WT and *Taz-KO* C2C12 myoblasts. VDAC1 is used as a loading control. (B) Quantification of relative MCU levels from (A) by densitometry using ImageJ software. Data shown as mean ± SD. n=3. $^{**}p < 0.005$. (C) BN-PAGE immunoblot analysis of MCU in digitonin-solubilized mitochondria isolated from WT and *Taz-KO* C2C12 myoblasts. Blot is representative of three independent experiments. (D) Permeabilized WT and *Taz-KO* cells were pulsed with 10 μM Ca^{2+} followed by FCCP (10 μM) as indicated. Traces show bath [Ca^{2+}] (μM). Traces are representative of three independent experiments. (E) MCU-mediated mitochondrial Ca^{2+} uptake rate calculated from (D). Data shown as mean ± SEM. n=3. $^{*}p < 0.05$. WT, wild type. (Figure reprinted from Ghosh et al., 2020).

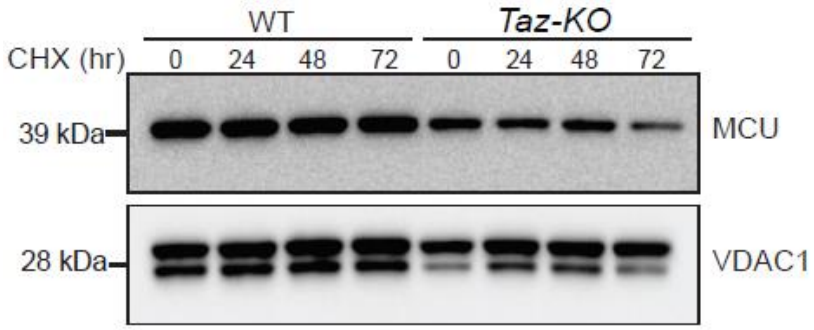

Figure 2.12 CL-deficiency causes increased protein turnover of MCU in *Taz-KO* C2C12 cells
SDS-PAGE immunoblot analysis of MCU in WT and *Taz-KO* C2C12 myoblasts treated with 10 μg/mL cycloheximide (CHX) for the indicated time-points. VDAC1 is used as loading control. Blot is representative of three independent experiments. (Figure reprinted from Ghosh et al., 2020).

MCU abundance is reduced in BTHS patient-derived cells and cardiac tissues

To test if our findings from yeast and C2C12 model systems of BTHS hold true in BTHS patient-derived cells and cardiac tissues, we procured a BTHS patient B-lymphocyte cell line and BTHS patient heart tissue samples. Phospholipid analysis of BTHS patient B-lymphocyte mitochondria showed reduced CL and elevated MLCL levels, validating the BTHS patient cell line (Figure 2.13A). Immunoblot analysis revealed a ~70% decrease in the steady-state levels of MCU in BTHS B-lymphocyte cells as compared to the control (Figure 2.13B). We also observed a reduction in assembly of the higher-order, MCU containing uniporter complexes in the patient cells (Figure 2.13C). Consistent with our *in vitro* data, we observed a reduction in MCU abundance in cardiac tissues obtained from five different BTHS patients, with MCU being reduced by ~40–90% as compared to the control sample (Figure 2.13D and E). Unlike MCU, other IMM proteins of the respiratory chain did not show reduced

abundance, except for respiratory complex I subunit NDUFB8 (Figure 2.13D and E). These data are consistent with our yeast model of BTHS (Figure 2.9A) and further demonstrate a specific requirement of CL for MCU abundance.

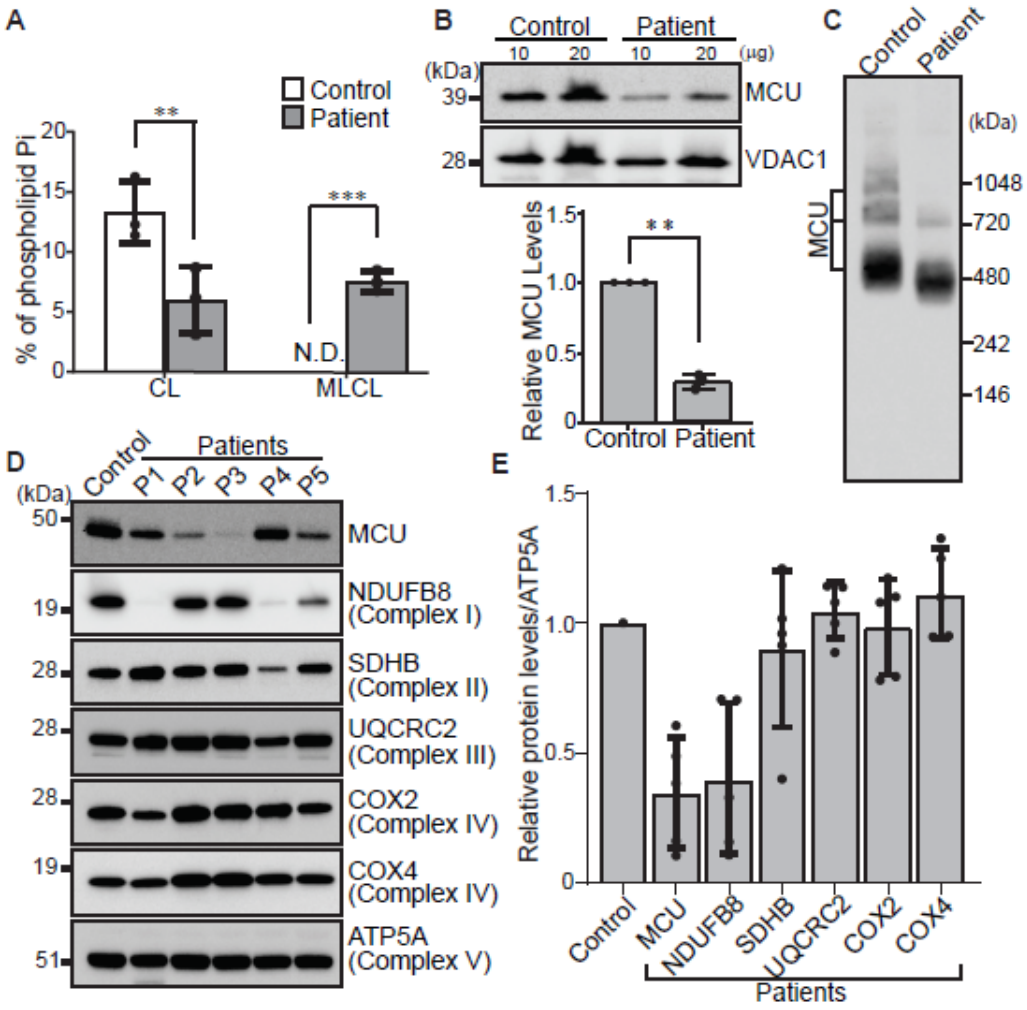

Figure 2.13 MCU is reduced in BTHS patient-derived lymphocyte and cardiac tissues

(A) CL and MLCL levels in mitochondria isolated from control and BTHS patient B-lymphocyte. Data shown as mean ± SD, n=3. $^{**}p < 0.005$. $^{***}p < 0.0005$. N.D., not detected. (B) (top) SDS-PAGE immunoblot analysis of MCU in mitochondria isolated from control and BTHS patient B-lymphocyte. VDAC1 is used as a loading control. (bottom) Quantification of relative MCU levels using ImageJ software. Data shown as mean ± SD, n=3. $^{**}p < 0.005$. (C) BN-PAGE immunoblot analysis of MCU in digitonin-solubilized mitochondria from control and BTHS patient B-lymphocyte. Blot is representative of three independent experiments. (D) SDS-PAGE immunoblot analysis of MCU and mitochondrial respiratory chain (MRC) complex

subunits in cardiac tissue lysates obtained from control and five BTHS patients (P1-P5). ATP5A is used as a loading control. (E) Quantification of immunoblots from (D) using ImageJ software. Data shown as mean ± SD, n=5. CL, cardiolipin; MLCL, monolysocardiolipin. (Figure reprinted from Ghosh et al., 2020).

Discussion

The assembly and activity of integral membrane proteins often depend on the surrounding membrane phospholipid composition (Dowhan et al., 2004, Lee 2004). Recent studies using yeast phospholipid mutants have uncovered some unexpected findings regarding the roles of individual mitochondrial membrane phospholipids in the function and formation of IMM proteins. Studies from yeast phospholipid mutants show that most mitochondrial membrane proteins are able to tolerate a large perturbation in membrane phospholipid composition (Baker et al., 2016, Schuler et al., 2016). However, some IMM proteins specifically rely on a particular class of phospholipid for their protein:protein interactions, higher-order assembly, and activity (Claypool et al., 2008, Baker et al., 2016, Bottinger et al., 2012). Here, we adapted a yeast heterologous expression system to uncover a CL-specific requirement for the stability and function of MCU. We demonstrate that the CL-specific requirement of MCU is conserved with a partial loss of CL reducing the stability of endogenous MCU in BTHS models and BTHS patient cardiac tissue, a finding that links MCU to BTHS disease pathology.

We attribute the decreased abundance of MCU in CL-deficient cells to its increased turnover (Figure 2.3C and D). We also considered the possibility that decreased MCU abundance could be due to the reduced mitochondrial membrane potential and protein import observed in CL-deficient yeast (Jiang et al., 2000).

However, this is unlikely because MCU levels were not decreased in PE-depleted *psd1*Δ cells (Figure 2.2 and Figure 2.3A and B) that also exhibit similarly reduced mitochondrial membrane potential and protein import (Bottinger et al., 2012). Moreover, we have shown that *crd1*Δ mitochondria could uptake Ca^{2+} via the membrane potential dependent Ca^{2+}-ionophore ETH129 (Figure 2.3F, H, and J), indicating that these CL-deficient mitochondria maintain sufficient mitochondrial membrane potential to support Ca^{2+} uptake.

Prior studies have typically used *in vitro* patch-clamp approaches to identify regulators of ion channels. For example, phosphatidylinositides were shown to regulate the activity of Ca^{2+} ion channel, TRPML1, in an intracellular compartment (Zhang et al., 2012). Similarly, M-type K^+ channel activity was shown to be regulated by phosphatidylinositides as well as a wide range of phospholipids (Telezhkin et al., 2012). Here, we provide a complementary *in vivo* approach to discover physiologically relevant phospholipid regulators of mitochondrial membrane localized ion channels. Our *in vivo* approach utilizing yeast phospholipid mutants provides information regarding the structural requirements of phospholipids in addition to their functional role, as seen in the case of MCU, where we found a specific requirement of CL for the stability of MCU (Figure 2.3A–D). Recently, it was shown that peripheral membrane proteins MICU1 and MICU2, which are two regulatory subunits of the uniporter, bind CL *in vitro* (Kamer et al., 2017). This observation, combined with our finding, provides compelling biochemical and genetic evidence that CL plays a critical role in uniporter holocomplex formation and function. A recent cryo-EM study of a fungal MCU channel identified the

presence of four acyl chains within the transmembrane helices of MCU that form lateral membrane openings, with basic residues on legs of the channel poised to interact with phospholipid head groups (Baradaran et al., 2018).

During the revision of this article, a new high-resolution cryo-EM structure of the human uniporter complex has been reported on a preprint server (Zhuo et al., 2020). The structure reports 8 CL and 16 PC molecules in the heterooctameric uniporter complex such that one CL and two PC molecules associate with each MCU subunit. The cavity formed by the two transmembrane helices of MCU is filled by these phospholipids, which the authors speculate may provide stability to the uniporter structure. However, in their report, functional studies were not included to establish the physiological roles of CL and PC. Our current *in vivo* work showing the requirement of CL for the stability of MCU (Figures 2.3, 2.7, 2.11, and 2.13) strongly supports its structural role. Of note, our work also shows that MCU stability is not impacted by depletion of PC (Figure 2.3A and B), which may be replaceable with other phospholipids that accumulate in *pem2*Δ cells (Table 2.1). Interestingly, the cryo-EM structure of the human uniporter complex also shows that acyl chain of CL interacts with EMRE, raising the possibility that the stabilizing effect of CL on MCU may be through its interactions with EMRE. However, since we find that CL is also required for the stability of DdMCU (Figure 2.3A), which does not contain EMRE, it is very likely that it is the direct CL-MCU interactions that provide stability to MCU. Additionally, this study by Zhuo et al. (Zhuo et al., 2020) showed that Arg297 residue of MCU forms hydrogen bonds with the phosphate moiety of CL as well as with the N-terminal domain of EMRE, and its mutation to Asp

abolished Ca^{2+} uptake. Our functional and biochemical studies perturbing CL are highly complementary to this structural observation and jointly support a specific role of CL in the stability and activity of MCU.

CL interacts strongly with many integral membrane proteins of the IMM and increases their stability (Musatov et al., 2017). A recent study has revealed that by virtue of remodeling its acyl chain composition, CL relieves the elastic stress imposed on the mitochondrial membrane due to protein crowding. In doing so, CL allows the formation of stable lipid:protein complexes resulting in the normal functioning of mitochondrial membrane proteins (Xu et al., 2019). Our finding that loss of CL increases the turnover of MCU (Figure 2.3C and D and Figure 2.12) points to an underlying biochemical mechanism of how CL impacts the stability of mitochondrial membrane protein complexes and could potentially be extrapolated to other key membrane proteins of mitochondria known to be interacting with CL.

CL requirement of MCU is particularly relevant to BTHS, a rare genetic disorder caused by mutations in the CL-remodeling enzyme, TAZ (Bione et al., 1996, Xu et al., 2003). The clinical presentations in BTHS patients and humans with loss-of-function mutations in MICU1 as well as the phenotypes observed in *Mcu*$^{-/-}$ or *Micu2*$^{-/-}$ mice show some overlapping features. For example, BTHS patients classically present with cardiomyopathy, skeletal muscle myopathy, proximal muscle myopathy, exercise intolerance, and fatigue (Clarke et al., 2013). Loss-of-function mutations in MICU1 also result in similar clinical presentations in humans (Logan et al., 2014, Lewis-Smith et al., 2016). *Mcu*$^{-/-}$ and *Micu2*$^{-/-}$ mice exhibit exercise intolerance and cardiovascular

phenotypes, respectively (Pan et al., 2013, Bick et al., 2017). Together, these studies suggest that some aspects of BTHS pathology may be attributable to defective mitochondrial Ca^{2+} signaling via the uniporter.

Materials and Methods

Yeast Strains and Growth Conditions

S. cerevisiae strains used in this study were obtained from Open Biosystems. All strains were isogenic to BY4741 WT and their authenticity was confirmed by PCR, replica plating on dropout plates, and phospholipid analyses. Yeast cells were precultured in standard growth media including YPD (1% yeast extract, 2% peptone and 2% dextrose) or YPGal (2% galactose). The final cultures were grown in synthetic complete (SC) medium, which contained 0.17% yeast nitrogen base without amino acids, 0.5% ammonium sulfate, 0.2% dropout mix containing amino acids, and 2% galactose (SC-galactose). Cells expressing either DdMCU or HsMCU and EMRE were grown in SC-galactose leucine drop-out or SC-galactose leucine/uracil double drop-out media, respectively, to resist plasmid curing. Growth in liquid media was measured spectrophotometrically at 600 nm. Final cultures were started at an optical density of 0.1 and were grown to late logarithmic phase at 30°C.

Mammalian Cell Culture and BTHS Heart Tissue Samples

The control (ND11500) and BTHS patient (GM22194) B-lymphocytes were obtained from the Coriell Institute for Medical Research. These cells were cultured in high glucose Roswell Park Memorial Institute (RPMI) 1640 medium supplemented with 15%

fetal bovine serum (FBS) (Sigma). C2C12 WT and *Taz-KO* myoblasts were cultured in Dulbecco's modified Eagle's medium supplemented with 10% FBS. All cell lines were cultured in 5% CO_2 at 37°C. Deidentified BTHS patient heart samples were obtained from Barth Syndrome Registry and DNA Bank. Whole-cell protein was extracted in lysis buffer (BP-115, Boston BioProducts) supplemented with protease inhibitor mixture (cOmplete Mini EDTA-free; Roche Diagnostics), and the protein concentrations were determined by bicinchoninic acid assay (Pierce BCA Protein Assay).

Mitochondria Isolation

Isolation of crude mitochondria from yeast cells was performed as previously described (Meisinger et al., 2006). Mitochondrial fractions were resuspended in SEM buffer (250 mM sucrose, 1 mM EDTA, 10 mM Mops-KOH, pH 7.2) and stored at −80°C for protein biochemistry experiments. Fresh mitochondrial isolates were used for Ca^{2+} uptake assays. Mitochondria from mammalian cells were isolated using the Mitochondria Isolation Kit from Abcam (110170; Abcam). Protein concentrations were determined by BCA assay (Pierce BCA Protein Assay).

SDS/PAGE, BN-PAGE, and Immunoblotting

Sodium dodecyl sulfate (SDS)/PAGE and BN-PAGE were performed to separate denatured and native protein complexes, respectively. For SDS/PAGE, mitochondrial lysate (10 μg, unless stated otherwise) was separated on NuPAGE 4–12% Bis-Tris gels (Thermo Fisher Scientific) and transferred onto polyvinylidene fluoride (PVDF) membranes using a Trans-Blot SD semidry transfer cell (Bio-Rad). For BN-PAGE, mitochondria were solubilized in buffer containing 1% digitonin (Thermo Fisher

Scientific) at 6 g/g of yeast mitochondrial protein or 9 g/g of mammalian mitochondrial protein, followed by incubation for 15 min at 4°C and centrifugation at 20,000 × g for 30 min. Clear supernatant was collected and 50X G-250 sample additive was added. Twenty micrograms of protein was loaded on 3–12% native PAGE Bis-Tris gel (Thermo Fisher Scientific) and transferred onto PVDF membranes using a wet transfer method. Following transfer, the membranes were probed with the following primary antibodies: For yeast proteins—Flag, 1:500,000 (F1804; Sigma); Pgk1, 1:50,000 (459250; Novex); Por1, 1:50,000 (ab110326; Abcam); Sdh1, 1:10,000; Sdh2, 1:5,000; Cor1, 1:5,000; Cor2, 1:80,000; Rip1, 1:50,000; Cox2, 1:5,000 (ab110271; Abcam); Cox4, 1:5,000 (ab110272; Abcam); Atp2, 1:40,000; Tim44, 1:5,000; Tom70, 1:5,000, and Aco1, 1:5,000. For mammalian proteins—MCU, 1:2,500 (14997S; Cell Signaling Technologies); VDAC1, 1:2,500 (ab14734; Abcam); NDUFB8, 1:2,500 (ab110242; Abcam); SDHB, 1:1,000 (ab14714; Abcam); UQCRC2, 1:2,500 (ab14745; Abcam); COX2, 1:2,500 (ab110258; Abcam); COX4, 1:2,500 (ab14744; Abcam); and ATP5A, 1:2,500 (ab14748; Abcam). Anti-mouse or anti-rabbit secondary antibodies (1:5,000) were incubated for 1 h at room temperature, and membranes were developed using Clarity Western ECL (Bio-Rad Laboratories).

Mitochondrial Phospholipid Measurement

Phospholipids were extracted from mitochondrial pellets of yeast and mammalian cells (~1.5 mg of protein) using the Folch method, as previously described (Baker et al., 2016, Folch et al., 1957). Phospholipids were separated by two-dimensional TLC (2D-TLC), as previously described (Baker et al., 2016), using the following solvent systems:

chloroform/methanol/ammonium hydroxide (32.5/17.5/2.5) in the first dimension, followed by chloroform/acetic acid/methanol/water (37.5/12.5/2.5/1.1) in the second dimension. Phospholipids were visualized with iodine vapor and scraped onto glass tubes to quantify phosphorus using the Bartlett assay (Bartlett et al., 1959).

Mitochondrial Ca^{2+} Uptake Measurement in Yeast

This method was performed as previously described (Kovács-Bogdán et al., 2014). For measuring mitochondrial Ca^{2+} uptake, freshly isolated yeast mitochondrial pellet was dissolved in resuspension buffer (0.6 M mannitol, 20 mM Hepes-KOH, pH 7.4, 1 mM EGTA, 0.2% [wt/vol] BSA supplemented with 1X protease inhibitor mixture). Mitochondrial protein concentration was measured by BCA assay. Five hundred micrograms of mitochondrial lysate was resuspended in assay buffer (0.6 M mannitol, 10 mM Hepes-KOH, pH 7.4, 10 mM potassium phosphate, 0.5 mg/mL BSA, 3 mM glutamate, 3 mM malate, 3 mM succinate, 10 μM EGTA, and 1 μM Calcium Green-5N, adjusted to pH 7.4 using KOH). Mitochondrial Ca^{2+} uptake was measured in the Spectramax M2 spectrofluorometer (Molecular Devices), by recording the fluorescence of Calcium Green-5N (Thermo Fisher Scientific) (excitation/emission at 506 nm/532 nm) every 2 s following repeated additions of 10 μM $CaCl_2$ into the assay mix. For Ca^{2+} uptake rate measurements, 25 μM $CaCl_2$ was added to the assay mix once and Calcium Green-5N fluorescence monitored every 2 s. Ten micromolar ETH129 (21193; Sigma), a Ca^{2+} ionophore, was used as a control. CCCP and antimycin (Sigma), 1 μM each, were used to uncouple and inhibit mitochondrial respiratory chain, respectively.

Protein Turnover Measurement

The method was performed as previously described (Veling et al., 2017). Briefly, yeast cells expressing DdMCU were precultured in YPD at 30°C overnight. Subsequently, cells were transferred into SC-galactose (leucine drop-out) media and allowed to grow for 6 h, after which cycloheximide (CHX) (C7698; Sigma) was added at a final concentration of 50 μg/mL. Cells (2 X 10^8) were subsequently collected at 0, 1, 3, and 5 h time intervals, added to stop-solution (20 mM NaN_3 and 0.5 mg/mL BSA) and pelleted down. Yeast cells were lysed using an alkaline lysis method. Briefly, cells were sequentially incubated in lysis buffer (0.2 M NaOH) at room temperature, followed by 0.1 M NaOH and LDS sample loading buffer at 70°C to extract proteins. The lysates were centrifuged to pellet insoluble materials and the supernatant analyzed by gel electrophoresis and immunoblotting. Mammalian MCU turnover in C2C12 cells was measured by SDS PAGE/immunoblotting of protein lysate extracted following 10 μg/mL CHX treatment for 0, 24, 48, and 72 h, respectively.

Mitochondrial Ca^{2+} Uptake Measurement in Permeabilized Cells

C2C12 cells (~4 X 10^6 cells) were resuspended and permeabilized with digitonin (40 μg/mL) in 1.5 mL of medium composed of 120 mM KCl, 10 mM NaCl, 1 mM KH_2PO_4, 20mM Hepes-Tris (pH 7.2), and 2 μM thapsigargin to block the SERCA pump. The experiments were performed in the presence of 5 mM succinate at 37°C with constant stirring. For measuring mitochondrial Ca^{2+} uptake, the permeabilized cells were suspended in medium containing 1.0 μM Fura-2FF. Fluorescence was monitored in a multiwavelength excitation, dual-wavelength emission fluorimeter (DeltaRAM, Photon

Technology International). Extramitochondrial Ca^{2+} was recorded at an excitation ratio (340 nm/380 nm) and emission at 510 nm of Fura-2FF fluorescence. Single 10 μM Ca^{2+} pulse was added at 500 s, and the changes in extramitochondrial Ca^{2+} fluorescence were monitored. Mitochondrial Ca^{2+} uptake rate was derived from the decay of bath [Ca^{2+}] after Ca^{2+} pulses.

Statistical Analyses

All statistical analyses were performed using two-tailed unpaired Student's *t* test using data obtained from three independent experiments.

CHAPTER III

MITOCHONDRIAL CALCIUM SIGNALING IS IMPAIRED IN CARDIOLIPIN-DEFICIENT BARTH SYNDROME CELLS*

Summary

Calcium signaling via mitochondrial calcium uniporter (MCU) coordinates mitochondrial bioenergetics with cellular energy demands. We recently showed that the stability and activity of MCU is dependent on the mitochondrial phospholipid, cardiolipin (CL), but how this impacts calcium-dependent mitochondrial bioenergetics in CL-deficiency disorder like Barth syndrome (BTHS) is not known. Here we utilized cellular models of BTHS as well patient cardiac tissue to show that CL is required for the *in vivo* stability and activity of MICU1, the principal regulator of MCU, however, the reduction in MICU1 in BTHS mitochondria is independent of MCU.

*Parts of this chapter have been reprinted with permission from "MCU-complex-mediated mitochondrial calcium signalling is impaired in Barth syndrome" by Ghosh S, Zulkifli M, et al. 2021. *Human Molecular Genetics.* https://doi.org/10.1093/hmg/ddab 254, Copyright (2021) by Oxford University Press.

We find that the requirement of CL is specific to MCU and MICU1 because other subunits of the uniporter complex, including EMRE and MCUR1, are not reduced in BTHS models. Consistent with the decrease in MICU1-levels, we show that MICU1-dependent mitochondrial calcium uptake is perturbed and acute stimulation of mitochondrial calcium signaling in BTHS myoblasts fails to activate pyruvate dehydrogenase, which in turn impairs generation of reducing equivalents and blunts mitochondrial bioenergetics. Taken together, our work suggests that defects in mitochondrial calcium signaling could contribute to cardiac and skeletal muscle pathologies observed in BTHS patients.

Introduction

Mitochondria respond to increased cellular energy demands through calcium (Ca^{2+}) uptake via the mitochondrial calcium uniporter complex (Clapham 2007, Kamer and Mootha, 2015). Elevation in mitochondrial Ca^{2+} stimulates the activities of mitochondrial matrix dehydrogenases resulting in increased NADH generation, which fuels an increase in mitochondrial respiration and ATP production. Ca^{2+} uptake through mitochondrial calcium uniporter (MCU), the pore-forming subunit, is regulated by a number of accessory factors, including the mitochondrial calcium uptake proteins 1, 2, and 3 (MICU1, MICU2, MICU3), essential MCU regulator (EMRE), dominant negative β-subunit (MCUb), and MCU Regulator 1 (MCUR1), which together form a holocomplex, often referred to as the uniporter complex or uniplex (Baughman et al., 2011, De Stefani et al., 2011, Perocchi et al., 2010, Sancak et al., 2013, Plovanich et al., 2013, Rafaello et al., 2013, Tomar et al., 2016).

MICU1 is the principal regulator of the MCU channel which monitors cytosolic Ca^{2+} $[Ca^{2+}]_i$ transients and allows its entry into the mitochondria only under conditions of high $[Ca^{2+}]_i$ (Mallilankaraman et al., 2012). MICU1 binds to Ca^{2+} and adopts a structural conformation conducive for Ca^{2+} inflow through the MCU pore (Wang et al., 2020, Fan et al., 2020). In addition, MICU1 governs the spatial distribution of MCU in the inner mitochondrial membrane, which is required for the activation of the uniporter complex (Gottschalk et al., 2019). As a result, the genetic ablation of MICU1 causes dysregulation of the uniporter complex function, both by allowing mitochondrial Ca^{2+} accumulation at low $[Ca^{2+}]_i$ and by abolishing cooperative activation of the complex

at high $[Ca^{2+}]_i$ (Csordas et al., 2013). The importance of MICU1 in mitochondrial Ca^{2+} signaling is further highlighted by the fact that loss-of-function mutations in MICU1 result in brain and skeletal muscle defects and a progressive and debilitating movement disorder in humans (Logan et al., 2014, Lewis-Smith et al., 2016). Till date, no patients have been identified with a mutation in any of the other subunits of the uniporter complex.

Utilizing a heterologous expression system consisting of yeast mutants of mitochondrial phospholipid biosynthesis, we recently reported a specific requirement of cardiolipin (CL) in the stability and activity of MCU (Ghosh et al., 2020). CL is a signature phospholipid of the mitochondria, and its deficiency results in Barth syndrome (BTHS), an X-linked cardio- and skeletal muscle myopathy that is caused by mutations in the CL remodeling enzyme *TAFAZZIN* (also referred to as *TAZ)* (Bione et al., 1996, Ghosh et al., 2019). Consistent with our findings in the yeast surrogate system, we showed that BTHS patient-derived cells and cardiac tissues also exhibit a reduction in MCU (Ghosh et al., 2020). However, currently we do not know if CL-deficiency in BTHS also impacts other subunits of uniporter complex and whether mitochondrial Ca^{2+} signaling-dependent downstream bioenergetic processes are disrupted in BTHS disease models. In this study, we utilized multiple BTHS models, including patient-derived cells, cardiac tissues, a murine skeletal muscle cell model of BTHS, and CL-deficient yeast to uncover an essential requirement of CL for MICU1 stability and MICU1-dependent mitochondrial Ca^{2+} signaling. Importantly, we found that the disruption of MCU and

MICU1 blunts up regulation of mitochondrial bioenergetic pathways in response to extra-mitochondrial Ca^{2+} signal in BTHS cells.

Results

MICU1 abundance and stability are reduced in a murine myoblast model of Barth syndrome

The abundance and stability of the pore-forming subunit, MCU, were found to be reduced across multiple cellular models and patient-derived cells and cardiac tissues of BTHS (Ghosh et al. 2020). However, it is not known if CL requirement is specific to MCU or is it also required for the abundance, assembly, or activity of the other regulatory components of the uniporter complex. A previous study had shown that MICU1, the principal regulatory subunit of the uniporter complex, binds CL *in vitro* (Kamer et al 2017). To uncover the role of CL in MICU1 function *in vivo*, we determined MICU1 abundance in a *Taz-KO* C2C12 murine myoblast cell line model of BTHS by SDS-PAGE/immunoblotting. We observed a ~50% reduction in the steady-state levels of MICU1 in *Taz-KO* C2C12 myoblasts as compared to the wild type (WT) cells (Figure 3.1A and B). Consistent with a decrease in the monomeric protein, the abundance of MICU1 containing uniporter complexes was also moderately reduced in *Taz-KO* cells, as observed by Blue Native Polyacrylamide gel electrophoresis/immunoblotting (BN-PAGE) (Figure 3.1C).

MICU1 associates with the inner mitochondrial membrane peripherally but its interactions with other integral membrane components of the uniporter complex, MCU and EMRE (Sancak et al., 2013, Phillips et al., 2019), and its ability to bind CL *in vitro*

(Kamer et al, 2017) suggests that loss of CL may prevent membrane anchoring of MICU1 *in vivo*, which in turn would trigger its degradation. To test whether the stability of MICU1 protein *in vivo* is dependent on CL, we performed a cycloheximide chase assay in WT and *Taz-KO* C2C12 cells. Inhibition of nascent protein synthesis by cycloheximide allows measurement of the turnover rate of a protein *in vivo*. Using this assay, we observed a more rapid rate of turnover of MICU1 in CL-depleted *Taz-KO* cells as compared to WT cells (Figure 3.1D and E).

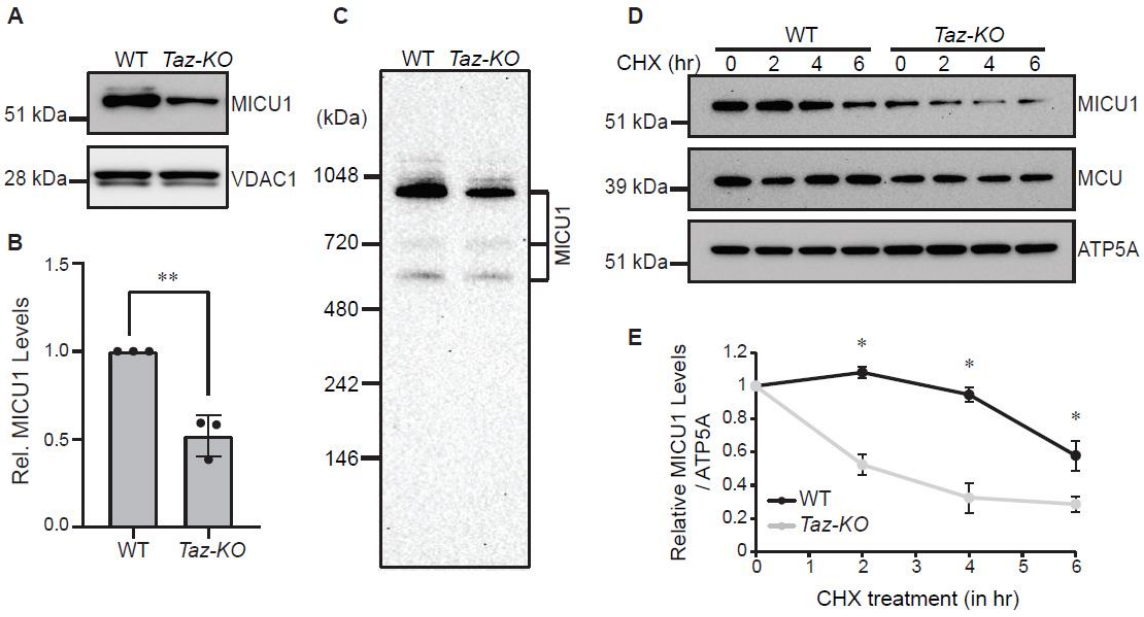

Figure 3.1 MICU1 abundance and stability are reduced in C2C12 *Taz-KO* cells
(A) SDS-PAGE immunoblot analysis of MICU1 in mitochondria isolated from WT and *Taz-KO* C2C12 myoblasts. VDAC1 is used as a loading control. (B) Quantification of relative MICU1 levels from (A) by densitometry using ImageJ software. Data shown as mean ± SD. n=3. $^{**}p < 0.005$. (C) BN-PAGE immunoblot analysis of MICU1 in digitonin-solubilized mitochondria isolated from WT and *Taz-KO* C2C12 myoblasts. Blot is representative of three independent experiments. (D) SDS-PAGE immunoblot analysis of MICU1 and MCU in WT and *Taz-KO* C2C12 myoblasts treated with 10 μg/mL cycloheximide (CHX) for the indicated time-points. ATP5A is used as loading control. Blot is representative of three independent experiments. (E) Quantification of relative MICU1 levels from (D) by densitometry using ImageJ software. Data are represented as mean ± SD. n=3 $^{*}p < 0.05$.

Since we had previously shown that MCU stability is also reduced in C2C12 *Taz-KO* cells (Ghosh et al., 2020), we next asked if the reduced stability of MICU1 is caused indirectly via degradation of MCU. Therefore, following cycloheximide treatment, we measured the levels of MCU at the same time-points at which MICU1 was degraded and found that MCU levels remained unchanged (Figure 3.1D). This result suggests that reduced MICU1 stability upon loss of CL is not dependent on MCU.

Uniporter components do not exhibit a generic requirement for CL

CL requirement for the abundance and stability of both MCU and MICU1 led us to ask if it was specific for these two proteins or a more generic requirement for the uniporter holocomplex. To answer this, we utilized yeast, *Saccharomyces cerevisiae*, which provides a "clean" background to test the effect of CL on the mitochondrial calcium uniporter components, as it does not contain any homologs of the core components of the uniporter machinery (Bick et al., 2012). We heterologously expressed the human MICU1 protein, without MCU and EMRE, in WT and CL-deficient *crd1Δ* yeast and observed a ~50% reduction in the abundance of MICU1 in CL-deficient *crd1Δ* yeast mitochondria compared to WT (Figure 3.2A and B). This data clearly establishes that the effect of CL on MICU1 abundance is independent of MCU. In contrast, the abundance of human MCUR1 remained unaltered when expressed in WT and *crd1Δ* cells (Figure 3.2C and D), suggesting that the requirement for CL is specific to MICU1.

Next, we measured the abundance of endogenous EMRE and MCUR1 in C2C12 WT and *Taz-KO* cells to test whether CL-depletion also affects these components of the uniporter complex. BN-PAGE/immunoblot analysis of EMRE in C2C12 WT and *Taz-*

KO mitochondria revealed that the abundance of EMRE containing oligomeric uniporter complexes were unaltered under CL deficiency (Figure 3.2E). Similarly, the levels of MCUR1 containing uniporter complexes also remained unchanged under CL deficiency (Figure 3.2F). Taken together, these data reveal that the uniporter subunits do not have a generic requirement of CL and that only the abundance of MCU and MICU1 are specifically reduced due to a loss of CL.

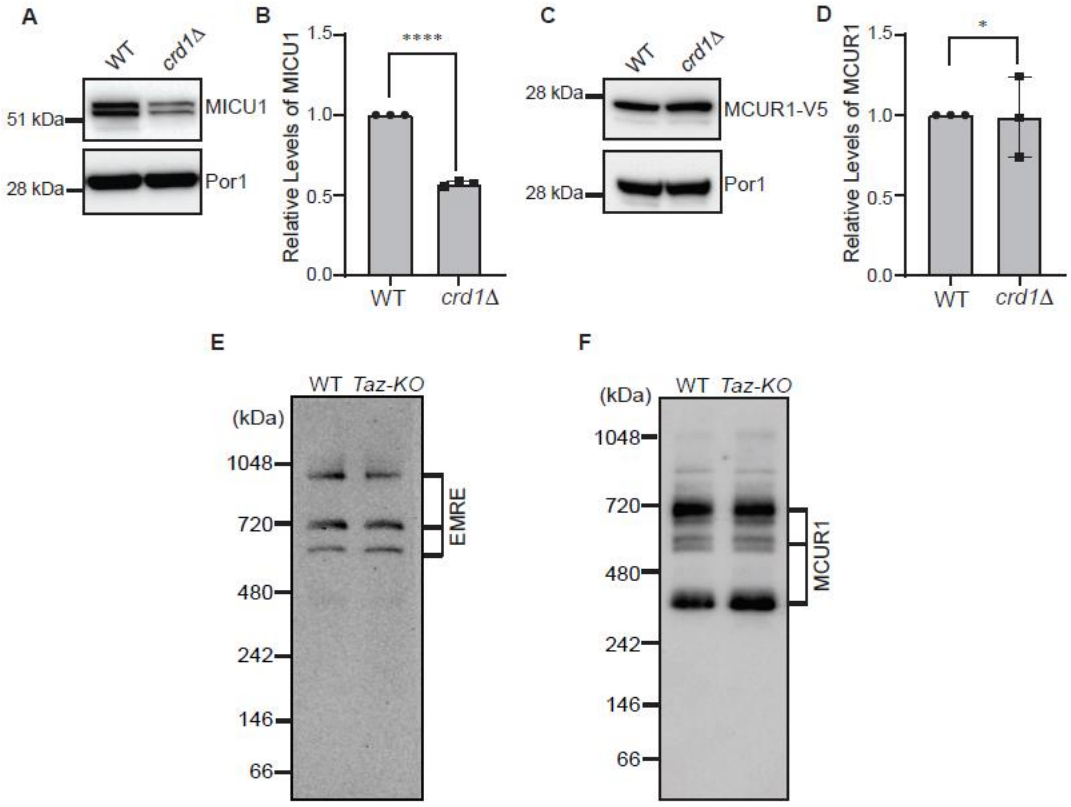

Figure 3.2 Loss of CL does not cause a generic decline in uniporter subunits
(A) SDS-PAGE immunoblot analysis of MICU1 in mitochondria isolated from WT and *crd1*Δ yeast expressing human MICU1. Por1 is used as a loading control. (B) Quantification of relative MICU1 levels from (A) using ImageJ software. Data shown as mean ± SD, n=3. ****p < 0.0001. (C) SDS-PAGE immunoblot of MCUR1-V5 in mitochondria isolated from WT and *crd1*Δ yeast expressing human MCUR1 tagged with V5. Por1 is used as a loading control. (D) Quantification of relative MCUR1 levels from (C) using ImageJ software. Data shown as mean ± SD, n=3. *p < 0.05. (E) BN-PAGE immunoblot of EMRE in mitochondria isolated from C2C12 WT and *Taz-KO* cells. Blot is representative of three independent experiments. (F) BN-

PAGE immunoblot of MCUR1 in mitochondria isolated from C2C12 WT and *Taz-KO* cells. Blot is representative of three independent experiments WT, wild type.

MICU1 abundance is reduced in BTHS patient-derived cells and cardiac tissues

To directly test if CL deficiency impacts MICU1 abundance in BTHS patient-derived samples we used a BTHS patient B-lymphocyte cell line, which have reduced CL (Ghosh et al 2020). Immunoblot analysis showed a marked reduction in the levels of MICU1 in the patient B-lymphocyte cells as compared to the control (Figure 3.3A and B). In addition, MICU1 containing higher-order uniporter complexes were also reduced in the BTHS patient B-lymphocytes (Figure 3.3C). Consistent with our cellular models, we found a reduction in MICU1 abundance in 4 out of 5 cardiac tissue samples obtained from 5 different BTHS patients (Figure 3.3D and E).

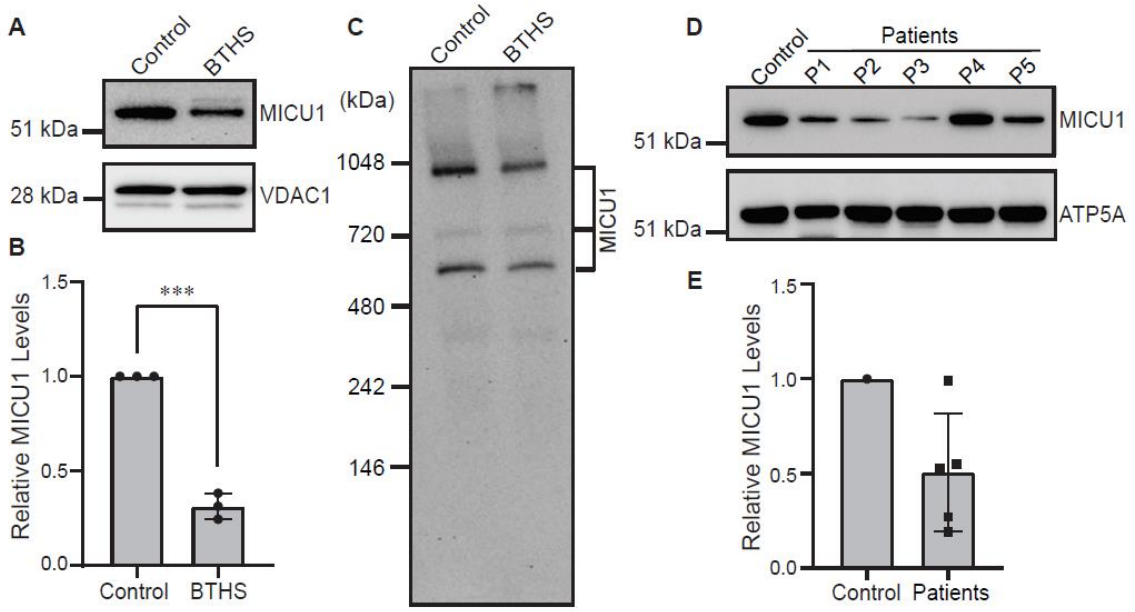

Figure 3.3 MICU1 is reduced in BTHS patient-derived B-lymphocytes and cardiac tissues

(A) SDS-PAGE immunoblot analysis of MICU1 in mitochondria isolated from control and BTHS patient B-lymphocytes. VDAC1 is used as a loading control. (B) Quantification of relative MICU1 levels using ImageJ software. Data shown as mean ± SD, n=3. ***$p < 0.0005$.

(C) BN-PAGE immunoblot analysis of MICU1 in digitonin-solubilized mitochondria from control and BTHS patient B-lymphocytes. Blot is a representative of three independent experiments. (D) SDS-PAGE immunoblot analysis of MICU1 in cardiac tissue lysates obtained from control and five BTHS patients (P1-P5). ATP5A is used as a loading control. (E) Quantification of immunoblots from (D) using ImageJ software. Data shown as mean ± SD, n=5.

MICU1-dependent mitochondrial Ca^{2+} uptake is disrupted in Taz-KO C2C12 myocytes

A decrease in MICU1 abundance predicts a reduction in MICU1-dependent Ca^{2+} uptake kinetics in *Taz-KO* C2C12 myoblasts. MICU1 has been previously shown to perform a "gatekeeper" role in mitochondrial Ca^{2+} uptake, such that under low $[Ca^{2+}]_i$ it blocks Ca^{2+} entry into the mitochondria and under high $[Ca^{2+}]_i$ it opens the MCU pore to facilitate rapid entry of Ca^{2+} into the mitochondria (Mallilankaraman et al., 2012; Csordas et al., 2013). Therefore, we measured mitochondrial Ca^{2+} uptake with increasing concentrations of exogenously added Ca^{2+}. We found that compared to WT mitochondria, at low concentrations of exogenous Ca^{2+}, BTHS mitochondria showed an increased tendency to uptake Ca^{2+} (Figure 3.4A-C) however, at higher concentrations we observed a significant reduction in mitochondrial Ca^{2+} uptake (Figure 3.4D). These results suggest a disruption in the MICU1-mediated control of the Ca^{2+} uptake threshold and cooperative activation of the MCU channel.

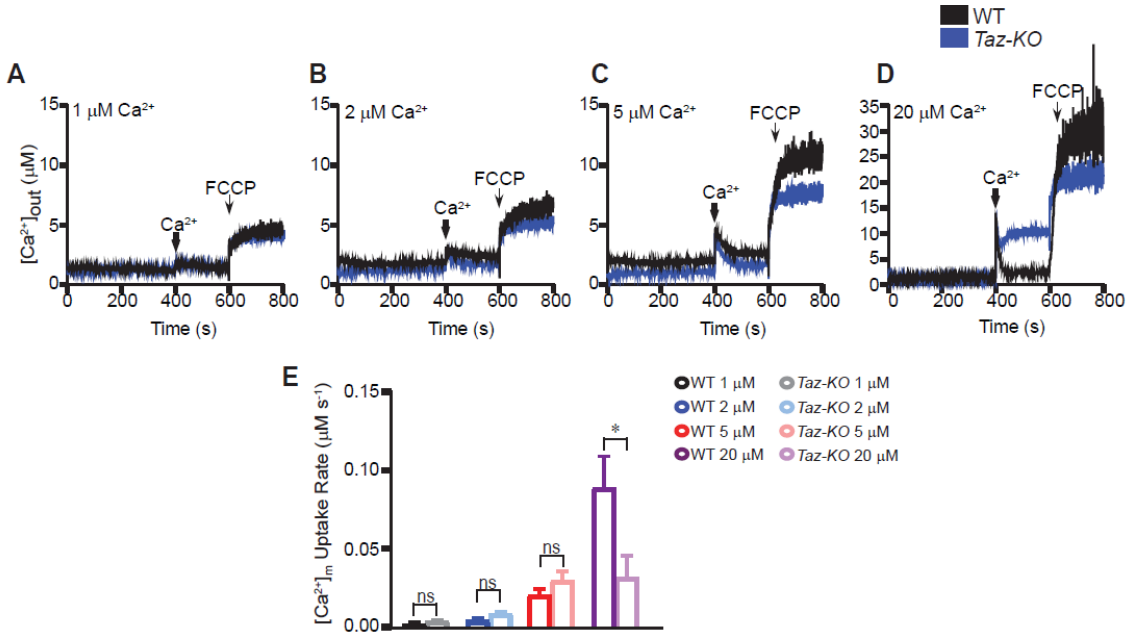

Figure 3.4 MCU-mediated mitochondrial Ca^{2+} uptake is reduced in C2C12 *Taz-KO* cells under high [Ca^{2+}]

(A-D) Permeabilized WT and *Taz-KO* C2C12 cells were pulsed with different [Ca^{2+}] as indicated. Representative traces show bath [Ca^{2+}] (μM). (E) Rate of $[Ca^{2+}]_m$ as function of MCU channel activity. Data is represented as mean ± SEM. n=3. *$p < 0.05$, ns; not significant. $[Ca^{2+}]_m$, mitochondrial Ca^{2+}.

Ca^{2+}- stimulated mitochondrial bioenergetics is disrupted in CL-deficient C2C12 cells

Mitochondrial Ca^{2+} regulates the activities of mitochondrial matrix dehydrogenases including the pyruvate dehydrogenase (PDH), α-ketoglutarate dehydrogenase, and isocitrate dehydrogenase (Kamer and Mootha, 2015). Mitochondrial matrix [Ca^{2+}] is known to stimulate the activity of the pyruvate dehydrogenase phosphatase, which dephosphorylates the E1-α subunit of the PDH complex, thereby activating the PDH enzyme. Previous studies have shown that genetic ablation of MCU in cardiac and skeletal muscle mitochondria result in increased levels of the phosphorylated form of PDH, which leads to a decrease in overall PDH activity

(Luongo et al., 2015, Pan et al., 2013). Thus, we asked whether decreased mitochondrial Ca^{2+} uptake in *Taz-KO* cells results in the accumulation of phosphorylated PDH in the mitochondria. To test this, we first validated our assay conditions and the antibodies against the phosphorylated form of PDH in C2C12 WT and *Taz-KO* cells by using a λ-phosphatase enzyme (Figure 3.5A).

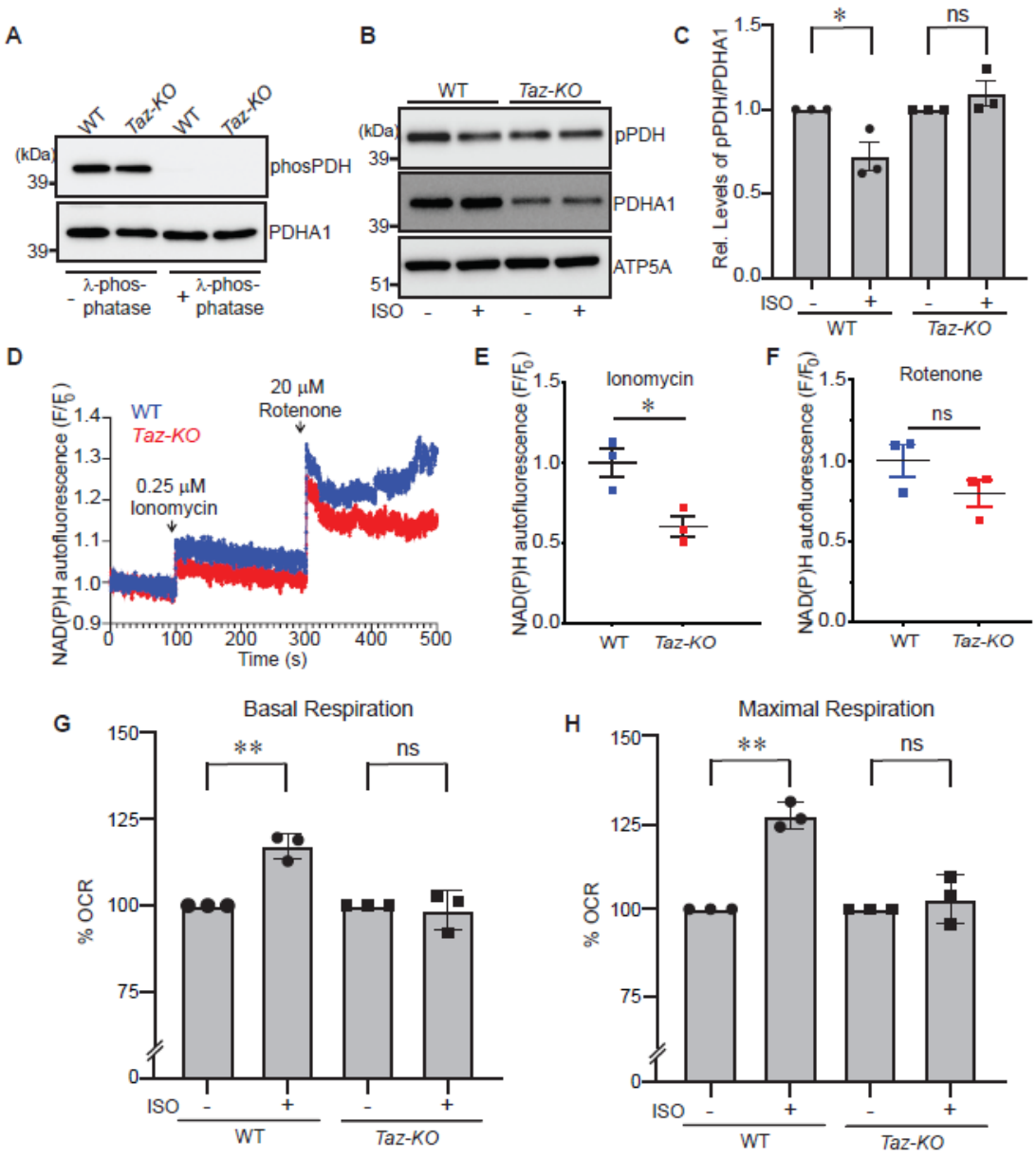

Figure 3.5 Ca^{2+}-stimulated mitochondrial bioenergetics is impaired in *Taz-KO* cells
(A) SDS-PAGE immunoblot analysis of phosphorylated PDH (pPDH) and total PDH (PDHA1) in C2C12 WT and *Taz-KO* mitochondrial lysate treated with or without λ-phosphatase for 10 mins. (B) SDS-PAGE immunoblot analysis of pPDH and total PDHA1 in mitochondria isolated from WT and *Taz-KO* myoblasts treated either with DMSO or 10 μM Isoprenaline hydrochloride (ISO) for 30 min. ATP5A is used to show equal loading. (C) Quantification of relative pPDH levels from (B) normalized to total PDHA1 by densitometry using ImageJ software. Data shown as mean ± SD. n=3. *$p < 0.05$. ns, not significant. (D) NAD(P)H fluorescence changes in WT and *Taz-KO* cells after sequential additions of ionomycin (0.25 μM) and rotenone (20 μM). (E) Quantification of ΔNAD(P)H fluorescence after ionomycin addition. (F) Quantification of ΔNAD(P)H fluorescence after rotenone addition. Data shown as mean ± SEM. n=3. *$p < 0.05$. ns, not significant. (G and H) Basal (G) and maximal (H) oxygen consumption rate (OCR) in intact WT and *Taz-KO* C2C12 cells treated with either DMSO or 10 μM ISO. Data represented as mean ± SEM (n = 15, three biological replicates each with 5 technical replicates per experiment) **$p < 0.005$. CCCP and antimycin A were used to measure maximum respiratory capacity and mitochondria-specific respiration, respectively. OCR data is reported as % OCR normalized to total protein content.

Next, we treated C2C12 WT and *Taz-KO* cells with Isoprenaline hydrochloride (ISO), a β-adrenergic agonist, known to elevate intracellular $[Ca^{2+}]_i$ followed by an increase in mitochondrial Ca^{2+} uptake (Luongo et al., 2015, Pan et al., 2013). Upon a 30 min treatment with 10 μM ISO, WT cells showed an expected decrease in the levels of PDH phosphorylation (Figure 3.5B and C). However, the *Taz-KO* cells were refractory to the mitochondrial Ca^{2+} uptake-mediated decrease in PDH phosphorylation status (Figure 3.5B and C). Additionally, we found that the overall abundance of the PDH subunit (PDHA1) was reduced and relative levels of phosphorylated PDH was higher in *Taz-KO* cells as compared to the WT cells (Figure 3.5B). These results show that mitochondrial Ca^{2+}-mediated dephosphorylation of PDH, a crucial step in the activation of PDH enzyme, is reduced in *Taz-KO* cells owing to diminished mitochondrial Ca^{2+} uptake in these cells.

Mitochondrial Ca^{2+} uptake-driven increase in the activities of matrix dehydrogenases results in an increase in mitochondrial NADH generation (Shanmughapriya et al., 2015, Luongo et al., 2015). Therefore, we measured NADH production in WT and *Taz-KO* cells after ionomycin treatment, which elevates intracellular Ca^{2+} levels, and found that NADH generation was reduced in *Taz-KO* cells compared to WT cells (Figure 3.5D and E). As expected, inhibiting NADH dehydrogenase by rotenone increased NADH signal in both WT and *Taz-KO* cells, albeit this increased NADH signal in *Taz-KO* cells was blunted (Figure 3.5F).

Elevation in mitochondrial Ca^{2+} has previously been shown to enhance mitochondrial respiration (Pan et al., 2013, Luongo et al., 2015). Therefore, we asked if reduction in the activation of PDH enzyme and a concomitant decrease in NADH generation result in a defect in mitochondrial respiration. To test this, we measured the oxygen consumption rate in intact WT and *Taz-KO* cells after stimulating them with ISO to increase $[Ca^{2+}]_i$ and subsequent mitochondrial Ca^{2+} uptake. WT cells showed a modest but significant increase in both basal and CCCP-driven maximal respiration following ISO stimulation (Figure 3.5G and H). However, CL-deficient *Taz-KO* cells were unable to stimulate either basal or maximal mitochondrial respiration following treatment with ISO (Figure 3.5G and H). This result suggests that mitochondrial Ca^{2+}-stimulated elevation in respiration following an acute stress signal is blunted in BTHS *Taz-KO* cells. Collectively, these results show that optimal levels of CL are essential for stimulating Ca^{2+}-driven mitochondrial bioenergetic functions in BTHS cells.

Discussion

Mitochondrial dysfunction caused by a decline in the levels and composition of CL is a hallmark of BTHS, an inherited X-linked genetic disorder characterized by debilitating cardiomyopathy and skeletal muscle myopathy (Clarke et al., 2013, Gaspard and McMaster 2015). Although mitochondrial and cellular functions of CL have been extensively studied (Joshi et al., 2009, Ren et al., 2014), we still do not know the full repertoire of CL-dependent mitochondrial functions that underlie BTHS disease pathogenesis (Ghosh et al., 2019). CL depletion leads to a decrease in mitochondrial energy generation and an increase in oxidative stress, both of which are regulated by mitochondrial Ca^{2+} signaling (Kamer and Mootha, 2015, Finkel et al., 2015). However, the biochemical link between CL depletion, mitochondrial Ca^{2+} signaling, and mitochondrial bioenergetics has not been determined in BTHS models. Here, we uncover the link by documenting a disruption in mitochondrial Ca^{2+} import machinery and a subsequent suppression of Ca^{2+}-stimulated mitochondrial bioenergetics in CL-depleted BTHS cells, a finding that could explain some of the clinical symptoms present in BTHS patients.

Our recent study demonstrating an essential requirement of CL for the stability and activity of MCU identified mitochondrial membrane phospholipid composition as a novel physiological determinant of the uniporter function *in vivo* (Ghosh et al., 2020). This functional study was later corroborated by a structural study, which mapped physical interactions between CL and MCU (Zhuo et al., 2021) and an *in vitro* proteoliposome-based study that demonstrated a requirement of CL for optimal MCU

activity (Wang et al., 2020). Although together these studies highlighted a critical role of CL in MCU structure and function, the requirement of CL for the other regulatory subunits of the uniporter complex and its impact on downstream mitochondrial bioenergetic pathways remained unexplored. To address these gaps in our knowledge, we utilized various CL-depleted BTHS models to uncover a requirement of CL for MICU1 stability and activity (Figures 3.1-3.4). Importantly, we show that due to reduced abundance of MCU and MICU1, BTHS cells fail to boost mitochondrial bioenergetics in response to Ca^{2+} stimulation (Figure 3.5). Our findings suggest that perturbation in mitochondrial Ca^{2+} signaling could contribute to cardiac arrhythmia and proximal muscle myopathy, typically observed in BTHS patients.

CL has previously been shown to closely interact and stabilize multiple integral inner mitochondrial membrane proteins (Musatov and Sedlak 2017). We have previously shown this to be true for MCU (Ghosh et al, 2020) but in this study, we found that the loss of CL in C2C12 *Taz-KO* cells does not affect the abundance of EMRE or MCUR1, two of the other integral membrane subunits of the uniporter complex (Figure 3.2). These observations suggest that the requirement of CL for the inner mitochondrial membrane proteins is not universal (Figure 3.2). In this study we found that CL is also required for the stability of a peripheral membrane protein like MICU1, but interestingly, its stability is independent of MCU because MICU1 turnover occurred with much faster kinetics compared to that of MCU (Figure 3.1D and E). We validated this assertion by showing that MICU1 abundance is reduced in CL-deficient *crd1*Δ yeast mitochondria, when expressed without MCU and EMRE (Figure 3.2A and B). Notably,

a previous study had shown that MICU1 could bind CL *in vitro* (Kamer et al, 2017). This *in vitro* study, together with our *in vivo* findings, jointly suggests that CL directly tethers MICU1 to the inner mitochondrial membrane and that this tethering is not mediated via MCU-MICU1 interactions. There could be important physiological consequences of the reduced abundance of MICU1, as it is the primary gatekeeper of the MCU channel that prevents mitochondrial Ca^{2+} accumulation under resting conditions.

Ca^{2+} signaling mediated up regulation of mitochondrial bioenergetics is primarily manifested by the enhanced activities of matrix dehydrogenases, such as PDH. Mitochondrial Ca^{2+} serves as a key regulator of PDH by stimulating the activity of the Ca^{2+}-dependent PDH-phosphatase, which dephosphorylates PDH, and thereby activating PDH. Utilizing protein-overlay techniques, a recent study showed that CL binds PDH (Li et al., 2019), a finding that could explain the lower baseline levels of total PDH in BTHS cells (Figure 3.5B). Interestingly, the same study showed increased levels of phosphorylated PDH in BTHS murine myoblasts, however the precise biochemical mechanism underlying the change in PDH phosphorylation status was not determined (Li et al., 2019). Our results showing ISO-based decrease in the levels of phosphorylated PDH in C2C12 WT cells, but not in *Taz-KO* cells (Figure 3.5B and C) suggests that the CL-mediated control of the PDH phosphorylation status observed in BTHS cells is likely through aberrant mitochondrial Ca^{2+} signaling.

A previous study comprising of 15 BTHS patients demonstrated diminished oxygen uptake and utilization in skeletal and cardiac muscles, when compared to age-matched controls while going from rest to peak exercise (Spencer et al., 2011). This

finding was recapitulated in a BTHS mouse model that showed significantly reduced mitochondrial oxygen consumption rates during increased workload with no changes at resting conditions (Powers et al., 2013). During aerobic exercise, β-adrenergic signaling mediates excitation-contraction coupling to stimulate mitochondrial bioenergetics in skeletal muscles by intracellular Ca^{2+} signaling (Voltarelli et al., 2021, Cairns et al., 2015, Blackwood et al., 2019). Our finding that BTHS myoblasts are unable to stimulate mitochondrial oxygen consumption in response to treatment with ISO, a β-adrenergic agonist (Figure 3.5G and H), suggests that reduced mitochondrial Ca^{2+} signaling could be responsible for the exercise intolerance defect often observed in BTHS patients. Additional evidence for the role of defective mitochondrial Ca^{2+} signaling in BTHS pathology comes from human genetic studies with MICU1 patients, who share overlapping clinical features with those seen in BTHS patients (Clarke et al., 2013, Logan et al., 2014, Lewis-Smith et al., 2016). In summary, our results highlight mitochondrial Ca^{2+} signaling as an important signaling pathway that could contribute to BTHS disease pathology.

Materials and Methods

Mammalian Cell Culture and BTHS Heart Tissue Samples

The control (ND11500) and BTHS patient (GM22194) B-lymphocytes were obtained from the Coriell Institute for Medical Research. B-lymphocytes were cultured in high glucose Roswell Park Memorial Institute (RPMI) 1640 medium supplemented with 15% fetal bovine serum (Sigma). Murine C2C12 WT and *Taz-KO* myoblasts were generously provided by Dr. Miriam L. Greenberg and were cultured in Dulbecco's Modified Eagle's

medium (DMEM) supplemented with 10% fetal bovine serum. All cell lines were incubated in 5% CO_2 at 37°C. De-identified BTHS patient heart samples were obtained from Barth syndrome Registry and DNA Bank. Whole cell protein was extracted in lysis buffer (BP-115, Boston BioProducts) supplemented with protease inhibitor cocktail (cOmplete Mini EDTA-free; Roche Diagnostics) and the protein concentrations were determined by BCA assay (Pierce™ BCA Protein Assay).

Yeast Strains and Growth Conditions

Yeast *Saccharomyces cerevisiae crd1*Δ mutant used in this study was purchased from Open Biosystems and the isogenic WT BY4741 strain was obtained from Dr. Miriam L. Greenberg. The authenticity of *crd1*Δ was confirmed by PCR, replica plating on dropout plates, and phospholipid analyses. Yeast cells were pre-cultured in YPD (1% yeast extract, 2% peptone and 2% dextrose). The final cultures were grown in synthetic complete (SC) medium, which contained 0.17% yeast nitrogen base without amino acids, 0.5% ammonium sulfate, 0.2% dropout mix containing amino acids, and 2% galactose (SC-galactose). Cells expressing MICU1 and V5-tagged MCUR1 were grown in SC-galactose histidine drop-out media and SC-galactose media supplemented with ClonNAT antibiotic, respectively, to resist plasmid curing. Growth in liquid media was measured spectrophotometrically at 600 nm. Final cultures were started at an optical density of 0.1 and were grown to late logarithmic phase at 30°C.

Mitochondria Isolation

Mitochondria from mammalian cells were isolated using the Mitochondria Isolation Kit from Abcam (110170; Abcam) and stored at -80˚C until further use. Protein

concentration was determined by BCA assay (Pierce™ BCA Protein Assay). Isolation of crude mitochondria from yeast was performed as previously described (Meisinger et al., 2006). Briefly, yeast cells grown to late logarithmic phase were pelleted and resuspended in DTT buffer (0.1 M Tris-HCl, pH 9.4, 10 mM DTT) for 20 min at 30°C. The cells in DTT buffer were pelleted by centrifugation at 3000 x g for 5 min and were resuspended in spheroplasting buffer (1.2 M sorbitol, 20 mM potassium phosphate, pH 7.4) and treated with 3 mg zymolyase (US Biological Life Sciences) per gram of cell pellet for 45 min at 30°C. Spheroplasts were homogenized in homogenization buffer (0.6 M sorbitol, 10 mM Tris-HCl, pH 7.4, 1 mM EDTA, 1 mM PMSF [Phenylmethanesulfonyl fluoride], 0.2% [w/v] BSA (fatty acid-free, Sigma-Aldrich) with 15 strokes using a glass teflon homogenizer. After subsequent centrifugation steps, the mitochondrial pellet was centrifuged at 12,000 x g for 15 min. Crude mitochondrial fractions were resuspended in SEM buffer (250 mM sucrose, 1 mM EDTA, 10 mM MOPS-KOH, pH 7.2) and stored at -80˚C.

SDS-PAGE, BN-PAGE, and Immunoblotting

Denatured and native proteins were separated using sodium dodecyl sulfate polyacrylamide gel electrophoresis (SDS-PAGE) and Blue Native PAGE (BN-PAGE), respectively. For SDS-PAGE, mitochondrial lysate (20 μg) was separated on NuPAGE 4-12% Bis-Tris gels (Thermo Fisher Scientific, Carlsbad, CA) and transferred onto polyvinylidene fluoride (PVDF) membranes using a Trans-Blot SD semi-dry transfer cell (Bio-Rad, Hercules, CA). For BN-PAGE, mitochondria were first solubilized in buffer containing 1% digitonin (Thermo Fisher Scientific, Carlsbad, CA) at 9g/g of

mammalian mitochondrial protein, followed by incubation for 15 min at 4°C and centrifugation at 20,000g for 30 min. Clear supernatant containing native protein complexes was collected and 50X G-250 sample additive was added. 20 µg of protein was loaded on 3-12% native PAGE Bis-Tris gel (Thermo Fisher Scientific, Carlsbad, CA) and transferred onto PVDF membranes using a wet transfer method. After transfer, the membranes were probed with the following primary antibodies: MICU1, 1:2,000 (12524S; Cell Signaling); MCU, 1:2,500 (14997S; Cell Signaling); VDAC1, 1:2,500 (ab14734; Abcam); and ATP5A, 1:2,500 (ab14748; Abcam). For PDH phosphorylation measurements, the following primary antibodies were used: pPDH (S293) (ab177461; Abcam) and PDHA1 (168379; Abcam). Anti-mouse or anti-rabbit secondary antibodies (1:5,000) were incubated for 1 h at room temperature, and membranes were developed using Clarity^{TM} Western ECL (Bio-Rad Laboratories).

Protein Turnover Measurement

C2C12 cells were grown in DMEM high glucose media supplemented with 10% FBS for ~14 hours. Cells were washed with PBS and treated with 10 µg/mL cycloheximide for 0, 2, 4, and 6 hours, respectively. At this point, cells were washed with PBS again and lysed using RIPA lysis buffer supplemented with 1X protease inhibitor cocktail. Total protein content of the lysate was quantified by BCA assay and 20 µg of protein was separated and detected by SDS PAGE/immunoblotting.

Mitochondrial Ca^{2+} Uptake Measurement in Permeabilized Cells

Wild type and *Taz-KO* C2C12 cells were washed with Ca^{2+} free PBS, pH 7.4. An equal number of cells (~4 X 10^6 cells) were resuspended and permeabilized with 40 µg/mL

digitonin in 1.5 mL of intracellular medium (ICM) composed of 120 mM KCl, 10 mM NaCl, 1 mM KH_2PO_4, 20 mM HEPES-Tris, pH 7.2. The experiments were performed in the presence of 5 mM succinate and 1 mM Mg-ATP at 37°C with constant stirring. For measuring mitochondrial Ca^{2+} uptake, the permeabilized cells were suspended in a medium containing 1.0 μM Fura-2FF. Fluorescence was monitored in a multiwavelength excitation, dual-wavelength emission fluorimeter (DeltaRAM, Photon Technology International). Extramitochondrial Ca^{2+} was recorded at an excitation ratio (340 nm/380 nm) and emission at 510 nm of Fura-2FF fluorescence. For individual experiments, Ca^{2+} pulses of 1 μM, 2 μM, 5 μM, and 20 μM were added at 400 s, and the changes in extramitochondrial Ca^{2+} fluorescence were monitored. Mitochondrial Ca^{2+} uptake rate was derived from the decay of bath [Ca^{2+}] after Ca^{2+} pulses.

NAD(P)H Measurement in Mammalian Cells

C2C12 WT and *Taz-KO* cells (~ 5×10^6 cells) were suspended in Hanks' balanced salt solution (Sigma). Autofluorescence of NAD(P)H was monitored at 350/460 nm (excitation/emission) using a multiwavelength excitation, dual-wavelength emission fluorimeter (DeltaRAM, Photon Technology International). These experiments were conducted at 37°C. C2C12 cells were stimulated with 0.25 μM ionomycin at 100 s after base line recording followed by 20 μM rotenone at 300 s.

PDH Phosphorylation Measurement in Mammalian Cells

C2C12 cells (~2 X 10^6) were seeded in 150 mm tissue-culture treated dishes and grown in DMEM media supplemented with 10% FBS at 37°C, 5% CO_2 for ~14 hours. At this point, cells were treated with 10 μM ISO or DMSO (vehicle) for 30 min and harvested.

Mitochondria were isolated using the Mitochondria Isolation Kit from Abcam (110170; Abcam). Proteins were extracted from the mitochondria using RIPA lysis buffer supplemented with 1X protease inhibitor cocktail (Roche) and 1X PhosSTOP phosphatase inhibitor (Roche) and the protein content was quantified by BCA Assay. Lysates (20 µg) were separated by SDS-PAGE, transferred onto PVDF membranes, and immunoblotted by the indicated primary antibodies.

Oxygen Consumption Rate Measurement in Intact Mammalian Cells

Oxygen consumption rate (OCR) measurements were carried out as previously described (Gohil et al., 2010) with minor modifications. Briefly, C2C12 WT and *Taz-KO* myoblasts were cultured in high glucose DMEM growth media supplemented with 10% FBS (Sigma) and 1 mM sodium pyruvate (Life Technologies). The cells were then seeded in XF24-well cell culture microplates (Agilent Technologies) at 10,000 cells/well in 250 µl of DMEM growth media supplemented with 10 mM galactose and incubated at 37°C, 5% CO_2 for ~16 hours. Before the oxygen consumption rate was measured, 475 µl of pre-warmed growth medium was added to each well and cells were incubated at 37°C for 30 min. OCR measurements were carried out in intact cells using Seahorse XF24 Extracellular Flux Analyzer (Agilent Technologies). Isoprenaline hydrochloride (Sigma) was injected through port A at a final concentration of 10 µM. Mix, wait and measure durations were set to 2, 3, and 2 min, respectively. For the mitochondrial stress test, oligomycin, carbonyl cyanide 3-cholorophenylhydrazone (CCCP) and antimycin A were sequentially injected through ports B, C, and D to achieve final concentrations of 1 µM, 10 µM and 1 µM, respectively. Immediately after the assay, the cell culture microplates

were washed twice with 500 µl PBS and 50 µl RIPA lysis buffer (25mM Tris. HCl pH 7.6, 150mM NaCl, 1% NP-40, 1% sodium deoxycholate, 0.1% SDS supplemented with 1X protease inhibitor cocktail) was added to each well and incubated on ice for 15 min. Protein concentration in each well was measured by BCA assay (Thermo Scientific) and the OCR values were normalized to the total protein content.

Statistical Analyses

All statistical analyses were performed using two-tailed unpaired Student's *t* test using data obtained from three independent experiments.

CHAPTER IV

CONCLUSIONS

The work described in this thesis is focused on understanding how the mitochondrial membrane phospholipid composition influences the structure and function of mitochondrial membrane proteins. I specifically focused on determining the phospholipid requirements of the inner mitochondrial membrane localized mitochondrial calcium (Ca^{2+}) uniporter complex, which imports cytosolic Ca^{2+} into the mitochondrial matrix and regulates mitochondrial bioenergetics. I primarily focused on mitochondrial Ca^{2+} uniporter (MCU), the ion-conducting pore-subunit of the multimeric uniporter complex, and MICU1, its principal regulator.

The assembly and activity of integral membrane proteins often depend on the surrounding membrane phospholipid composition (Dowhan et al., 2004, Lee 2004). Membrane lipids are known to influence integral membrane protein conformation, oligomerization, topology, stability, and activity (Dowhan et al., 2011, Harayama et al., 2018, Shevchenko et al., 2010, van Meer et al., 2008). This is achieved either through direct lipid-protein interactions or through modulation of the bulk physicochemical properties of the membrane such as viscosity, thickness, surface charge, intrinsic curvature, lipid packing density, and lateral pressure (Harayama et al., 2018, Lee et al., 2011, Ernst et al., 2018). The mitochondrial membrane phospholipid composition has previously been shown to influence mitochondrial respiratory chain biogenesis and function (Baker et al., 2016). However, the identities and role of lipid regulators of MCU

remained elusive until recently. Being an integral membrane protein, I hypothesized that MCU function can be influenced by the surrounding membrane phospholipids.

Deciphering the phospholipid requirements of MCU was challenging in part because, there is a lack of a robust *in vitro* biochemical reconstitution system in which to investigate the channel complex. I circumvented this problem by utilizing yeast, *Saccharomyces cerevisiae*, as a facile *in vivo* reconstitution system to heterologously express MCU and dissect its specific phospholipid requirements in a physiologically relevant mitochondrial membrane (Ghosh et al., 2020). Yeast served as a powerful reconstitution system, because 1) the mitochondrial phospholipid composition is highly conserved (Basu Ball et al., 2018), 2) mitochondrial phospholipid composition can be genetically and nutritionally manipulated in yeast (Baker et al., 2016), and 3) *S. cerevisiae* does not contain the uniporter machinery (Bick et al., 2012), providing a suitable system to study the effect of phospholipids on heterologously expressed MCU. I engineered isogenic yeast mutants with defined perturbations in the levels of most abundant mitochondrial phospholipids, including phosphatidylcholine (PC), phosphatidylethanolamine (PE), and cardiolipin (CL), by deleting their respective biosynthetic enzymes and identified an essential role for CL in the abundance and activity of the protozoan and human MCU. I found that the reduction in MCU levels in CL-deficient yeast was due to increased turnover of MCU, suggesting that CL is essential for MCU stability. In addition to decreased abundance of MCU, I showed that the specific activity of MCU was also reduced in CL-deficient mitochondria. Consistent with findings in yeast, I found reduced abundance of endogenous MCU in CL-depleted

murine skeletal muscle cells. These findings was in agreement with a recently released cryo-EM structure of the multimeric human MCU complex, which reported one CL and two PC molecules bound to individual MCU subunits of the complex (Zhuo et al., 2021). My functional data (Ghosh et al., 2020) and the recently published structure (Zhuo et al., 2021) jointly showed that CL provides stability and elasticity to the channel by filling in the cavity between the transmembrane helices of MCU. Although PC was identified in the structure, I found it to be dispensable for MCU assembly in yeast, suggesting that it might not play a direct role in MCU complex formation, or its loss might be compensated for by other phospholipids that are accumulated upon PC depletion (Ghosh et al., 2020). Importantly, I found that MCU abundance and activity was markedly reduced in CL-deficient mammalian cell line models as well as patient-derived cardiac tissues of Barth syndrome (BTHS), a rare and debilitating X-linked disease affecting young boys.

A reduction in the stability and activity of MCU in multiple BTHS disease models and BTHS patient-derived samples led me to ask if defective mitochondrial Ca^{2+} signaling by the uniporter complex could drive BTHS disease pathogenesis. To this end, I first determined if any of the accessory uniporter subunits required CL for their stability, activity, and assembly into the mature uniporter complex. I found reduced abundance and activity of MICU1, the principal regulator of the uniporter complex, in BTHS cellular models and patient-derived cardiac tissue. Interestingly, I found that requirement of CL for MICU1 was independent of MCU and depletion of CL in BTHS cells did not disrupt other components of the uniporter including EMRE or MCUR1.

These findings suggest that CL mediates its effect on the uniporter complex via protein:lipid interactions rather than impacting the bulk biophysical properties of mitochondrial membranes. Decreased abundance and activity of MCU and MICU1 predicted impaired mitochondrial Ca^{2+} signaling, which is triggered in response to increased cellular energy demands. Consistent with this prediction, I found that β-adrenergic stress signal failed to stimulate Ca^{2+}-dependent mitochondrial bioenergetics in BTHS cells. The failure to couple Ca^{2+}-stimulated mitochondrial bioenergetics to increased cellular energy demands provides biochemical basis of clinical defects observed in BTHS patients such as exercise intolerance and muscle myopathy.

While uncovering the biochemical bases for clinal defects observed in BTHS, I became interested in neutropenia, another important pathological feature observed in ~70% of all BTHS patients registered to date (Jefferies 2013). However, the biochemical basis of neutropenia in BTHS remains unclear. To uncover a mechanistic link, I initiated collaboration with Dr. Scot C. Leary's Lab at University of Saskatchewan, Saskatoon, Canada. Dr. Leary's lab has recently identified an immunosuppressive factor, α-fetoprotein (AFP), which is secreted in response to mitochondrial dysfunction in mouse liver and heart and causes peripheral white blood cell deficiency. Although known to primarily have a hepatic origin, I found that AFP synthesis was cell autonomous and was expressed in multiple cell types, including skeletal muscles, fibroblasts, and lymphoblasts, and its expression increased in response to pharmacological inhibition of mitochondrial respiratory chain. These findings raised the hypothesis that elevated AFP could be the cause of neutropenia in BTHS patients. Utilizing a murine skeletal muscle

cell model of BTHS, I found that AFP levels were indeed increased in BTHS cells compared to wild type cells.

Future Directions

One of the major contributions of my thesis research was the development of yeast *Saccharomyces cerevisiae* phospholipid mutants as a facile *in vivo* reconstitution system to identify the lipid requirements of non-native mitochondrial membrane proteins. Yeast offers following advantages over currently used biophysical techniques to probe for phospholipid requirements of membrane proteins: 1) phospholipid requirements can be probed in a physiologically relevant mitochondrial membrane milieu, 2) it does not require complex preparatory steps including purification of integral membrane proteins, and 3) it does not involve the use of non-native lipids or non-physiological concentrations of lipids that might often give misleading results. The mitochondrial membrane phospholipid composition of yeast is highly conserved, which can tolerate large perturbations without a loss of viability or gross ultrastructural change to the mitochondria. Thus, yeast phospholipid mutants can be leveraged to uncover the lipid requirements of other mitochondrial ion channels and membrane proteins. In short term, the yeast system could be used to elucidate the assembly of the uniporter complex and determine the function of MCUb, one of the least studied subunit of the complex.

My work established an *in vivo* requirement of CL for MICU1 in multiple model systems, which now raises the obvious next question: what are the precise molecular interactions between CL and MICU1? To identify specific MICU:CL interactions, Ion Mobility Mass Spectrometry (IM-MS) could be used, which measures collision induced

unfolding of membrane protein complexes in the gas phase, where resistance to unfolding correlates with specific lipid-binding events (Liu et al., 2017). IM-MS enables the identification of distinct lipid-protein interactions that might modulate the function of MICU1 from a host of lipids that merely bind to these proteins (Liu et al., 2017). Consequently, a functional analysis of the resultant MICU1:CL interactions could be performed by using mutated proteins and measuring their Ca^{2+}-conducting activities. In addition to phospholipid:protein interactions, IM-MS would also allow us to identify if CL is required for any protein-protein interactions between the uniporter subunits that facilitate their hetero-oligomeric modular assemblies, a process that remains largely unclear. Along the same lines, the application of BN-PAGE and gel-filtration on knockout cell lines of uniporter subunits could be used to determine the composition of various oligomeric assemblies and elucidate the assembly pathway of this multimeric complex. These studies in conjunction with the yeast heterologous system could help identify any mammalian-specific factors that are needed for building or regulating the uniporter complex.

My finding that Ca^{2+}-dependent mitochondrial bioenergetics is impaired in BTHS models motivates animal studies to understand the physiological consequences of impaired Ca^{2+}-signaling in BTHS pathology. Measurement of various Ca^{2+}-dependent physiological parameters of the cardiac and skeletal muscle function, including ventricular dysfunction, cardiac arrhythmia, muscle hypertrophy, force production, and muscle growth and wasting, in BTHS mice will shed light on clinical features seen in BTHS patients. Understanding these processes will allow development of therapeutic

approaches or symptom management regimens for BTHS patients, for which currently no treatment option is available.

REFERENCES

Abelev GI. (1971). Alpha-fetoprotein in ontogenesis and its association with malignant tumors. Adv Cancer Res. 14, 295-358.

Acehan D, Vaz F, Houtkooper RH, James J, Moore V, Tokunaga C, Kulik W, Wansapura J, Toth MJ, Strauss A, Khuchua Z. (2011). Cardiac and skeletal muscle defects in a mouse model of human Barth syndrome. J Biol Chem. 286, 899–908.

Alevriadou BR, Patel A, Noble M, Ghosh S, Gohil VM, Stathopulos PB, Madesh M. (2021). Molecular nature and physiological role of the mitochondrial calcium uniporter channel. Am J Physiol Cell Physiol. 320, C465-C482.

Baile MG, Sathappa M, Lu YW, Pryce E, Whited K, McCaffery JM, Han X, Alder NN, Claypool SM. (2014). Unremodeled and remodeled cardiolipin are functionally indistinguishable in yeast. J Biol Chem. 289, 1768–1778.

Baker CD, Basu Ball W, Pryce EN, Gohil VM. (2016). Specific requirements of nonbilayer phospholipids in mitochondrial respiratory chain function and formation. Mol Biol Cell. 27, 2161–2171.

Ban T, Ishihara T, Kohno H, Saita S, Ichimura A, Maenaka K, Oka T, Mihara K, Ishihara N. (2017). Molecular basis of selective mitochondrial fusion by heterotypic action between OPA1 and cardiolipin. Nat Cell Biol. 19, 856–863.

Baradaran R, Wang C, Siliciano AF, Long SB. (2018). Cryo-EM structures of fungal and metazoan mitochondrial calcium uniporters. Nature. 559, 580–584.

Barth PG, Scholte HR, Berden JA, van der Klei-van Moorsel JM, Luyt-Houwen IE, Van't Veer-Korthof ET, Van der Harten JJ, Sobotka-Plojhar MA. (1983) An X-linked mitochondrial disease affecting cardiac muscle, skeletal muscle and neutrophil leucocytes. J Neurol Sci. 62, 327–355.

Barth PG, Van Den Bogert C, Bolhuis PA, Scholte HR, Van Gennip AH, Schutgens RB, Ketel AG. (1996). X-linked cardioskeletal myopathy and neutropenia (Barth syndrome): respiratory-chain abnormalities in cultured fibroblasts. J Inherit Metab Dis. 19, 157–160.

Bartlett GR. (1959). Phosphorus assay in column chromatography. J Biol Chem. 234, 466–468.

Basu Ball W, Baker CD, Neff JK, Apfel GL, Lagerborg KA, Žun G, Petrovič U, Jain M, Gohil VM. (2018). Ethanolamine ameliorates mitochondrial dysfunction in cardiolipin-deficient yeast cells. J Biol Chem. 293, 10870–10883.

Basu Ball W, Neff JK, Gohil VM. (2018). The role of non-bilayer phospholipids in mitochondrial structure and function. FEBS Lett. 592, 1273–1290.

Baughman JM, Perocchi F, Girgis HS, Plovanich M, Belcher-Timme CA, Sancak Y, Bao XR, Strittmatter L, Goldberger O, Bogorad RL, Koteliansky V, Mootha VK. (2011). Integrative genomics identifies MCU as an essential component of the mitochondrial calcium uniporter. Nature. 476, 341–345.

Bazán S, Mileykovskaya E, Mallampalli VK, Heacock P, Sparagna GC, Dowhan W. (2013). Cardiolipin-dependent reconstitution of respiratory supercomplexes from purified Saccharomyces cerevisiae complexes III and IV. J Biol Chem. 288, 401–411.

Belayew A, Tilghman SM. (1982). Genetic analysis of alpha-fetoprotein synthesis in mice. Mol Cell Biol. 2, 1427-1435.

Beranek A, Rechberger G, Knauer H, Wolinski H, Kohlwein SD, Leber R. (2009). Identification of a Cardiolipin-specific phospholipase encoded by the gene CLD1 (YGR110W) in yeast. J Biol Chem. 284, 11572–11578.

Bick AG, Calvo SE, Mootha VK. (2012). Evolutionary diversity of the mitochondrial calcium uniporter. Science. 336, 886.

Bick AG, Wakimoto H, Kamer KJ, Sancak Y, Goldberger O, Axelsson A, DeLaughter DM, Gorham JM, Mootha VK, Seidman JG, Seidman CE. (2017). Cardiovascular homeostasis dependence on MICU2, a regulatory subunit of the mitochondrial calcium uniporter. Proc Natl Acad Sci USA. 114, E9096–E9104.

Bione S, D'Adamo P, Maestrini E, Gedeon AK, Bolhuis PA, Toniolo D. (1996). A novel X-linked gene, G4.5. is responsible for Barth syndrome. Nat Genet. 12, 385–389.

Bissler JJ, Tsoras M, Göring HH, Hug P, Chuck G, Tombragel E, McGraw C, Schlotman J, Ralston MA, Hug G. (2005). Infantile dilated X-linked cardiomyopathy, G4.5 mutations, altered lipids, and ultrastructural malformations of mitochondria in heart, liver, and skeletal muscle. Lab Invest. 82, 335–344.

Blackwood SJ, Katz A. (2019). Isoproterenol enhances force production in mouse glycolytic and oxidative muscle via separate mechanisms. Pflugers Arch. 471, 1305-1316.

Blumson NJ, Gomez-Espinosa E, Ashlin TG, Cockcroft S. (2018). Mitochondrial CDP-diacylglycerol synthase activity is due to the peripheral protein, TAMM41 and not due to the integral membrane protein, CDP diacylglycerol synthase 1. Biochim Biophys Acta Mol Cell Biol Lipids. 1863, 284–298.

Böttinger L, Horvath SE, Kleinschroth T, Hunte C, Daum G, Pfanner N, Becker T. (2012). Phosphatidylethanolamine and cardiolipin differentially affect the stability of mitochondrial respiratory chain supercomplexes. J Mol Biol. 423, 677–686.

Bowron A, Honeychurch J, Williams M, Tsai-Goodman B, Clayton N, Jones L, Shortland GJ, Qureshi SA, Heales SJR, Steward CG. (2015). Barth syndrome without tetralinoleoyl cardiolipin deficiency: a possible ameliorated phenotype. J Inherit Metab Dis. 38, 279–286.

Brandner K, Mick DU, Frazier AE, Taylor RD, Meisinger C, Rehling P. (2005). Taz1, an outer mitochondrial membrane protein, affects stability and assembly of inner membrane protein complexes: implications for Barth syndrome. Mol Biol Cell 16, 5202–5214.

Brini M, Calì T, Ottolini D, Carafoli E. (2014). Neuronal calcium signaling: function and dysfunction. Cell Mol Life Sci. 71, 2787–2814.

Brini M, Manni S, Pierobon N, Du GG, Sharma P, MacLennan DH, Carafoli E. (2005). Ca2+ signaling in HEK-293 and skeletal muscle cells expressing recombinant ryanodine receptors harboring malignant hyperthermia and central core disease mutations. J Biol Chem. 280, 15380–15389.

Cadalbert LC, Ghaffar FN, Stevenson D, Bryson S, Vaz FM, Gottlieb E, Strathdee D. (2015). Mouse Tafazzin is required for male germ cell meiosis and spermatogenesis. PLoS One. 10, e0131066.

Cairns SP, Borrani F. (2015). β-Adrenergic modulation of skeletal muscle contraction: key role of excitation-contraction coupling. J Physiol. 593, 4713-4727.

Calvo-Rodriguez M, Hou SS, Snyder AC, Kharitonova EK, Russ AN, Das S, Fan Z, Muzikansky A, Garcia-Alloza M, Serrano-Pozo A, Hudry E, Bacskai BJ. (2018). Increased mitochondrial calcium levels associated with neuronal death in a mouse model of Alzheimer's disease. Nat Commun. 11, 2146.

Chen E, Kiebish MA, McDaniel J, Niedzwiecka K, Kucharczyk R, Ravasz D, Gao F, Narain NR, Sarangarajan R, Seyfried TN, Adam-Vizi V, Chinopoulos C. (2018). Perturbation of the yeast mitochondrial lipidome and associated membrane proteins following heterologous expression of Artemia-ANT. Sci Rep. 8, 5915.

Clapham DE. (2007). Calcium signaling. Cell. 131, 1047–1058.

Clarke SL, Bowron A, Gonzalez IL, Groves SJ, Newbury-Ecob R, Clayton N, Martin RP, Tsai-Goodman B, Garratt V, Ashworth M, Bowen VM, McCurdy KR, Damin MK, Spencer CT, Toth MJ, Kelley RI, Steward CG. (2013). Barth syndrome. Orphanet J Rare Dis. 8, 23.

Claypool SM, Oktay Y, Boontheung P, Loo JA, Koehler CM. (2008). Cardiolipin defines the interactome of the major ADP/ATP carrier protein of the mitochondrial inner membrane. J Cell Biol. 182, 937–950.

Csordás G, Golenár T, Seifert EL, Kamer KJ, Sancak Y, Perocchi F, Moffat C, Weaver D, Perez SF, Bogorad R, Koteliansky V, Adijanto J, Mootha VK, Hajnóczky G. (2013). MICU1 controls both the threshold and cooperative activation of the mitochondrial Ca^{2+} uniporter. Cell Metab. 17, 976-987.

Cui TZ, Conte A, Fox JL, Zara V, Winge DR. (2014). Modulation of the respiratory supercomplexes in yeast: enhanced formation of cytochrome oxidase increases the stability and abundance of respiratory supercomplexes. J Biol Chem. 289, 6133–6141.

De Stefani D, Raffaello A, Teardo E, Szabò I, Rizzuto R. (2011). A forty-kilodalton protein of the inner membrane is the mitochondrial calcium uniporter. Nature. 476, 336–340.

Debattisti V, Horn A, Singh R, Seifert EL, Hogarth MW, Mazala DA, Huang KT, Horvath R, Jaiswal JK, Hajnóczky G. (2019). Dysregulation of mitochondrial Ca^{2+} uptake and sarcolemma repair underlie muscle weakness and wasting in patients and mice lacking MICU1. Cell Rep. 29, 1274–1286.

DeVay RM, Dominguez-Ramirez L, Lackner LL, Hoppins S, Stahlberg H, Nunnari J. (2009). Coassembly of Mgm1 isoforms requires cardiolipin and mediates mitochondrial inner membrane fusion. J Cell Biol. 186, 793–803.

Dowhan W, Bogdanov M. (2011). Lipid-protein interactions as determinants of membrane protein structure and function. Biochem Soc Trans. 39, 767–774.

Dowhan W, Mileykovskaya E, Bogdanov M. (2004). Diversity and versatility of lipid-protein interactions revealed by molecular genetic approaches. Biochim Biophys Acta. 1666, 19–39.

Drago I, Davis RL. (2016). Inhibiting the mitochondrial calcium uniporter during development impairs memory in adult *Drosophila*. Cell Rep. 16, 2763–2776.

Drago I, De Stefani D, Rizzuto R, Pozzan T. (2012). Mitochondrial Ca^{2+} uptake contributes to buffering cytoplasmic Ca^{2+} peaks in cardiomyocytes. Proc Natl Acad Sci USA. 109, 12986–12991.

Dudek J, Cheng IF, Balleininger M, Vaz FM, Streckfuss-Bomeke K, Hübscher D, Vukotic M, Wanders RJA, Rehling P, Guan K. (2013). Cardiolipin deficiency affects respiratory chain function and organization in an induced pluripotent stem cell model of Barth syndrome. Stem Cell Res. 11, 806–819.

Dudek J, Cheng IF, Chowdhury A, Wozny K, Balleininger M, Reinhold R, Grunau S, Callegari S, Toischer K, Wanders RJ, Hasenfuß G, Brügger B, Guan K, Rehling P. (2016). Cardiac-specific succinate dehydrogenase deficiency in Barth syndrome. EMBO Mol Med. 8, 139–154.

Eisner V, Csordás G, Hajnóczky G. (2013). Interactions between sarcoendoplasmic reticulum and mitochondria in cardiac and skeletal muscle-pivotal roles in Ca^{2+} and reactive oxygen species signaling. J Cell Sci. 126, 2965–2978.

Ernst R, Ballweg S, Levental I. (2018). Cellular mechanisms of physicochemical membrane homeostasis. Curr Opin Cell Biol. 53, 44–51.

Fan M, Zhang J, Tsai CW, Orlando BJ, Rodriguez M, Xu Y, Liao M, Tsai MF, Feng L. (2020). Structure and mechanism of the mitochondrial Ca^{2+} uniporter holocomplex. Nature. 582, 129–133.

Fieni F, Lee SB, Jan YN, Kirichok Y. (2012). Activity of the mitochondrial calcium uniporter varies greatly between tissues. Nat Commun. 3, 1317.

Finkel T, Menazza S, Holmström KM, Parks RJ, Liu J, Sun J, Liu J, Pan X, Murphy E. (2015). The ins and outs of mitochondrial calcium. Circ Res. 116, 1810-1819.

Flarsheim CE, Grupp IL, Matlib MA. (1996). Mitochondrial dysfunction accompanies diastolic dysfunction in diabetic rat heart. Am J Physiol Heart Circ Physiol. 271, H192–H202.

Folch J, Lees M, Stanley GHS. (1957). A simple method for the isolation and purification of total lipides from animal tissues. J Biol Chem. 226, 497–509.

Francy CA, Clinton RW, Fröhlich C, Murphy C, Mears JA. (2017). Cryo-EM studies of Drp1 reveal cardiolipin interactions that activate the helical oligomer. Sci Rep. 7, 10744.

Friedman JR, Mourier A, Yamada J, McCaffery JM, Nunnari J. (2015). MICOS coordinates with respiratory complexes and lipids to establish mitochondrial inner membrane architecture. Elife. 28, 4.

Gaspard GJ, McMaster CR. (2015). Cardiolipin metabolism and its causal role in the etiology of the inherited cardiomyopathy Barth syndrome. Chem Phys Lipids. 193, 1–10.

Ghosh S, Basu Ball W, Madaris TR, Srikantan S, Madesh M, Mootha VK, Gohil VM. (2020). An essential role for cardiolipin in the stability and function of the mitochondrial calcium uniporter. Proc Natl Acad Sci USA. 117, 16383-16390.

Ghosh S, Iadarola DM, Basu Ball W, Gohil VM. (2019). Mitochondrial dysfunctions in Barth syndrome. IUBMB Life. 71, 791-801.

Gohil VM and Greenberg ML. (2009). Mitochondrial membrane biogenesis: phospholipids and proteins go hand in hand. J Cell Biol. 184, 469-472.

Gohil VM, Sheth SA, Nilsson R, Wojtovich AP, Lee JH, Perocchi F, Chen W, Clish CB, Ayata C, Brookes PS, Mootha VK. (2010). Nutrient-sensitized screening for drugs that shift energy metabolism from mitochondrial respiration to glycolysis. Nat Biotechnol. 28, 249-255.

Gohil VM, Thompson MN, Greenberg ML. (2005). Synthetic lethal interaction of the mitochondrial phosphatidylethanolamine and cardiolipin biosynthetic pathways in *Saccharomyces cerevisiae*. J Biol Chem. 280, 35410–35416.

Gottschalk B, Klec C, Leitinger G, Bernhart E, Rost R, Bischof H, Madreiter-Sokolowski CT, Radulović S, Eroglu E, Sattler W, Waldeck-Weiermair M, Malli R, Graier WF. (2019). MICU1 controls cristae junction and spatially anchors mitochondrial Ca^{2+} uniporter complex. Nat Commun. 10, 3732.

Griffiths EJ, Rutter GA. (2009). Mitochondrial calcium as a key regulator of mitochondrial ATP production in mammalian cells. Biochim Biophys Acta. 1787, 1324–1333.

Gu Z, Valianpour F, Chen S, Vaz FM, Hakkaart GA, Wanders RJA, Greenberg ML. (2004). Aberrant cardiolipin metabolism in the yeast *taz1* mutant: a model for Barth syndrome. Mol Microbiol. 51, 149–158.

Hajnóczky G, Csordás G, Das S, Garcia-Perez C, Saotome M, Roy SS, Yi M. (2006). Mitochondrial calcium signalling and cell death: approaches for assessing the role of mitochondrial Ca^{2+} uptake in apoptosis. Cell Calcium. 40, 553-560.

Harayama T, Riezman H. (2018). Understanding the diversity of membrane lipid composition. Nat Rev Mol Cell Biol. 19, 281–296.

Horn A, Van der Meulen JH, Defour A, Hogarth M, Sreetama SC, Reed A, Scheffer L, Chandel NS, Jaiswal JK. (2017). Mitochondrial redox signaling enables repair of injured skeletal muscle cells. Sci Signal. 10, eaaj1978.

Horvath SE and Daum G. (2013). Lipids of mitochondria. Prog Lipid Res. 52, 590-614.

Jefferies JL. (2013). Barth syndrome. Am J Med Genet C Semin Med Genet. 163C, 198-205.

Jiang F, Ryan MT, Schlame M, Zhao M, Gu Z, Klingenberg M, Pfanner N, Greenberg ML. (2000). Absence of cardiolipin in the crd1 null mutant results in decreased mitochondrial membrane potential and reduced mitochondrial function. J Biol Chem. 275, 22387–22394.

Jiang F, Ryan MT, Schlame M, Zhao M, Gu Z, Klingenberg M, Pfanner N, Greenberg ML. (2000). Absence of cardiolipin in the crd1 null mutant results in decreased mitochondrial membrane potential and reduced mitochondrial function. J Biol Chem. 275, 22387–22394.

Johnston J, Kelley RI, Feigenbaum A, Cox GF, Iyer GS, Funanage VL, Proujansky R. (1997). Mutation characterization and genotype-phenotype correlation in Barth syndrome. Am J Hum Genet. 61, 1053–1058.

Joshi AS, Zhou J, Gohil VM, Chen S, Greenberg ML. (2009). Cellular functions of cardiolipin in yeast. Biochim Biophys Acta. 1793, 212-218.

Kamer KJ, Grabarek Z, Mootha VK. (2017). High-affinity cooperative Ca^{2+} binding by MICU1-MICU2 serves as an on-off switch for the uniporter. EMBO Rep. 18, 1397-1411.

Kamer KJ, Mootha VK. (2015). The molecular era of the mitochondrial calcium uniporter. Nat Rev Mol Cell Biol. 16, 545–553.

Khuchua Z, Yue Z, Batts L, Strauss AW. (2006). A zebrafish model of human Barth syndrome reveals the essential role of tafazzin in cardiac development and function. Circ Res. 99, 201–208.

Kiebish MA, Yang K, Liu X, Mancuso DJ, Guan S, Zhao Z, Sims HF, Cerqua R, Cade WT, Han X, Gross RW. (2013). Dysfunctional cardiac mitochondrial bioenergetic, lipidomic, and signaling in a murine model of Barth syndrome. J Lipid Res. 54, 1312–1325.

Koshkin V, Greenberg ML. (2002). Cardiolipin prevents rate-dependent uncoupling and provides osmotic stability in yeast mitochondria. Biochem J. 364, 317–322.

Kovács-Bogdán E, Sancak Y, Kamer KJ, Plovanich M, Jambhekar A, Huber RJ, Myre MA, Blower MD, Mootha VK. (2014). Reconstitution of the mitochondrial calcium uniporter in yeast. Proc Natl Acad Sci USA. 111, 8985–8990.

Krumlauf R, Chapman VM, Hammer RE, Brinster R, Tilghman SM. (1986). Differential expression of alpha-fetoprotein genes on the inactive X chromosome in extraembryonic and somatic tissues of a transgenic mouse line. Nature. 319, 224-226.

Kuo TH, Zhu L, Golden K, Marsh JD, Bhattacharya SK, Liu BF. (2002). Altered Ca^{2+} homeostasis and impaired mitochondrial function in cardiomyopathy. Mol Cell Biochem. 238, 119–127.

Kwong JQ, Lu X, Correll RN, Schwanekamp JA, Vagnozzi RJ, Sargent MA, York AJ, Zhang J, Bers DM, Molkentin JD. (2015). The mitochondrial calcium uniporter selectively matches metabolic output to acute contractile stress in the heart. Cell Rep. 12, 15-22.

Lee AG. (2004). How lipids affect the activities of integral membrane proteins. Biochim Biophys Acta. 1666, 62–87.

Lee AG. (2011). Lipid-protein interactions. Biochem Soc Trans. 39, 761–766.

Lee KS, Huh S, Lee S, Wu Z, Kim AK, Kang HY, Lu B. (2018). Altered ER-mitochondria contact impacts mitochondria calcium homeostasis and contributes to neurodegeneration *in vivo* in disease models. Proc Natl Acad Sci USA. 115, E8844–E8853.

Lewis-Smith D, Kamer KJ, Griffin H, Childs AM, Pysden K, Titov D, Duff J, Pyle A, Taylor RW, Yu-Wai-Man P, Ramesh V, Horvath R, Mootha VK, Chinnery PF.

(2016). Homozygous deletion in MICU1 presenting with fatigue and lethargy in childhood. Neurol Genet. 2, e59.

Li Y, Lou W, Raja V, Denis S, Yu W, Schmidtke MW, Reynolds CA, Schlame M, Houtkooper RH, Greenberg ML. (2019). Cardiolipin-induced activation of pyruvate dehydrogenase links mitochondrial lipid biosynthesis to TCA cycle function. J Biol Chem. 294, 11568-11578.

Liu Y, Cong X, Liu W, Laganowsky A. (2017). Characterization of membrane protein-lipid interactions by mass spectrometry ion mobility mass spectrometry. J Am Soc Mass Spectrom. 28, 579-586.

Logan CV, Szabadkai G, Sharpe JA, Parry DA, Torelli S, Childs AM, Kriek M, Phadke R, Johnson CA, Roberts NY, Bonthron DT, Pysden KA, Whyte T, Munteanu I, Foley AR, Wheway G, Szymanska K, Natarajan S, Abdelhamed ZA, Morgan JE, Roper H, Santen GWE, Niks EH, van der Pol WL, Lindhout D, Raffaello A, De Stefani D, den Dunnen JT, Sun Y, Ginjaar I, Sewry CA, Hurles M, Rizzuto R, UK10K Consortium; Duchen MR, Muntoni F, Sheridan E. (2014). Loss-of-function mutations in MICU1 cause a brain and muscle disorder linked to primary alterations in mitochondrial calcium signaling. Nat Genet. 46, 188–193.

Lou W, Reynolds CA, Li Y, Liu J, Hüttemann M, Schlame M, Stevenson D, Strathdee D, Greenberg ML. (2018). Loss of tafazzin results in decreased myoblast differentiation in C2C12 cells: A myoblast model of Barth syndrome and cardiolipin deficiency. Biochim Biophys Acta Mol Cell Biol Lipids. 1863, 857–865.

Lu FH, Fu SB, Leng X, Zhang X, Dong S, Zhao YJ, Ren H, Li H, Zhong X, Xu CQ, Zhang WH. (2013). Role of the calcium-sensing receptor in cardiomyocyte apoptosis via the sarcoplasmic reticulum and mitochondrial death pathway in cardiac hypertrophy and heart failure. Cell Physiol Biochem. 31, 728–743.

Luongo TS, Lambert JP, Yuan A, Zhang X, Gross P, Song J, Shanmughapriya S, Gao E, Jain M, Houser SR, Koch WJ, Cheung JY, Madesh M, Elrod JW. (2015). The mitochondrial calcium uniporter matches energetic supply with cardiac workload during stress and modulates permeability transition. Cell Rep. 12, 23–34.

M'Angale PG, Staveley BE. (2017). Inhibition of mitochondrial calcium uptake 1 in *Drosophila* neurons. Genet Mol Res. 16.

Ma L, Vaz FM, Gu Z, Wanders RJ, Greenberg ML. (2004). The human *TAZ* gene complements mitochondrial dysfunction in the yeast *taz1*Δ mutant. Implications for Barth syndrome. J Biol Chem. 279, 44394–44399.

Malhotra A, Edelman-Novemsky I, Xu Y, Plesken H, Ma J, Schlame M, Ren M. (2009). Role of calcium-independent phospholipase A_2 in the pathogenesis of Barth syndrome. Proc Natl Acad Sci USA. 106, 2337–2341.

Mallilankaraman K, Doonan P, Cardenas C, Chandramoorthy HC, Muller M, Miller R, Hoffman NE, Gandhirajan RK, Molgo J, Birnbaum MJ, Rothberg BS, Mak DO, Foskett JK, Madesh M. (2012). MICU1 is an essential gatekeeper for MCU-mediated mitochondrial Ca^{2+} uptake that regulates cell survival. Cell. 151, 630–644.

Mammucari C, Gherardi G, Zamparo I, Raffaello A, Boncompagni S, Chemello F, Cagnin S, Braga A, Zanin S, Pallafacchina G, Zentilin L, Sandri M, De Stefani D, Protasi F, Lanfranchi G, Rizzuto R. (2015). The mitochondrial calcium uniporter controls skeletal muscle trophism *in vivo*. Cell Rep. 10, 1269–1279.

Mammucari C, Raffaello A, Vecellio Reane D, Gherardi G, De Mario A, Rizzuto R. (2018). Mitochondrial calcium uptake in organ physiology from molecular mechanism to animal models. Pflugers Arch-Eur J Physiol. 470, 1165–1179.

McKenzie M, Lazarou M, Thorburn DR, Ryan MT. (2006). Mitochondrial respiratory chain supercomplexes are destabilized in Barth syndrome patients. J Mol Biol. 361, 462–469.

Meisinger C, Pfanner N, Truscott KN. (2006). Isolation of yeast mitochondria. Methods Mol Biol. 313, 33–39.

Mileykovskaya E, Penczek PA, Fang J, Mallampalli VK, Sparagna GC, Dowhan W. (2012). Arrangement of the respiratory chain complexes in Saccharomyces cerevisiae supercomplex III_2IV_2 revealed by single particle cryo-electron microscopy. J Biol Chem. 287, 23095–23103.

Mink JW, Blumenschine RJ, Adams DB. (1981). Ratio of central nervous system to body metabolism in vertebrates: its constancy and functional basis. Am J Physiol Regul Integr Comp Physiol. 241, R203–R212.

Musatov A, Sedlák E. (2017). Role of cardiolipin in stability of integral membrane proteins. Biochimie. 142, 102–111.

Nakano Y, Nakao S, Sumiyoshi H, Mikami K, Tanno Y, Sueoka M, Kasahara D, Kimura H, Moro T, Kamiya A, Hozumi K, Inagaki Y. (2017). Identification of a novel alpha-fetoprotein-expressing cell population induced by the Jagged1/Notch2 signal in murine fibrotic liver. Hepatol Commun. 1, 215-229.

Paillard M, Csordás G, Szanda G, Golenár T, Debattisti V, Bartok A, Wang N, Moffat C, Seifert EL, Spät A, Hajnóczky G. (2017). Tissue-specific mitochondrial decoding of cytoplasmic Ca^{2+} signals is controlled by the stoichiometry of MICU1/2 and MCU. Cell Rep. 18, 2291–2300.

Pan X, Liu J, Nguyen T, Liu C, Sun J, Teng Y, Fergusson MM, Rovira II, Allen M, Springer DA, Aponte AM, Gucek M, Balaban RS, Murphy E, Finkel T. (2013). The physiological role of mitochondrial calcium revealed by mice lacking the mitochondrial calcium uniporter. Nat Cell Biol. 15, 1464–1472.

Pchitskaya E, Popugaeva E, Bezprozvanny I. (2018). Calcium signaling and molecular mechanisms underlying neurodegenerative diseases. Cell Calcium. 70, 87–94.

Perincheri S, Cameron Dingle RW, Peterson ML, Spear BT. (2005). Hereditary persistence of alpha-fetoprotein and *H19* expression in liver of BALB/cJ mice is due to a retrovirus insertion in the *Zhx2* gene. Proc Natl Acad Sci USA. 102, 396-401.

Perocchi F, Gohil VM, Girgis HS, Bao XR, McCombs JE, Palmer AE, Mootha VK. (2010). MICU1 encodes a mitochondrial EF hand protein required for Ca^{2+} uptake. Nature. 467, 291–296.

Pfeiffer K, Gohil V, Stuart RA, Hunte C, Brandt U, Greenberg ML, Schägger H. (2003). Cardiolipin stabilizes respiratory chain supercomplexes. J Biol Chem. 278, 52873–52880.

Phillips CB, Tsai CW, Tsai MF. (2019). The conserved aspartate ring of MCU mediates MICU1 binding and regulation in the mitochondrial calcium uniporter complex. Elife. 8, e41112.

Phoon CK, Acehan D, Schlame M, Stokes DL, Edelman-Novemsky I, Yu D, Xu Y, Viswanathan N, Ren M. (2012). Tafazzin knockdown in mice leads to a developmental cardiomyopathy with early diastolic dysfunction preceding myocardial noncompaction. J Am Heart Assoc. 1, 1–13.

Plovanich M, Bogorad RL, Sancak Y, Kamer KJ, Strittmatter L, Li AA, Girgis HS, Kuchimanchi S, De Groot J, Speciner L, Taneja N, Oshea J, Koteliansky V, Mootha VK. (2013). MICU2, a paralog of MICU1, resides within the mitochondrial uniporter complex to regulate calcium handling. PLoS One. 8, e55785.

Powers C, Huang Y, Strauss A, Khuchua Z. (2013). Diminished exercise capacity and mitochondrial *bc1* complex deficiency in tafazzin-knockdown mice. Front Physiol. 4, 74.

Raffaello A, De Stefani D, Sabbadin D, Teardo E, Merli G, Picard A, Checchetto V, Moro S, Szabò I, Rizzuto R. (2013). The mitochondrial calcium uniporter is a multimer that can include a dominant-negative pore-forming subunit. EMBO J. 32, 2362–2376.

Rampelt H, Wollweber F, Gerke C, de Boer R, van der Klei IJ, Bohnert M, Pfanner N, van der Laan M. (2018). Assembly of the mitochondrial cristae organizer Mic10 is regulated by Mic26-Mic27 antagonism and cardiolipin. J Mol Biol. 430, 1883–1890.

Rangaraju V, Calloway N, Ryan TA. (2014). Activity-driven local ATP synthesis is required for synaptic function. Cell. 156, 825–835.

Ren M, Phoon CKL, Schlame M. (2014). Metabolism and function of mitochondrial cardiolipin. Prog Lipid Res. 55, 1-16.

Robert V, Massimino ML, Tosello V, Marsault R, Cantini M, Sorrentino V, Pozzan T. (2001). Alteration in calcium handling at the subcellular level in mdx myotubes. J Biol Chem. 276, 4647–4651.

Ronvelia D, Greenwood J, Platt J, Hakim S, Zaragoza MV. (2012). Intrafamilial variability for novel *TAZ* gene mutation: Barth syndrome with dilated cardiomyopathy and heart failure in an infant and left ventricular noncompaction in his great-uncle. Mol Genet Metab. 107, 428–432.

Sancak Y, Markhard AL, Kitami T, Kovács-Bogdán E, Kamer KJ, Udeshi ND, Carr SA, Chaudhuri D, Clapham DE, Li AA, Calvo SE, Goldberger O, Mootha VK. (2013). EMRE is an essential component of the mitochondrial calcium uniporter complex. Science. 342, 1379–1382.

Schägger H, Pfeiffer K. (2000). Supercomplexes in the respiratory chains of yeast and mammalian mitochondria. EMBO J. 19, 1777–1783.

Schlame M, Towbin JA, Heerdt PM, Jehle R, DiMauro S, Blanck TJJ. (2002). Deficiency of tetralinoleoyl-cardiolipin in Barth syndrome. Ann Neurol. 51, 634–637.

Schuler MH, Di Bartolomeo F, Mårtensson CU, Daum G, Becker T. (2016). Phosphatidylcholine affects inner membrane protein translocases of mitochondria. J Biol Chem. 291, 18718–18729.

Shanmughapriya S, Rajan S, Hoffman NE, Zhang X, Guo S, Kolesar JE, Hines KJ, Ragheb J, Jog NR, Caricchio R, Baba Y, Zhou Y, Kaufman BA, Cheung JY, Kurosaki T, Gill DL, Madesh M. (2015). Ca^{2+} signals regulate mitochondrial metabolism by stimulating CREB-mediated expression of the mitochondrial Ca^{2+} uniporter gene MCU. Sci Signal. 8, ra23.

Shevchenko A, Simons K. (2010). Lipidomics: coming to grips with lipid diversity. Nat Rev Mol Cell Biol. 11, 593–598.

Soman SK, Bazała M, Keatinge M, Bandmann O, Kuznicki J. (2019). Restriction of mitochondrial calcium overload by MCU inactivation renders a neuroprotective effect in zebrafish models of Parkinson's disease. Biol Open. 8, bio044347.

Soustek MS, Falk DJ, Mah CS, Toth MJ, Schlame M, Lewin AS, Byrne BJ. (2011). Characterization of a transgenic short hairpin RNA-induced murine model of *Tafazzin* deficiency. Hum Gene Ther. 22, 865–871.

Spencer CT, Byrne BJ, Bryant RM, Margossian R, Maisenbacher M, Breitenger P, Benni PB, Redfearn S, Marcus E, Cade WT. (2011). Impaired cardiac reserve and severely diminished skeletal muscle O_2 utilization mediate exercise intolerance in Barth syndrome. Am J Physiol Heart Circ Physiol. 301, H2122-H2129.

Stepanyants N, Macdonald PJ, Francy CA, Mears JA, Qi X, Ramachandran R. (2015). Cardiolipin's propensity for phase transition and its reorganization by dynamin-related protein 1 form a basis for mitochondrial membrane fission. Mol Biol Cell 26, 3104–3116.

Su X, Dowhan W. (2006). Translational regulation of nuclear gene COX4 expression by mitochondrial content of phosphatidylglycerol and cardiolipin in *Saccharomyces cerevisiae*. Mol Cell Biol. 26, 743–753.

Tasseva G, Bai HD, Davidescu M, Haromy A, Michelakis E, Vance JE. (2013). Phosphatidylethanolamine deficiency in mammalian mitochondria impairs oxidative phosphorylation and alters mitochondrial morphology. J Biol Chem. 288, 4158–4173.

Telezhkin V, Reilly JM, Thomas AM, Tinker A, Brown DA. (2012). Structural requirements of membrane phospholipids for M-type potassium channel activation and binding. J Biol Chem. 287, 10001–10012.

Tomar D, Dong Z, Shanmughapriya S, Koch DA, Thomas T, Hoffman NE, Timbalia SA, Goldman SJ, Breves SL, Corbally DP, Nemani N, Fairweather JP, Cutri AR, Zhang X, Song J, Jaña F, Huang J, Barrero C, Rabinowitz JE, Luongo TS, Schumacher SM, Rockman ME, Dietrich A, Merali S, Caplan J, Stathopulos P, Ahima RS, Cheung JY, Houser SR, Koch WJ, Patel V, Gohil VM, Elrod JW, Rajan S, Madesh M. (2016). MCUR1 is a scaffold factor for the MCU complex function and promotes mitochondrial bioenergetics. Cell Rep. 15, 1673-1685.

Van Meer G, Voelker DR, Feigenson GW. (2008). Membrane lipids: where they are and how they behave. Nat Rev Mol Cell Biol. 9, 112–124.

Veling MT, Reidenbach AG, Freiberger EC, Kwiecien NW, Hutchins PD, Drahnak MJ, Jochem A, Ulbrich A, Rush MJP, Russell JD, Coon JJ, Pagliarini DJ. (2017). Multi-omic mitoprotease profiling defines a role for Oct1p in coenzyme Q production. Mol Cell. 68, 970–977.e11.

Voltarelli VA, Coronado M, Fernandes LG, Campos JC, Jannig PR, Ferreira JCB, Fajardo G, Brum PC, Bernstein D. (2021). β_2-Adrenergic signaling modulates mitochondrial function and morphology in skeletal muscle in response to aerobic exercise. Cells. 10, 146.

Walkinshaw E, Gai Y, Farkas C, Richter D, Nicholas E, Keleman K, Davis RL. (2015). Identification of genes that promote or inhibit olfactory memory formation in *Drosophila*. Genetics. 199, 1173–1182.

Wang C, Baradaran R, Long SB. (2020). Structure and reconstitution of an MCU-EMRE mitochondrial Ca^{2+} uniporter complex. J Mol Biol. 432, 5632-5648.

Wang G, McCain ML, Yang L, He A, Pasqualini FS, Agarwal A, Yuan H, Jiang D, Zhang D, Zangi L Geva J, Roberts AE, Ma Q, Ding J, Chen J, Wang D, Li K, Wang J, Wanders RJA, Kulik W, Vaz FM, Laflamme MA, Murry CE, Chien KR, Kelley RI, Church GM, Parker KK, Pu WT. (2014). Modeling the mitochondrial cardiomyopathy of Barth syndrome with induced pluripotent stem cell and heart-on-chip technologies. Nat Med. 20, 616–623.

Wang Y, Han Y, She J, Nguyen NX, Mootha VK, Bai XC, Jiang Y. (2020). Structural insights into the Ca^{2+}-dependent gating of the human mitochondrial calcium uniporter. Elife. 9: e60513.

Wenz T, Hielscher R, Hellwig P, Schägger H, Richers S, Hunte C. (2009). Role of phospholipids in respiratory cytochrome bc(1) complex catalysis and supercomplex formation. Biochim Biophys Acta. 1787, 609–616.

West AP, Shadel GS, Ghosh S. (2011). Mitochondria in innate immune responses. Nat Rev Immunol. 11, 389-402.

Whited K, Baile MG, Currier P, Claypool SM. (2013). Seven functional classes of Barth syndrome mutation. Hum Mol Genet. 22, 483–492.

Wu M, Gu J, Guo R, Huang Y, Yang M. (2016). Structure of mammalian respiratory supercomplex $I_1III_2IV_1$. Cell. 167, 1598–1609.

Wu Y, Rasmussen TP, Koval OM, Joiner ML, Hall DD, Chen B, Luczak ED, Wang Q, Rokita AG, Wehrens XH, Song LS, Anderson ME. (2015). The mitochondrial uniporter controls fight or flight heart rate increases. Nat Commun. 6, 6081.

Xie Z, Zhang H, Tsai W, Zhang Y, Du Y, Zhong J, Szpirer C, Zhu M, Cao X, Barton MC, Grusby MJ, Zhang WJ. (2008). Zinc finger protein ZBTB20 is a key repressor of alpha-fetoprotein gene transcription in liver. Proc Natl Acad Sci USA. 105, 10859-10864.

Xu Y, Anjaneyulu M, Donelian A, Yu W, Greenberg ML, Ren M, Owusu-Ansah E, Schlame M. (2019). Assembly of the complexes of oxidative phosphorylation triggers the remodeling of cardiolipin. Proc Natl Acad Sci USA. 116, 11235–11240.

Xu Y, Condell M, Plesken H, Edelman-Novemsky I, Ma J, Ren M, Schlame M. (2006). A *Drosophila* model of Barth syndrome. Proc Natl Acad Sci USA. 103, 11584–11588.

Xu Y, Kelley RI, Blanck TJ, Schlame M. (2003). Remodeling of cardiolipin by phospholipid transacylation. J Biol Chem. 278, 51380–51385.

Xu Y, Malhotra A, Ren M, Schlame M. (2006). The enzymatic function of tafazzin. J Biol Chem. 281, 39217–39224.

Xu Y, Phoon CK, Berno B, D'Souza K, Hoedt E, Zhang G, Neubert TA, Epand RM, Ren M, Schlame M. (2016). Loss of protein association causes cardiolipin degradation in Barth syndrome. Nat Chem Biol. 12, 641–647.

Yamamoto T, Yamagoshi R, Harada K, Kawano M, Minami N, Ido Y, Kuwahara K, Fujita A, Ozono M, Watanabe A, Yamada A, Terada H, Shinohara Y. (2016).

Analysis of the structure and function of EMRE in a yeast expression system. Biochim Biophys Acta. 1857, 831–839.

Ye C, Lou W, Li Y, Chatzispyrou IA, Hüttemann M, Lee I, Houtkooper RH, Vaz FM, Chen S, Greenberg ML. (2014). Deletion of the cardiolipin-specific phospholipase Cld1 rescues growth and life-span defects in the tafazzin mutant: implications for Barth syndrome. J Biol Chem. 289, 3114–3125.

Zaglia T, Ceriotti P, Campo A, Borile G, Armani A, Carullo P, Prando V, Coppini R, Vida V, Stølen TO, Ulrik W, Cerbai E, Stellin G, Faggian G, De Stefani D, Sandri M, Rizzuto R, Di Lisa F, Pozzan T, Catalucci D, Mongillo M. (2017). Content of mitochondrial calcium uniporter (MCU) in cardiomyocytes is regulated by microRNA-1 in physiologic and pathologic hypertrophy. Proc Natl Acad Sci USA. 114, E9006–E9015.

Zampieri S, Mammucari C, Romanello V, Barberi L, Pietrangelo L, Fusella A, Mosole S, Gherardi G, Höfer C, Löfler S, Sarabon N, Cvecka J, Krenn M, Carraro U, Kern H, Protasi F, Musaró A, Sandri M, Rizzuto R. (2016). Physical exercise in aging human skeletal muscle increases mitochondrial calcium uniporter expression levels and affects mitochondria dynamics. Physiol Rep. 4, e13005.

Zhang M, Mileykovskaya E, Dowhan W. (2002). Gluing the respiratory chain together. Cardiolipin is required for supercomplex formation in the inner mitochondrial membrane. J Biol Chem. 277, 43553–43556.

Zhang X, Li X, Xu H. (2012). Phosphoinositide isoforms determine compartment-specific ion channel activity. Proc Natl Acad Sci USA. 109, 11384–11389.

Zhuo W, Zhou H, Guo R, Yi J, Yu L, Sui Y, Zhang L, Zeng W, Wang P, Yang M. (2020). Structure of intact human MCU supercomplex with the auxiliary MICU subunits. (Preprint). bioRxiv.

Zhuo W, Zhou H, Guo R, Yi J, Zhang L, Yu L, Sui Y, Zeng W, Wang P, Yang M. (2021). Structure of intact human MCU supercomplex with the auxiliary MICU subunits. Protein Cell. 12, 220–229.

APPENDIX A

CARDIOLIPIN DEFICIENCY IN BARTH SYNDROME TRIGGERS INCREASED EXPRESSION OF IMMUNOSUPPRESIVE FACTOR A-FETOPROTEIN

Mounting evidence indicates that mitochondria are key regulators of the mammalian immune system that impacts antiviral and antibacterial immunity (West et al., 2011). Neutropenia is one such clinical manifestation of mitochondrial dysfunction-induced immune suppression observed in BTHS patients (Clarke et al., 2013, Jefferies 2013). It is defined as an abnormally low count of neutrophils, a type of white blood cells, that makes BTHS patients susceptible to life-threatening secondary bacterial infections and resultant sepsis (Clarke et al., 2013, Jefferies 2013). To date, the underlying cause of neutropenia in BTHS is not known. To this end, I initiated collaboration with Dr. Scot C. Leary who recently discovered that mitochondrial dysfunction in mice triggers production of an immunosuppressive factor, α-fetoprotein (AFP), which is responsible for suppression of the peripheral immune system. The Leary lab utilized mouse models with liver-specific genetic perturbations in mitochondrial respiratory chain (MRC) complex IV biogenesis and found a robust increase in the levels of secreted AFP in these mice as compared to the control mice.

AFP is a major serum protein expressed by the developing embryo under tight temporal and spatial regulation (Belayew and Tilghman, 1982, Krumlauf et al., 1986). Post-birth, multiple genetic factors coordinate a conserved developmental program to repress its transcription (Perincheri et al., 2005, Xie et al., 2008). However, liver dysfunction in adults can reactivate AFP expression in hepatocytes, most notably with

hepatic cellular carcinoma (Abelev, 1971, Nakano et al., 2017). Here, I utilized different cell types including skeletal muscle cells, fibroblasts, and B-lymphoblasts to determine if non-hepatic cells could synthesize AFP. I found that all three cell types synthesized AFP (Figure A.1). Moreover, the AFP levels were responsive to a disruption in the MRC complexes as observed by an increase in AFP abundance in C2C12 myoblasts and B-lymphoblasts upon treatment with potassium cyanide, a pharmacological inhibitor of the MRC complex IV (Figure A.1) These findings suggest that AFP is not exclusively hepatic in origin and its expression is elevated in response to mitochondrial dysfunction.

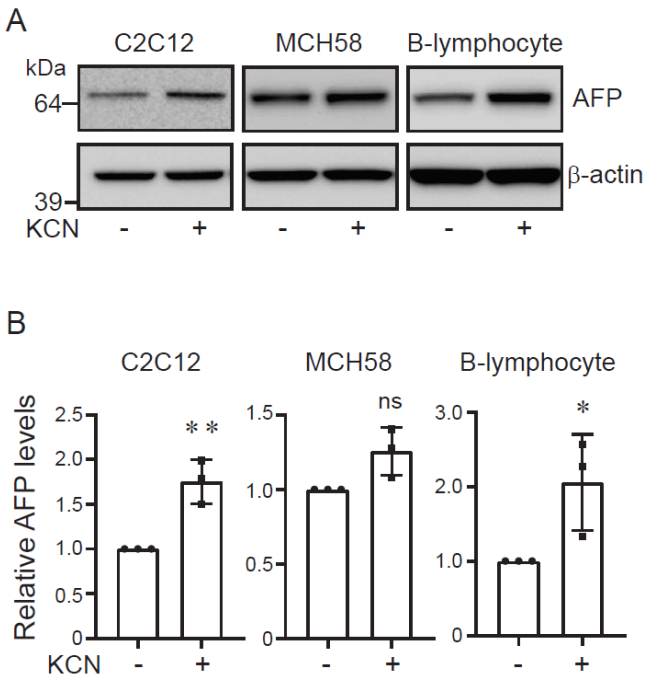

Figure A.1 Inhibition of MRC complex IV leads to increased AFP abundance in multiple cell types.
(A) Western blot analysis of AFP levels in cell lysates obtained from C2C12 myoblasts, MCH58 fibroblasts, and human B-lymphoblasts treated with DMSO or KCN (1 mM) for 24 h. β-actin is used as a loading control. Blots are representative of three independent experiments. (B) Quantification of relative AFP levels in indicated cell lines in (A) using ImageJ software. Data shown as mean ± SD, n=3, *$p < 0.05$, **$p < 0.005$. ns, not significant.

Next, we wondered if the AFP response was specific to MRC complex IV disruption or was it a more generic response to a disruption in any of the MRC complexes. To answer this, I treated mouse skeletal muscle cells with pharmacological inhibitors of MRC complexes I through V, respectively (Figure A.2). I found that AFP levels were elevated in response to a disruption of all MRC complexes, except for Complex II, suggesting that the immunological response of AFP owing to mitochondrial dysfunctions is not limited to Complex IV (Figure A.2).

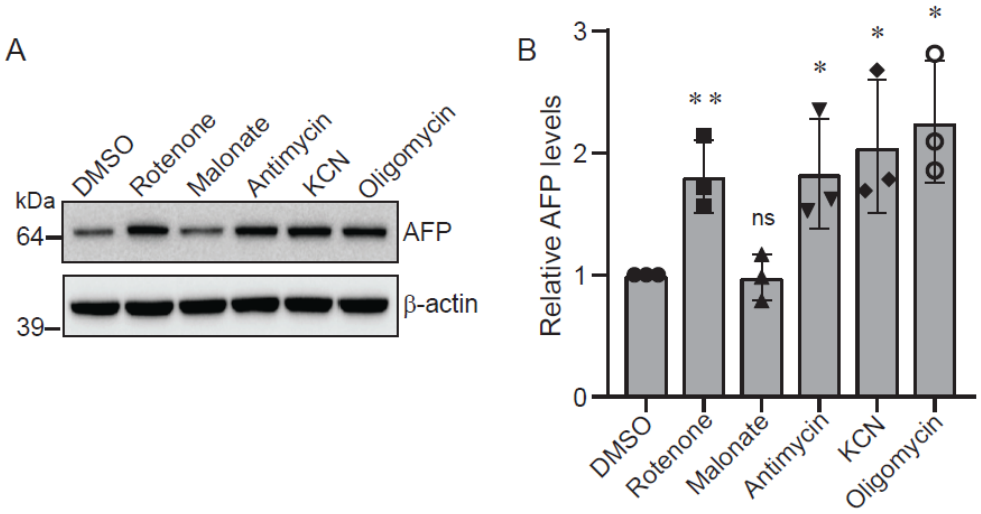

Figure A.2 Pharmacological inhibition of different MRC complexes increases AFP abundance

(A) Western blot analysis of AFP levels in C2C12 myoblasts treated with DMSO or the indicated mitochondrial respiratory chain complex inhibitors for 24 h. β-actin is used as a loading control. Blot is representative of three independent experiments. (B) Quantification of relative AFP levels from (A) using ImageJ software. Data shown as mean ± SD, n=3, *$p < 0.05$, **$p < 0.005$. ns, not significant.

The above findings motivated me to determine if AFP was also involved in BTHS disease pathology. To this end, I utilized a C2C12 murine myoblast model of BTHS and found that the abundance of AFP was increased by ~2.5 fold in BTHS *Taz*-

KO cells as compared to wild type cells (Figure A.3). This finding implicates AFP in neutropenia and associated immunosuppression defects observed in BTHS patients.

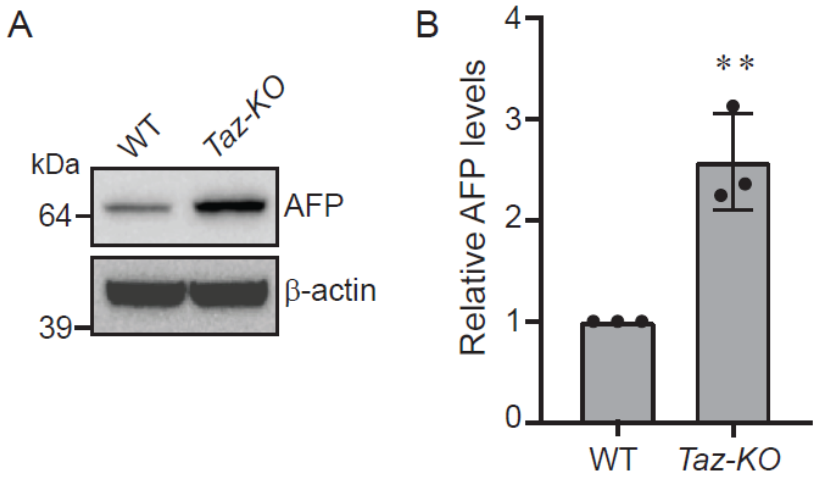

Figure A.3 AFP expression is increased in murine myoblast model of BTHS
(A) Western blot analysis of AFP in cell lysates obtained from WT and *Taz-KO* C2C12 myoblasts. Blot is representative of three independent experiments. (B) Quantification of immunoblots from (A) using ImageJ software. Data shown as mean ± SD, n=3, $^{**}p < 0.005$. WT, wild type.

Next, I utilized BTHS patient-derived serum and cardiac tissues to determine the abundance of AFP in these samples. Utilizing Enzyme-Linked Immunosorbent Assay (ELISA) (Quantikine ELISA, R&D Systems), I found a trend towards an increased level of AFP in BTHS patient-derived serum as compared to control serum (Figure A.4). The results did not meet statistical significance, which could be due to: 1) variations in the age and genetic backgrounds of the control and patient-derived samples, 2) type of mutations in the patient samples (not all BTHS patients exhibit neutropenia), 3) small sample size. Additionally, I found that AFP levels are increased in 2 out of 5 cardiac tissue samples obtained from BTHS patients (Figure A.5), which could be due to the above discussed scenarios.

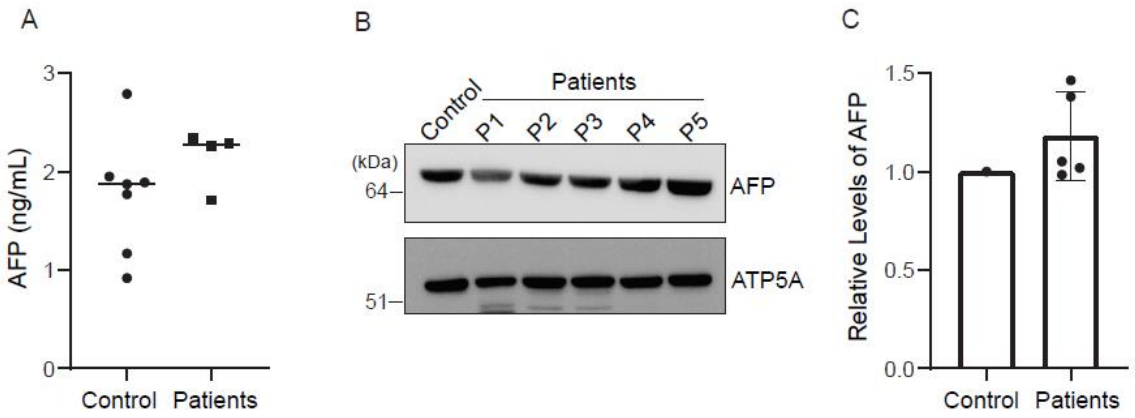

Figure A.4 AFP expression shows an increasing trend in BTHS patient-derived serum and cardiac tissues

(A) Enzyme-linked immunosorbent assay of AFP in serum samples obtained from 7 different human controls and 4 different BTHS patients. Data represented as mean from two technical replicates. (B) SDS-PAGE immunoblot analysis of AFP in cardiac tissues obtained from 5 different BTHS patients (P1-P5). ATP5A is used as a loading control. (C) Quantification of AFP levels from (B) by densitometry using ImageJ software. Data represented as mean ± SD.

In summary, my findings suggest a cell autonomous nature of AFP expression which is responsive to robust disruptions in mitochondrial respiration, both by genetic and pharmacological means. This work suggests that AFP could be a novel physiological factor in BTHS disease pathology that could explain neutropenia and immune suppression, a commonly observed clinical feature in these patients.